

7-Dec-2005

Technical Proposal for the Design, Construction, Commissioning and Operation of

R³B**A universal setup for kinematical complete measurements of
Reactions with Relativistic Radioactive Beams****The R³B collaboration****Abstract**

A versatile reaction setup with high efficiency, acceptance, and resolution for kinematically complete measurements of reactions with high-energy radioactive beams is proposed. The setup will be located at the focal plane of the high-energy branch of the Super-FRS. The experimental configuration is based on a concept similar to the existing LAND reaction setup at GSI introducing substantial improvement with respect to resolution and an extended detection scheme, which comprises the additional detection of light (target-like) recoil particles and a high-resolution fragment spectrometer. The setup is adapted to the highest beam energies (corresponding to 20 Tm magnetic rigidity) provided by the Super-FRS capitalizing on the highest possible transmission of secondary beams. The experimental setup is suitable for a wide variety of scattering experiments, i.e., such as heavy-ion induced electromagnetic excitation, knockout and breakup reactions, or light-ion (in)elastic and quasi-free scattering in inverse kinematics, thus enabling a broad physics programme with rare-isotope beams to be performed.

Spokesperson: Thomas Aumann

GSI

Tel.: +49 6159 71 1408

e-mail: t.aumann@gsi.de

Deputy: Björn Jonson

Chalmers University of Technology

Tel.: +46 31 772 3262

e-mail: bjn@fy.chalmers.se

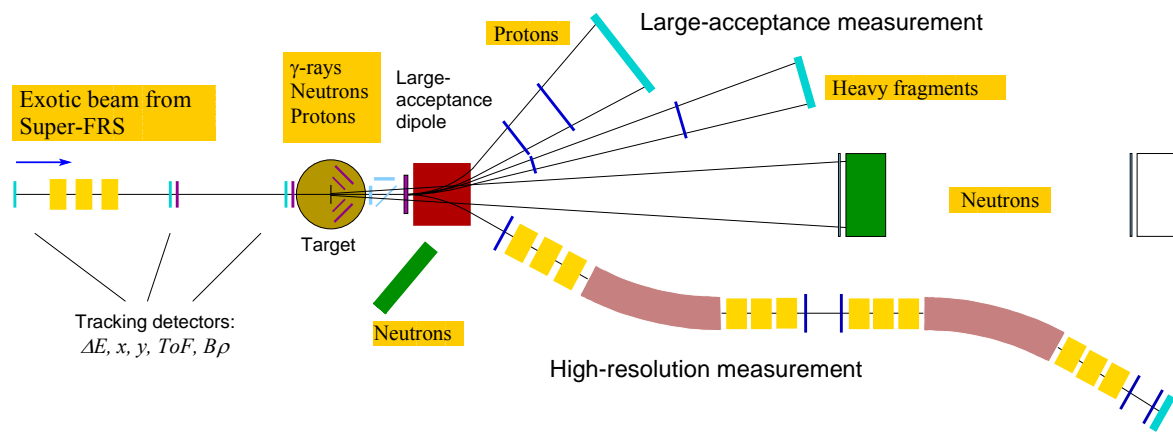


Figure 1: Schematic drawing of the experimental setup comprising γ -ray and target recoil detection, a large-acceptance dipole magnet, a high-resolution magnetic spectrometer, neutron and light-charged particle detectors, and a variety of heavy-ion detectors.

The R³B Collaboration

Aarhus, Denmark, University of Aarhus
D.V. Fedorov, H.O.U. Fynbo, A.S. Jensen, K. Riisager

Argonne, USA, Argonne National Laboratory
J. Nolen

Barcelona, Spain, Universidad Politecnica de Cataluna
F. Calvino

Basel, Switzerland, Universität Basel
K. Hencken

Bergen, Norway, University of Bergen
J.S. Vaagen

Birmingham, UK, University of Birmingham
M. Freer

Bucharest, Romania, Institute of Space Sciences
M. Haiduc, D. Hasegan, C. Mitu, M.Potlog, A. Sevcenco

Caen, France, GANIL
D. Boilley, W. Mittig, F. Rejmund, P. Roussel-Chomaz, H. Savajols

Daresbury, UK, CCLRC Daresbury Laboratory
P. Coleman-Smith, I. Lazarus, R. Lemmon, S. Letts, V. Pucknell, J. Simpson

Darmstadt, Germany, Technische Universität
F. Aksouh, J. Enders, S. Mueller, A. Richter, G. Schrieder, A. Zilges

Darmstadt, Germany, GSI
T. Aumann, F. Becker, K. Boretzky, A. Chatillon, P. Egelhof, H. Emling, H. Feldmeier, H. Geissel, J. Gerl,
M. Górska, V. Henzl, D. Henzlova, J. Hoffmann, H. Johansson, A. Kelic, I. Kojouharov, N. Kurz, K. Langanke,
T. Le Bleis, Y. Leifels, K. Mahata, G. Münzenberg, T. Neff, M.V. Ricciardi, T. Saito, K.-H. Schmidt, H. Simon,
K. Sümmerer, W. Trautmann, S. Typel, H. Weick, M. Winkler

Debrecen, Hungary, ATOMKI
A. Algora, M. Csatlós, Z. Gácsi, J. Gulyás, M. Hunyadi, A. Krasznahorkay

Dresden, Germany, Forschungszentrum Rossendorf
E. Grosse, A. Junghans, A. Wagner

Dubna, Russia, Joint Institute for Nuclear Research
S.N. Ershov, L. Grigorenko

East Lansing, USA, NSCL, MSU
B. Sherrill

Frankfurt, Germany, Universität Frankfurt
C. Müntz, J. Stroth, C. Wimmer

Gatchina, Russia, Petersburg Nuclear Physics Institute, PNPI
A. Khanzadeev

Giessen, Germany, Justus-Liebig-Universität
H. Lenske

Gif sur Yvette, France, DAPNIA, CEA Saclay
A. Boudard, J.-E. Ducret, B. Gastineau, K. Kezzar, E. Le Gentil, V. Lapoux, S. Leray,
E. Pollacco, C. Simenel, C. Volant

Göteborg, Sweden, Chalmers University of Technology
B. Jonson, M. Meister, T. Nilsson, G. Nyman, M. Zhukov

Guildford, UK, University of Surrey
J. Al Khalili, W. Catford, W. Gelletly, R. Johnson, S. Pietri, M. Oi, Z. Podolyak, P. Regan,
P. Stevenson, I. Thompson, J. Tostevin

Heidelberg, Germany, Max-Planck-Institut
Heiko Scheit

Köln, Germany, Universität zu Köln
P. Reiter

Kolkata, Saha Institute of Nuclear Physics, India
S. Bhattacharya, U. Datta Pramanik

Krakow, Poland, Jagellonski University
P. Adrich, A. Klimkiewicz, R. Kulesa, W. Walus

Krakow, IFJ PAN Krakow
M. Kmiecik, A. Maj, M. Zieblinski

Lanzhou, China
Yu-Hu Zhang

Liverpool, UK, University of Liverpool
M. Chartier, C.E. Demonchy, B. Fernandez Dominguez, P. Nolan, S. Paschalis

Lyon, IPN Lyon, France
Ch. Schmitt

Madrid, Spain, Instituto de Estructura de la Materia, CSIC
M.J.G. Borge, E. Garrido, D. Obradors, O. Tengblad, M. Turrión

Madrid, Spain, Universidad Complutense
L.M. Fraile, J.M. Udias

Mainz, Germany, Johannes Gutenberg Universität
O. Kiselev, J.V. Kratz

Manchester, UK, University of Manchester
D. Cullen, S. Freeman

Moscow, Russia, Kurchatov Institute
L. Chulkov, B. Danilin

Moscow, Russia, Institute for Nuclear Research, Russian Academy of Sciences
A. Botvina

Mumbai, India, Bhabha Atomic Research Centre
S. Kailas, A. Shrivastava

Mumbai, India, Tata Institute of Fundamental Research
R. Palit

München, Germany, TU München
M. Böhmer, T. Faestermann, J. Friese, R. Gernhäuser, T. Kröll, R. Krücken

Obninsk, Russia, IPPE Obninsk
A. Ignatyuk

Orsay, France, IN2P3/IPN Orsay
F. Azaiez, D. Beaumel, Y. Blumenfeld, B. Genolini, E. Khan, J. Peyré, J. Pouthas,
J.A. Scarpaci, F. Skaza, T. Zerguerras

Paisley, UK, University of Paisley
R. Chapman, M. Labiche, X. Liang, K. Spohr

Pyhäsalmi, Finland, CUPP project
T. Enqvist

Santiago de Compostela, Spain, University of SdC
H. Alvarez-Pol, J. Benlliure, E. Casarejos, D. Cortina-Gil, I. Duran

Sao Paulo, Brazil, Instituto de Fisica, Universidade de São Paulo
Alinka Lepine-Szily

Tokyo, Japan, Tokyo Institute of Technology
T. Nakamura

Tucson, University of Arizona
C. Bertulani

Valencia, Spain, IFIC, CSIC-University Valencia
B. Rubio, J.L. Tain

Vancouver, Canada, TRIUMF
R. Kanungo, I. Tanihata

Yale University, USA
A. Heinz

York, UK, University of York
Ch. Barton

Contents

A.	Introduction and overview	6
A.1.	Introductory Remarks	6
A.2.	Experimental concept	6
A.3.	Physics and reactions to be studied with R^3B	8
A.3.1.	Knockout reactions	8
A.3.2.	Quasi-free scattering	8
A.3.3.	Total-absorption measurements	9
A.3.4.	Elastic proton scattering	10
A.3.5.	Electromagnetic excitation	10
A.3.6.	Charge-exchange reactions	10
A.3.7.	Fission	11
A.3.8.	Spallation reactions	11
A.3.9.	Projectile fragmentation and multifragmentation	11
A.3.10.	Astrophysics	12
A.4.	Overview on subsystems	13
B.	Systems	14
B.1.	Detector Subsystems	
B.1.1.	Large-acceptance dipole	14
B.1.2.	High-resolution magnetic spectrometer	16
B.1.3.	Heavy-ion tracking detectors and velocity measurements	20
B.1.4.	Proton tracking	27
B.1.5.	Large-area ToF wall for fission and spallation measurements	28
B.1.6.	Total γ -absorption spectrometer	31
B.1.7.	Target recoil detector	36
B.1.8.	Active target	43
B.1.9.	Low-energy neutron detector	47
B.1.10.	High-resolution neutron time-of-flight spectrometer	49
B.1.11.	Multi-track ion detector for spallation and fission measurements	55
B.2.	Data acquisition system	65
B.3.	Beam/Target Requirements	69
B.4.	Physics performance	69
C.	Implementation and Installation	72
D.	Commissioning	73
E.	Operation	73
F.	Safety	73
G.	Organization and Responsibilities, Planning	75
H.	Relation to other Projects	81

A. Introduction and overview

A.1. Introductory remarks

This technical proposal follows the Letter of Intent (LoI) of the R³B collaboration which was submitted in April 2004. The progress in the technical design of the proposed experiment since then is reported. For completeness, the physics case and the reactions to be studied as described already in the LoI and the Conceptual Design Report of the facility are briefly summarized again. In following the recommendations of the PAC, special emphasis is given to the description of the individual subsystems, the requirements, the design concepts and expected performances. Based on this, an updated cost estimate is given. The collaboration intends to build and implement the basic subsystems of the experiment until end of 2009 in order to be ready for commissioning and first physics experiments in 2010. Working groups for the individual tasks have been formed and the individual participants have documented their intention to develop and build certain detector subsystems by signing a Memorandum of Understanding (MoU).

A.2. Experimental concept

During the past decade it has been demonstrated that reactions with high-energy secondary beams are an important tool to explore properties of nuclei far off stability, which allows detailed spectroscopic information to be extracted. The physics motivation for studying reactions with exotic nuclei is described extensively in various reports in the context of next-generation facilities, see, e.g., the 'Conceptual Design Report' (CDR) (<http://www.gsi.de/GSI-Future/cdr>) for the future FAIR project. High beam energies, in the range of a few hundred MeV/nucleon, allow a more quantitative description of the reaction mechanisms [Han03, AIK03], while also having experimental merits, such as the possibility of using relatively thick targets (in the order of 1 g/cm²). Moreover, due to the kinematical forward focusing full-acceptance measurements are feasible with moderately sized detectors. This makes it possible to gain nuclear-structure information from reaction studies even with very low beam intensities, as low as about 1 ion/s.

R³B will cover experimental reaction studies with exotic nuclei far off stability, with emphasis on nuclear structure and dynamics. Astrophysical aspects and technical applications are also concerned. A survey of reaction types and associated physics goals that can be achieved is given in Table 1.

Table 1. Reaction types with high-energy beams measurable with R³B and corresponding achievable information

<i>Reaction type</i>	<i>Physics goals</i>
Knockout	Shell structure, valence-nucleon wave function, many-particle decay channels unbound states, nuclear resonances beyond the drip lines
Quasi-free scattering	Single-particle spectral functions, shell-occupation probabilities, nucleon-nucleon correlations, cluster structures
Total-absorption measurements	Nuclear matter radii, halo and skin structures
Elastic p scattering	Nuclear matter densities, halo and skin structures
Heavy-ion induced electromagnetic excitation	Low-lying transition strength, single-particle structure, astrophysical S factor, soft coherent modes, low-lying resonances in the continuum, giant dipole (quadrupole) strength
Charge-exchange reactions	Gamow-Teller strength, soft excitation modes, spin-dipole resonance, neutron skin thickness
Fission	Shell structure, dynamical properties
Spallation	Reaction mechanism, astrophysics, applications: nuclear-waste transmutation, neutron spallation sources
Projectile fragmentation and multifragmentation	Equation-of-state, thermal instabilities, structural phenomena in excited nuclei, γ -spectroscopy of exotic nuclei

A brief description follows subsequently in the next sub-section. For a more detailed discussion we refer to the CDR. In case of light-ion scattering, the experiments at R³B are complementary to the ones proposed for the internal target in the NESR (see the LoI of the EXL collaboration). Here, the R³B programme will focus on the most exotic short-lived nuclei, which cannot be stored and cooled efficiently, and on reactions with large-momentum transfer allowing the use of thick targets. The proposed experimental setup is adapted to the highest beam energies delivered by the Super-FRS, thus exploiting fully the highest possible transmission efficiency of secondary beams.

The proposed experimental scheme is based on that of the LAND apparatus which is used successfully in experiments with secondary beams from the FRS facility at GSI. The most essential upgrades concern the target recoil detector and the two magnetic spectrometers. A schematic view of the R³B experimental setup is shown in Figure 1. The incoming secondary beams are tracked and identified on an event-by-event basis. Measurements of the magnetic rigidity $B\rho$ (position measurement at the dispersive focus in the Super-FRS), time-of flight ToF, and energy loss ΔE provide unique isotope identification and momentum determination. Although the secondary beam has a momentum spread of $\pm 2.5\%$, the momentum will be determined to an accuracy $\Delta p/p \sim 10^{-4}$ (event-wise). After the secondary target, the kinematically forward focused projectile residues are again identified and momentum analyzed.

Two modes of operation are foreseen depending on the demands of the experiments: i) A large-acceptance mode: Heavy fragments and light charged particles (i.e. protons) are deflected by a large-acceptance dipole and detected with full solid-angle acceptance, for most reactions envisaged (left bend in Figure 1). Relative resolutions for velocity and $B\rho$ measurements amount to about 10^{-3} allowing unique identification in mass and nuclear charge of also heavy fragments. ii) A high-resolution mode: here, the dipole magnet is operated in reversed mode, deflecting the fragments into a magnetic spectrometer (right bend in Figure 1). The envisaged resolution of $\Delta p/p = 10^{-4}$ will allow, e.g., a precise measurement of the fragment recoil momentum in single-nucleon knockout and quasi-free scattering experiments even for heavy nuclei.

The large gap of the dipole provides a free cone of ± 80 mrad for the neutrons, which are detected in forward direction by the large area neutron detector (new LAND). At beam energies around 500 MeV/nucleon, this corresponds to a 100% acceptance for neutrons with kinetic energies up to 5 MeV in the projectile rest frame. Depending on the requirements on resolution and acceptance, the detector with an active area of 2×2 m² is placed at a distance of 10 m to 35 m from the target.

The target is surrounded by a γ -ray spectrometer. For most of the experiments envisaged, a high-efficiency total-absorption spectrometer (cooled CsI or NaI) is the optimum solution, which is also used to measure the energy of recoiling protons. For specific experiments requiring ultimate energy resolution for γ -detection, the Germanium spectrometer AGATA might be used alternatively. For elastic, inelastic and quasi-free scattering experiments or charge-exchange reactions, liquid hydrogen or frozen hydrogen targets are considered. Recoiling protons and neutrons are detected by a Si-strip array and plastic scintillators, respectively. For measurements at low momentum transfer, the use of an active target is foreseen. Fast neutrons stemming from (p,pn) type knockout processes can be measured by placing part of the LAND detector at angles around 45°. The Si-strip array is also used as a high-granularity multiplicity detector array for measuring charged particles from the fire-ball, created in semi-peripheral collisions. The detector subsystems needed to achieve such a kinematical complete measurement of reactions with high efficiency and acceptance, which is of key importance for experiments with radioactive beams, are described in section B of this document.

A.3. Physics and reactions to be studied with R³B

A.3.1. Knockout reactions

If we are to understand exotic nuclei and use them as a tool to progress our description of the nuclear many-body problem, it will be essential to explore their single-particle structure in detail. The most direct way to do this is by exploiting reactions where we add or remove single nucleons. The technique of knockout reactions induced by high-energy beams of exotic nuclei has recently been developed. It allows the exploration of *ground-state configurations* and of excited states. Due to limitations in beam intensity for heavier nuclei, this method has been restricted mainly to light nuclei so far. In particular, the method has been used to map the halo-nucleon wave function in momentum space, from which their *spatial distribution* is derived via Fourier transformation [Sme99]. By γ -coincidence measurements, different single-particle configurations (including core-excited states) can be identified and corresponding *spectroscopic factors* may be obtained [Aum00]. The coincident measurement of neutrons allows the method to be utilized even if unbound states are involved. As an example, we mention the one-neutron knockout from the two-neutron halo nucleus ^{11}Li populating states in the unbound nucleus ^{10}Li , from which the occupancy of the $(s_{1/2})^2$ and $(p_{1/2})^2$ configurations of the two halo neutrons in the ^{11}Li ground state were deduced [Sim99]. Recently, knockout has been developed into a tool to allow the extraction of *absolute* spectroscopic factors and hence the determination of the spectroscopic strength for single-particle states. This has confirmed the findings of $(e,e'p)$ reactions that the spectroscopic strength in valence orbits is only 60% of that expected in the independent-particle shell model (IPSM). This fundamental result indicates the presence of short- and long-range correlations in the nuclear wavefunction. Unlike $(e,e'p)$ reactions, knockout reactions can also probe the neutron wavefunction and it has now been found that the spectroscopic strength for valence neutrons is also 60% of the value of the IPSM. Another very intriguing result is that, when the spectroscopic strength for a halo neutron is measured using knockout, it has a value closer to 100% of the IPSM as would be expected for an almost free nucleon. Extending such measurements to more and heavier exotic nuclei to fully explore the effects of correlations in the nuclear system is clearly of fundamental interest.

At the new facility heavy neutron-rich nuclei, produced by in-flight fission can be studied. With high detection efficiency, secondary beam intensities in the order of ten ions/s are sufficient to extract detailed spectroscopic information, thus making nuclear structure studies possible even very far from stability. The *key instrument* in this programme is the *high resolution magnetic spectrometer*. This is because in order to determine the angular momentum l of the knocked out nucleon, the momentum of the recoil fragment has to be measured with high precision and this device will provide a relative momentum resolution of about 10^{-4} , which is essential for studying medium-mass and heavy nuclei. Other important devices will be efficient high-resolution γ -ray spectrometers, like the proposed cooled CsI (or NaI) array or AGATA in cases where the ultimate energy resolution is essential.

Another promising field is the study of *resonant states in the continuum* [Mei02] or even *nuclei beyond the drip lines*, see [Mei03] for a recent study of the unbound ^5H nucleus.

A.3.2. Quasi-free scattering

As described in the previous section, knockout reactions using light targets, e.g., Be or C, have proven in the past to be very useful in gaining information on the wave function of the valence nucleons. However, the strong absorption concentrates the reaction probability at the surface. Similar arguments hold for transfer and Coulomb break-up reactions. Nucleon knockout reactions using protons, on the other side, allow one to determine the *spectral functions* of protons and neutrons in a wide range from the weakly bound valence nucleons to the deeply bound core states. Thus, in neutron rich nuclei one gains access to the hitherto unknown region of the strongly bound protons and simultaneously to the valence neutrons. Beside the single-particle shell-structure, *nucleon-nucleon correlations* may be investigated as well as *cluster* knockout reactions. For stable nuclei and in normal kinematics, (p,pN) reactions have been used in the past as spectroscopic tool [Kre95].

We intend to develop and apply the technique of quasi-free scattering using radioactive beams in inverse kinematics. At energies around 700 MeV/nucleon (which is high enough to ensure that the conditions for quasi-free scattering are met), both outgoing nucleons have energies in the range where the nucleon-

nucleon cross section is at minimum, thus maximizing the transparency of the nucleus and minimizing final state interaction. Measurements such as (p,2p), (p,pn), (p,pd) etc. will become possible in a kinematically complete geometry, allowing a background-free measurement and also for a better control of final state interactions. As in the knockout programme, a *key instrument* for the quasi-free scattering programme is the *high resolution magnetic spectrometer*. It will allow the momentum of the recoil fragment to be measured with a relative momentum resolution of 10^{-4} , which will be essential for studying medium-mass and heavy nuclei. To detect the proton recoils and other charged particles, we foresee two shells of Si microstrip detectors that surround the liquid hydrogen target integrated into a 4π gamma calorimeter. For (p,pn) reactions, part of the LAND neutron detector can be placed at angles around 45° to detect the knocked-out neutrons with energies of few hundred MeV. Thus, the experiment determines the complete kinematics of quasi-free knockout reactions including those to continuum states (by measuring the invariant mass of the decaying system). Even reactions populating states *beyond the dripline* such as, e.g., $^{14}\text{Be}(p,p')^{13}\text{Li}$, $^{14}\text{Be}(p,p'\alpha)^{10}\text{He}$, $^{11}\text{Li}(p,p'\alpha)^7\text{H}$, or $^8\text{He}(p,p'\alpha)^4\text{n}$, can be studied.

A thick liquid hydrogen target (200 mg/cm^2 , $\sim 3\text{ cm}$ thickness) will be used. The tracking of both protons and the beam will allow reconstruction of the interaction point with an accuracy much better than 3 mm , corresponding to an effective target thickness of less than 20 mg/cm^2 . Thus, the relative momentum resolution of 10^{-4} for the fragment can be preserved. Experiments can be performed with intensities of 1000 ions/s corresponding to a luminosity of $10^{26}\text{ cm}^{-2}\text{s}^{-1}$.

In a further development of our experimental programme, we wish to exploit *polarized* quasi-free hadronic scattering, such as (p,2p) and (p,pn) reactions. The interest is twofold. Firstly, polarized measurements will allow the j -values of the hole states to be determined experimentally, in addition to the l -values. Secondly, such measurements can be used to study *in-medium effects*. Modification of meson and nucleon properties in the nuclear medium is one of the most interesting topics in current nuclear physics. There have been speculations on modifications of nucleon and meson masses and sizes, and of meson-nucleon coupling constants. These speculations have been motivated from a variety of theoretical points of view, which include renormalization effects due to strong relativistic nuclear fields, deconfinement of quarks, and chiral symmetry restoration. Such modifications cause a density dependence of the nucleon-nucleon interaction and are expected to play an important role in nucleon-induced reactions. Hence, exclusive measurements of nucleon quasi-free scattering, and in particular polarized scattering, give a direct way to study the nucleon-nucleon interaction in nuclei and, therefore, to study meson and nucleon properties in the nuclear medium. For example, analyzing power measurements from (p,2p) reactions on several stable nuclei have recently been reported. It is found that A_y is a monotonically decreasing function of the averaged nuclear density, strongly suggesting the existence of a nuclear medium effect on the nucleon-nucleon interaction. Clearly measurements on unstable nuclei where the averaged nuclear density can be varied systematically could be invaluable. Measurements on unstable nuclei will have the possibility to probe the nucleon-nucleon interaction in a nuclear medium with very different values of isospin and also low-density nuclear matter, for example in the diffuse surface of neutron-rich nuclei. Clearly, the polarized quasi-free scattering programme will require the development of a polarized hydrogen target, which is one of the future avenues we wish to pursue within R³B.

A.3.3. Total-absorption measurements

Nuclear *matter radii* may be inferred from total interaction cross sections derived from total-absorption measurements of radioactive ions in thick targets. This technique requires intensities of the order of only one ion/s. For instance, interesting results were obtained by a RIKEN-GSI collaboration [Suz95] by using beams of unstable sodium isotopes. These data, together with isotope-shift measurements, provide a first experimental manifestation of *neutron skins*. Beam intensities available at the new facility will allow systematic studies of this phenomenon in heavy nuclei. Such experiments can be performed using the high-resolution spectrometer after the dipole magnet.

A.3.4. Elastic proton scattering

The radial shape of the *nuclear density distribution* of exotic nuclei may be extracted from high-energy proton elastic scattering in inverse kinematics. Previous measurements [Ege02] using secondary beams at 700 MeV/nucleon have demonstrated the power of the method to investigate *halo* and *skin* structures in nuclei far off stability. Complementary to the experiments proposed at the storage ring, elastic scattering will be measured at R³B using (thick) liquid hydrogen or frozen hydrogen targets, and focusing on larger momentum transfer and very short-lived nuclei, which are produced with low intensity only.

A.3.5. Electromagnetic excitation

Electromagnetic processes in heavy-ion interactions at energies far above the Coulomb barrier give access to a wealth of nuclear-structure information on exotic nuclei [Ber88]. At energies of the order of 1 GeV/nucleon, collective nuclear states at low and at high excitation energies are excited in peripheral heavy-ion collisions with large cross sections. Due to Lorentz contraction, the mutual electromagnetic field contains high frequencies up to several tens of MeV/h. *Surface vibrations* and particular *giant resonances* can be studied even with moderate beam intensities. The large cross sections allow experiments with minimum beam intensities of 1 to 1000 ions/s, provided efficient devices for γ -ray and particle detection are implemented.

Electromagnetic excitation of the *giant dipole resonance* induced by high-energy beams on targets of high nuclear charge was pioneered at GSI in exploring the multi-phonon states of the dipole resonance [Aum98]. This method was recently extended to secondary beams of exotic nuclei [Leis01]. It was shown that, e.g., for neutron-rich oxygen isotopes, *low-lying strength* appears and that the usual pattern of the dipole resonance strength distribution dissolves [Leis01]. With the proposed new facility, the measurement of the dipole strength of neutron-rich nuclei relevant for the *astrophysical r-process* will be feasible. In the region of the $N=82$ closed shell, for instance, the giant dipole strength can be deduced even beyond ¹³²Sn. For these heavier neutron-rich nuclei, the appearance of a new collective mode is predicted, the collective oscillation of valence neutrons (neutron skin) against the core, the so called *soft dipole mode*. The higher beam intensities also allow the study of giant quadrupole strength. Compared to dipole excitations, the required beam intensities are an order of magnitude larger. Giant resonance studies, in particular monopole and quadrupole excitations, will also be investigated at the NESR using the internal target and at the e-A collider (see the LoI's by the EXL and ELISE collaborations).

Besides resonant excitations, direct non-resonant transitions to the continuum occur for weakly bound nuclei. This 'threshold strength' is characteristic for the *single-particle structure*, being extremely sensitive to the spatial distribution of the valence nucleons. Similar to knockout, the l -value of the removed nucleon and spectroscopic factors can be deduced [Dat03]. For a halo-like structure, cross sections become very large, and spectroscopic information can be obtained with beam intensities down to 0.1 ions/s.

The continuum structure of drip-line nuclei was studied so far only for very light nuclei. From a kinematically complete measurement of the decay not only the excitation spectrum, but also correlations can be studied as, e.g., in the three-body decay of Borromean halo nuclei like ¹¹Li or ⁶He [Aum99,Ers01]. The experimental technique discussed here also allows the extraction of (p,γ) and (n,γ) reaction rates, which essentially determine the *astrophysical r-, and rp-reaction paths*. While the direct measurement of these rates is very difficult, the (γ,p) and (γ,n) reaction can be measured by electromagnetic excitation using high-energy secondary beams [Sch03] (see subsection A.3.10).

A.3.6. Charge-exchange reactions

The (p,n) charge-exchange reaction can be used to excite *Gamow-Teller (GT)* and *spin-dipole* resonances by utilizing a liquid hydrogen target and measuring the slow neutrons with plastic scintillators surrounding the target. Studies of the GT strength are beside their importance in nuclear structure of particular astrophysical interest. Electron-capture reactions leading to *stellar collapse and supernova formation* are mediated by GT transitions. Basic understanding of all these processes requires reliable knowledge of the GT strength distribution in a large excitation energy range as well as in nuclei far off stability. Cross sections of the spin-dipole giant resonance excited in (p,n) reactions are rather directly

related to the *neutron-skin* thickness. Corresponding measurements were performed so far only for stable isotopes [Kra99]. With exotic nuclear beams, such measurements require secondary beam intensities of the order of 1000 ions/s, and thus a systematic study of neutron skins will be feasible by a method alternative to that consisting of a combination of proton and electron scattering data.

A.3.7. Fission

Since fission corresponds to a typical large-scale motion process, it has been recognised as one of the most promising tools for deducing information on *nuclear viscosity*, and on *shell effects* and *collective excitations at extreme deformation*. This is not only important from the fundamental point of view but is of the prime interest in many challenging fields in nuclear physics, like e.g. *super-heavy element synthesis* or nuclide production in secondary-beam facilities. However, many questions still remain open, mainly due to the fact that experiments were restricted up to very recently to spontaneously fissioning isotopes and primordial or long-lived target nuclei. First-generation experiments performed at GSI have proven that the use of secondary beams indeed opens new prospects for studies of nuclear fission [Sch00]. More than 100 short-lived neutron-deficient nuclei will become available for such investigations. It will be possible, for the first time, to identify both fission fragments in A and Z at different excitation energies. This information in combination with fission-fragment velocities would give new insight into the dynamics of the fission process. The full isotopic distribution of the fission fragments is a sensitive signature of the excitation energy at which fission occurs in the statistical deexcitation cascade. The knowledge of the emitted neutrons and γ radiation accompanying the fission process allows determining the excitation energies of the final products.

A.3.8. Spallation reactions

Spallation reactions are important in various fields of research such as *astrophysics*, *neutron sources* and *production of radioactive beams*. To get a quantitative understanding of the spallation mechanism and to improve its modeling, which is needed for accurate simulations of, e.g., sub-critical reactors coupled with high-intensity proton beams designed as *radioactive waste burners*, exclusive measurements of the reaction channels are mandatory. First experiments in this direction were performed [Duc03] at GSI at the ALADIN/LAND facility with high-energy (1 GeV/nucleon) Fe beams impinging on a liquid hydrogen target. Such studies are most interesting to be extended to heavier systems, which is prohibited at present, however, due to experimental limitations. We intend to measure spallation with two heavy beams, ^{208}Pb and ^{238}U . The first one constitutes the main component of the spallation target in accelerator driven systems, while the second allows studying the role of fission in spallation reactions. The R³B facility provides the ideal setup for such studies making use of the large-acceptance dipole magnet with its large bending power. The goal will be to identify all the products in mass and nuclear charge (isotopic distributions) of the reactions and measure their velocities so that a complete reconstruction of the excited system at the end of the first stage of the reaction could be achieved. This would allow, for the first time for heavy projectiles, for a detailed study of the competition between the different de-excitation mechanisms (evaporation, fission, emission of intermediate-mass fragments, see also the sections on fission, projectile fragmentation).

A.3.9. Projectile fragmentation and multifragmentation

Heavy-ion collisions offer the possibility to probe nuclear matter under different conditions of densities and temperatures. At high excitation energies the nuclei may break-up into many intermediate-mass fragments, the so called multifragmentation. In multifragmentation, nuclear matter at low densities and, more generally, modes of disintegration of dynamically unstable systems are probed. In particular, the expected link with the *nuclear liquid-gas phase transition* provides a continuing motivation for studying multifragmentation. In these reactions, systems of small and intermediate-mass nuclei surrounded by a nucleon gas may be produced, with properties close to what is expected in stellar processes as, e.g., supernova II explosions [Bot04]. Experimental extraction of in-medium modifications of the properties of hot nuclei, in particular, their symmetry energy [LeF05] will be important for understanding the production of nuclei and their interaction in stellar matter. Also properties of the high-density zones of the collision may be studied in the fragmentation of excited projectile spectators. The velocities of

projectile residues are predicted to be sensitive to the non-local features of the nuclear mean field [Ric03].

Isotopic effects originating from the two-fluid nature of nuclear matter [Mue95], reflect the strength of the *symmetry term* in the *equation of state* whose density dependence is of importance for astrophysical applications. Experiments using the existing GSI facilities [Ala03] have shown that secondary beams of exotic nuclei are useful and necessary for obtaining systems with a sufficiently broad range of isotopic composition. With the new facility, this can be further extended, in particular to neutron-rich asymmetric matter for which the effects of the symmetry term are most strongly pronounced.

Projectile fragmentation of secondary beams in conjunction with *γ -ray spectroscopy* is a powerful method to explore *excited states in exotic nuclei*. This method is also addressed in the LEB LoI. The R³B setup is particularly well suited for cases at the very limits of the production rates, i.e., for the most exotic nuclei. Here, the better transmission using high-energy beams and the high efficiency of the γ -calorimeter is advantageous.

A.3.10. Astrophysics

Reactions which are of particular interest for astrophysics were already mentioned in the previous subsections. These are Gamow-Teller transitions measured by charge-exchange reactions, spallation reactions, and Coulomb dissociation [Ber88]. The nuclei that will be accessible with the NUSTAR facility will allow exploring the reactions inverse to those relevant for the astrophysical rp- and r-processes by utilizing the electromagnetic-excitation process at high beam energy. The cross sections for the direct capture reactions in the stellar environment are very small due to the stellar temperature (~ 20 keV) and the Coulomb barrier, while the cross sections for the inverse process, Coulomb dissociation, are much larger. Of special interest are the (γ,p) and (γ,n) cross section at very low fragment-nucleon relative energy. The proton tracking through the magnetic field of the large-acceptance dipole will result in a momentum resolution of $\Delta p/p \sim 10^{-3}$. For the neutrons, a similar resolution is achievable by making use of a long time-of-flight path of ~ 35 m (ToF resolution < 100 ps), resulting in an invariant-mass resolution of better than 20 keV (at 100 keV relative energy), thus making cross-section measurement feasible at energies relevant for astrophysics, down to about 10 keV. Here, the lead target thickness is limited to about 100 mg/cm² due to multiple scattering and energy loss. Still, with beam intensities of $\sim 10^4$ ions/s differential cross sections of 100 $\mu\text{b}/(10 \text{ keV bin})$ can be measured within a few days.

A.4. Overview on subsystems

The following table gives an overview of the subsystems needed for the different type of experiments as indicated by crosses. In several cases, a detector might not necessarily be required but would, however, improve the quality. Those are marked with a cross in brackets.

Subsystems:	(1) Large-acceptance dipole	(7) Target recoil detector
	(2) High-resolution spectrometer	(8) Active target
	(3) Tracking detectors	(9) Low-energy neutron detector
	(4) Proton tracking	(10) Neutron ToF spectrometer
	(5) Large-area ToF wall	(11) Multi-track detector
	(6) Gamma spectrometer	

Reaction/Physics	Subsystem										
	1	2	3	4	5	6	7	8	9	10	11
Knockout	x	x	x	-	-	x		-	-	x	-
Quasi-free scattering	x	x	x	(x)	-	x	x	-	-	x	-
Total-absorption meas.	x	(x)	x	-	-	-	-	-	-	-	-
(In-)elastic scattering	x	(x)	x	-	-	x ¹⁾	x ¹⁾	x	-	-	-
Electromagnetic exc.	x	(x)	x	x	-	x	-	-	-	x	-
Charge-exchange	x	(x)	x	-	-	-	-	-	x	x	-
Fission	x	x ²⁾	x	-	x	x	-	-	-	x	x
Spallation	x	-	x	-	x	x	-	-	-	x	x
Projectile fragmentation	x	(x)	x	-	-	x	x	-	-	x	-
Multifragmentation	x	-	x	-	x	-	x	-	-	x	x

¹⁾ The target recoil detector and calorimeter will be used for large-momentum transfer reactions only, low-energy recoils will be detected in the active target

²⁾ For high precision (velocity) measurements the spectrometer is needed (only one fission fragment is detected). Kinematically complete measurements of fission will be done using the large-acceptance mode

References

- [Ala03] K. Kezzar *et al.*, (ALADIN-FRS-LAND collaborations), SIS experiment S254.
 [AlK03] J. Al-Khalili and F. Nunes, *J. Phys. G* 29 (2003) R89.
 [Aum98] T. Aumann, P.F. Bortignon, H. Emling, *Annu. Rev. Nucl. Part. Sci.* 48 (1998) 351.
 [Aum99] T. Aumann *et al.*, *Phys. Rev. C* 59 (1999) 1252.
 [Aum00] T. Aumann *et al.*, *Phys. Rev. Lett.* 84 (2000) 35.
 [Ber88] C.A. Bertulani and G. Baur, *Phys. Rep.* 163 (1988) 299.
 [Bot04] A.S. Botvina and I.N. Mishustin, *Phys. Lett. B* 584 (2004) 233.
 [Dat03] U. Datta Pramanik *et al.*, *Phys. Lett. B* 551 (2003) 63.
 [Duc03] J.E. Ducret *et al.*, SPALADIN experiment, performed at GSI, proposal S248.
 [Ege02] P. Egelhof *et al.*, *Eur. Phys. J. A* 15 (2002) 27.
 [Ers01] S.N. Ershov, B.V. Danilin and J.S. Vaagen, *Phys. Rev. C* 64 (2001) 064609.
 [Han03] P.G. Hansen and J.A. Tostevin, *Annu. Rev. Nucl. Part. Sci.* 53 (2003) 219.
 [Kra99] A. Kraznahorkay *et al.*, *Phys. Rev. Lett.* 82 (1999) 3216.
 [Kre95] G. Krein, Th.A.J. Maris, B.B. Rodrigues, E.A. Veit, *Phys. Rev. C* 51 (1995) 2646.
 [LeF05] A. Le Fevre *et al.*, *Phys. Rev. Lett.* 94 (2005) 162701.
 [Lei01] A. Leistenschneider *et al.*, *Phys. Rev. Lett.* 86 (2001) 5442.
 [Mei02] M. Meister *et al.*, *Phys. Rev. Lett.* 88 (2002) 102501.
 [Mei03] M. Meister *et al.*, *Phys. Rev. Lett.* 91 (2003) 162504.
 [Mue95] H. Müller and B.D. Serot, *Phys. Rev. C* 52 (1995) 2072.
 [Ric03] M.V. Ricciardi *et al.*, *Phys. Rev. Lett.* 90 (2003) 212302.
 [Sch00] K.-H. Schmidt *et al.*, *Nucl. Phys. A* 665 (2000) 221.
 [Sch03] F. Schümann *et al.*, *Phys. Rev. Lett.* 90 (2003) 232501.
 [Sme99] M.H. Smedberg *et al.*, *Phys. Lett. B* 452 (1999) 1.
 [Sim99] H. Simon *et al.*, *Phys. Rev. Lett.* 83 (1999) 496.
 [Suz95] T. Suzuki *et al.*, *Phys. Rev. Lett.* 75 (1995) 3241.

B. Systems

B.1. Detector subsystems

B.1.1. Large-acceptance dipole

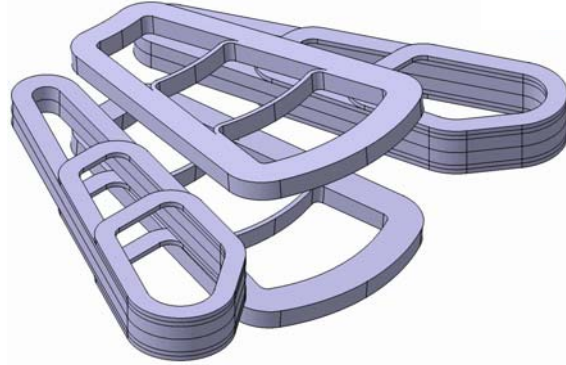


Figure 1: Layout of the four superconducting coils of the R³B dipole. The side coils are optimized to reduce the fringe fields. The field integral amounts to about 5 Tm.

For the variety of experiments to be performed, a zero-degree superconducting dipole magnet was designed by CEA Saclay for the R³B project. The main parameters of the spectrometer are: (i) A large vertical gap providing an angular acceptance of ± 80 mrad for neutrons; (ii) A maximum bending angle of 40° , ensuring an acceptance close to 100% even for experiments with very different magnetic rigidities of the beam and the fragments; (iii) A high field integral of about 5 Tm, which allows a bending angle of 18° for a 15 Tm beam (e.g. 1 GeV/nucleon ^{132}Sn or 500 MeV/nucleon ^8He) or 14° for 20 Tm beams, the maximum rigidity provided by the Super-FRS. A momentum resolution $\Delta p/p$ of around 10^{-3} can be achieved by tracking the particles with high resolution, see section B.4. The design includes four superconducting coils, shown in Figure 1, which are tilted to match the required acceptance angle for the particles of interest. The side coils are optimized to reduce the fringe field, and guarantee a low magnetic field in the target region, where detectors have to be placed.

A technical design report is available (<http://www-land.gsi.de/r3b/docu/TDR-R3B-dipole.pdf>). The magnet will be built by CEA Saclay within the framework of the EU construction contract DIRAC-Phase 1. According to the time schedule outlined in the contract with the European Commission (see Table 2), a construction period of three years is foreseen. In year 4 of the project, installation and commissioning of the device in the R³B experimental area including field mapping is foreseen (see table with milestones and detailed time schedule below). This means that the dipole would be fully operational end of 2009 if the project will start as anticipated end of 2005 (Q4).

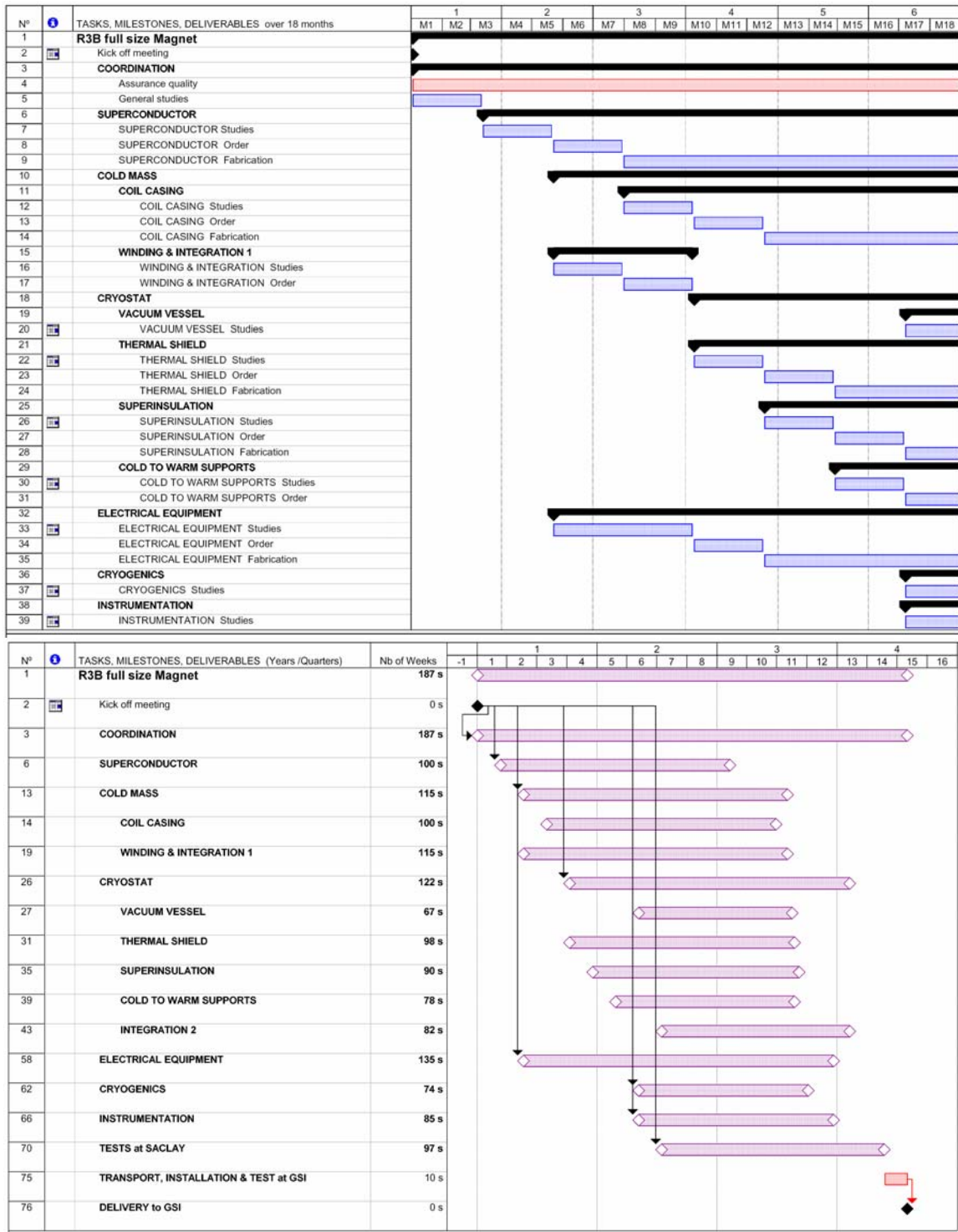
This project is coordinated by CEA Saclay.

Table 1. Milestones and deliverables.

Milestones/Deliverables	Year	Quarter
<i>Kick-off meeting</i>		
<i>End of the Studies</i>	Y1	Q3
<i>Superconducting cable delivery</i>	Y3	Q1
<i>End of the winding</i>	Y3	Q3
<i>Integration in the cryostat</i>	Y4	Q1
<i>Tests at Saclay</i>	Y4	Q2
<i>Installation at R³B/FAIR</i>	Y4	Q3

Time schedule

Table 2. Detailed time plan for the task construction of the R³B superconducting large-acceptance dipole. For the first 18 months (upper part) and for the whole duration of the project (lower panel).



B.1.2. High-resolution magnetic spectrometer

Requirements on precision

The tracking of heavy ion trajectories through the magnetic field of the large-acceptance dipole provides a $B\rho$ measurement with a precision of $\Delta B\rho/B\rho \sim 10^{-3}$ (sigma), see section B.4. In conjunction with energy-loss and time-of-flight measurements fragments are uniquely identified also for heavy nuclei. For a precise measurement of the momentum of recoiling fragments produced in reactions an additional momentum analysis is required. Experiments demanding high momentum resolution are discussed in section A of this document. For the further more detailed discussion, we use knockout reactions and quasi-free scattering experiments as an example. Those reactions rely on a precise momentum measurement and constitute a key part of the R³B experimental programme, namely the investigation of the single-particle and shell structure of exotic nuclei.

In knockout reactions and quasi-free scattering experiments, the momentum of the recoiling nucleus after one-nucleon removal provides information on the wave function of the removed nucleon. The states populated in the reaction are characterized by means of a γ coincidence measurement and the tracking of the target recoil proton and the knocked-out nucleon in case of quasi-free scattering. The intrinsic momentum distribution of a nucleon in the nucleus has a typical width in the order of 100 MeV/c. The shape and the width of the momentum distribution depend thereby on the spatial extension of the wave function, i.e. the separation energy of the nucleon and the quantum numbers of the single-particle configuration from which the nucleon is removed. The angular momentum l of the nucleon is deduced from the measured momentum distribution of the recoiling $A-1$ fragment in the rest frame of the projectile. As an example, we give the widths of the momentum distributions for a knockout reaction of a neutron bound in a medium-mass nucleus with a separation energy of 5 MeV: For the angular momenta $l=0,1,2,3,4$ a momentum width of 75, 100, 140, 200, 270 MeV/c is estimated, respectively, in the rest frame of the projectile, which is broadened in the laboratory frame by a factor of about γ ($\gamma=1.75$ at 700 GeV/nucleon).

In case of high beam energies and medium-heavy to heavy nuclei a precision of this measurement in the order of 10^{-4} is needed. Assuming typical beam energies in the range of 700 to 1000 GeV/nucleon to be used for these types of reactions, the beam momentum is in the range of 1.3-1.7 AGeV/c. For a medium-mass nucleus this corresponds to a total momentum of 170-220 GeV/c. For the measurement of heavy nuclei in the mass range $A=200$, the highest beam energies have to be used in order to have fully stripped ions. In such a case the beam momentum will be around 340 GeV/c. A momentum resolution of 10^{-4} corresponding to about 20-30 MeV/c (sigma) would thus allow distinguishing different angular momenta from a measurement of the momentum distributions. The corresponding resolution of the momentum distribution in the rest frame of the projectile would amount to about 30 MeV/c (FWHM), which has to be compared to the difference in widths given above.

Possible solutions

Four possible solutions for high-resolution momentum measurements are considered:

1) Experiment at the mid focal plane of the SUPER-FRS

High-resolution measurements are performed at the present facility directly at the FRS. Thereby, the first half of the separator is used to select radioactive ions, and the second half is used as a spectrometer. The two stages operate thereby in a dispersion-matched mode. This scheme is, however, rather limited because of several reasons. 1) A clean separation of the radioactive beams with only one stage of the separator is often not possible. This will be in particular difficult with the larger acceptance of the Super-FRS. 2) The background rates at the reaction target placed at the mid focus of the separator are rather high. 3) Due to the dispersion-matching mode, the focus at the reaction target is dispersive implying a beam spot size of about 40 cm (in the dispersive plane), which makes an efficient coincident measurement of γ -rays very difficult. The γ -spectrometer would have to be very large and thus very expensive. 4) Coincident measurement of other particles like neutrons or recoiling target protons would be difficult. Again, a tracking detector for proton recoils would have to have an enormous size in order to achieve a high-acceptance measurement. This option would thus not only imply a doubling of many detection schemes but also the detection would be much more expensive with worse performance compared to those at the R³B target.

2) Magnetic spectrometer behind the large-acceptance dipole operated together with the Super-FRS in dispersion matched mode

This option overcomes many of the limitations discussed above for option 1). The main limitation we see here is the extended beam spot size discussed already above. Compromises concerning the performance would have to be made and the consequently large detector sizes would increase the costs dramatically. Therefore, we do not consider this option in the further discussion.

3) A high-resolution ToF spectrometer

The envisaged momentum resolution of $\Delta p/p=10^{-4}$ could be in principle also achieved by a velocity measurement. The corresponding accuracy in the velocity determination amounts to 3.2×10^{-5} for a beam energy of 700 GeV/nucleon, and 2.3×10^{-5} for 1 GeV/nucleon beams. Since the resolution of Cerenkov detectors is limited to about 10^{-3} , a time-of-flight (ToF) measurement seems to be the only option. By placing a quadrupole triplet behind the dipole magnet, a rather long flight path could be realized for a ToF measurement keeping the size of the vacuum beam pipe moderate (<50 cm diameter). Assuming a flight path similar to the maximum flight path envisaged for the neutron measurement of about 35 m (length of the R³B hall ~50 m), a ToF resolution of about 5 psec (sigma) would be required to achieve a momentum resolution of 10^{-4} at 700 GeV/nucleon and 3 psec at 1 GeV/nucleon. Such marvellous time resolutions have not been reached so far. We note, however, that time resolutions in the order of 10 psec have been reached for heavy ions with small fast plastic scintillators and fast phototubes already at the RIKEN accelerator [Nis03]. Although it seems to us difficult to reach the required resolution also due to electronics limitations, the collaboration intends to devote some R&D work on this subject in order to approach the limits. At present, we do not see a technical solution providing the time resolution needed.

4) Magnetic spectrometer behind the large-acceptance dipole operated as tracking spectrometer

The solution we propose is a spectrometer placed behind the large-acceptance dipole. The spectrometer will be placed at an angle of 18°, which is the maximum bending angle of the dipole (5 Tm field integral) for a beam with magnetic rigidity of 15 Tm (corresponding to, e.g., 1 GeV/nucleon ¹³²Sn), and will be operated as a zero-degree spectrometer. The focus at the R³B target is an achromatic focus with a beam spot size of around $2 \times 2 \text{ cm}^2$, as in the usual operation mode. The momentum resolution will be obtained by tracking the particles through the spectrometer. The position at the focal plane will thus not be directly related to the momentum transfer in the reaction but rather reflect the momentum spread of the incoming beam.

The following discussion refers to option 4).

Parameters of the spectrometer

Acceptance

The Super-FRS has an acceptance of $\pm 2.5\%$ in momentum and $\pm 40(\pm 20)$ mrad in the (non)dispersive direction, respectively. The spectrometer has to provide at least the same acceptance. This has to be compared to the momentum transfer in the reactions of interest. As mentioned above, typical recoil momenta in the rest frame of the projectile are in the order of few hundred MeV/c, which is small compared to the momentum spread of the incoming beam (the same holds for longitudinal and transverse components). We conclude that the acceptance of the spectrometer should be the same as the one of the Super-FRS. A solution utilizing the same layout as for one half of the main separator would thus be a possible option.

Rigidity

The maximum rigidity of the Super-FRS amounts to 20 Tm in order to allow separation of fully stripped ions also for heavy nuclei. Considering energy-loss in two degraders at the pre-separator and at the mid-focal plane of the main separator, it seems reasonable to limit the maximum rigidity of the spectrometer to 15 Tm. The costs of the magnets as compared to the Super-FRS will approximately scale down with the same factor.

Tracking

Since the spectrometer is not operated in a dispersion matched mode, the momenta of incoming and outgoing ions have to be determined with the same precision. In both cases, this is realized by tracking the ions through the separator and the spectrometer, respectively. The measurement of trajectories starts

at the mid-focal plane of the main separator behind the degrader. The position and angle is measured at this dispersive focus by two diamond detector arrays (size about $5 \times 40 \text{ cm}^2$). The position in the dispersive plane already determines the momentum with a precision corresponding to the resolving power of the Super-FRS of 1500. Two position measurements in front of the R³B target are utilized for determination of incident position and angle on the target. The four position measurements will be utilized to calculate the momentum of the projectile incident on the target on an event-by-event basis. A simulation, based on ion-optical calculations including the large-acceptance dipole, and including position resolution and straggling due to the tracking detectors will be carried out in the near future.

Other limiting factors for the resolution: target contributions

There are several contributions related to the target thickness which limit the obtainable momentum resolution. These are: 1) the width of the energy-loss distribution (energy-loss straggling), 2) transverse components introduced due to small-angle scattering (angular straggling), and 3) the fact that the momentum loss in the target is different for beam and reaction product. In the following we consider a thick liquid hydrogen target with 10% total reaction probability. For the example of ^{132}Sn this corresponds to 140 mg/cm^2 , or a length of 2.0 cm. We shall use a beam energy of 700 MeV/nucleon. The code ATIMA is used for the following estimates.

1) *Energy-loss straggling* In case of the chosen example of 0.7 GeV/nucleon ^{132}Sn ; the beam will loose about 14 MeV/nucleon in the target. A width in momentum of $\Delta p/p = 0.9 \times 10^{-1}$ (sigma) is introduced due to this energy loss. It means that even for a very thick target (10% reaction probability) a momentum resolution of 10^{-4} is reachable.

2) *Angular straggling* The multiple scattering in the hydrogen target introduces an angular spread of 0.23 mrad, which does not disturb the momentum measurement. This can be compared to the transverse momentum of the recoiling fragment in case of one-nucleon knockout with typical width of 100 to 200 MeV/c corresponding to deflection angles of 0.6 to 1.1 mrad. The measurement of position and angle incident on the target can be done with a resolution of 0.2 mm and 0.2 mrad, respectively. The scattering angle could be determined with a resolution of 0.3 mrad. Here, we assumed three diamond detectors with 0.5 mm pitch size and thickness of 0.1 mm (straggling in the detector 0.14 mrad). A measurement of the transverse-momentum distribution would thus be in principle possible, although with worse resolution than the longitudinal component measured with the spectrometer.

3) *Location straggling* Since in knockout or (p,pn) and (p,2p) type of reactions the charge and/or the mass changes in the reaction, the total energy loss in the target depends on the location of the reaction in the target. This results in an uncertainty of the recalculated recoil momentum of the fragment in the rest frame of the projectile. The worst case is the proton knockout. Here the energy loss of the fragment is significant smaller than for the projectile. For the example chosen, one-proton knockout from ^{132}Sn , the difference in $\beta\gamma$ for ^{132}Sn and ^{131}In after passing 2.0 cm liquid hydrogen amounts to 4.2×10^{-4} , 4 times larger than the envisaged resolution. The point of interaction, however, can be reconstructed easily from the proton measurement (see section about target recoil detector) with a precision of 1 mm. The energy loss can thus be precisely calculated corresponding to an effective target thickness of less than 10 mg/cm^2 . The contribution to the resolution can thus be neglected.

In summary, the largest effect due to the target thickness results from the energy-loss straggling which reaches, however, a value comparable to the spectrometer resolution only for a rather thick target corresponding to 10% reaction probability. The envisaged momentum resolution of $\Delta p/p = 10^{-4}$ for knockout reactions is thus achievable even with thick liquid-hydrogen targets.

Design, construction

A detailed design study of the spectrometer is planned for the next years. Considering the requirements on acceptance, maximum magnetic rigidity, and resolution, a design close to that of the Super-FRS immediately comes to mind. Detailed ion-optical calculations, however, have to be done. A solution close to that of the Super-FRS using the same magnet technology also brings the advantage of saving costs for R&D as well as for the production of the magnets. We consider a reduced rigidity in order to reduce the costs further.

Assuming a solution close to that of the Super-FRS, design, delivery of the technical design report, and construction of the device will follow closely that of the Super-FRS. Assuming that the magnets will be

produced by the same manufacturer, construction and delivery should be foreseen directly following those of the Super-FRS. The high-energy beam line will deliver first beams in 2010. During 2010/2011 Super-FRS magnets and beam lines will be installed for the storage rings and the low-energy branch. After that, the magnets for the spectrometer could be installed. The spectrometer should thus be setup and commissioned in the experimental hall in 2012. The R³B experiment would thus run the first two years without the spectrometer (phase I).

Space requirements

The length of the spectrometer will be similar to one half of the main separator, amounting to about 40 m. Some reduction of this length can be expected if the rigidity is limited to 15 Tm. The total length of the R³B experimental hall needs to be about 50 m to 60 m in order to house the spectrometer. A similar requirement on the length, however, comes from the high-resolution neutron time-of-flight measurement. The time-of-flight option for the momentum measurement of heavy fragments would require a similar length of the hall.

Working group

The members of the working group are given in section G. This project is coordinated by CCLRC Daresbury for the UK collaboration.

References

[Nis03] S. Nishimura et al., Nucl. Instr. and Meth. in Phys. Res. A 510 (2003) 377.

B.1.3. Heavy ion tracking detectors and velocity measurements

In most cases experiments using exotic beams have to include a twofold setup for identifying particles and their kinematic properties before and after the secondary reaction target. For the large variety of different experiments proposed for the R³B setup, various tracking-detector systems with different demands are required.

The incoming beam will be tracked (starting from the dispersive focus at the Super-FRS (S-FRS)) in order to determine beam momentum, angle and position of incidence on the target, and, similarly, for the spectrometer after the target. The velocity of the incoming beam as well as of the fragments has to be determined with a resolution of $\delta\beta/\beta < 10^{-3}$ in order to achieve unique isotope identification after the target also for heavy beams. Using 40 m distance between the dispersive focus at the Super-FRS and the reaction target the requirements for time-of-flight (TOF) detectors are quite moderate ($\sigma_t < 100$ ps) in this case. Also moderate position resolution of $\Delta x = 3$ mm would be sufficient. But even using quite exotic beams (e.g. ¹³²Sn) the detectors should be able to cope with rates of 10^7 to 10^8 s⁻¹ heavy ions at the dispersive focus (FX) of the S-FRS.

For the large-acceptance mode, large-area detectors are placed behind the R³B dipole magnet. For detection of light charged particles drift chambers with a size of about 1.2×0.8 m² including dedicated front-end electronics are presently being considered, see section on proton tracking. For heavy ions, a position detector with the size of 30×20 cm² is needed. For fission and spallation studies, even larger detectors are needed. Those are described in the sections 'Multi-track detector' and 'Large-area ToF wall' and are not discussed in this section.

In view of the high momentum resolution mode ($\sigma_{p/p} < 10^{-4}$) needed for several experiments, the situation is quite different. The position resolution of all tracking devices has to be better than $\Delta x < 0.5$ mm. Especially the vertex and angle reconstruction at the secondary target will need much better resolution of $\Delta x \sim 0.1$ mm. The angular scattering and momentum spread introduced by the tracking detectors in the target region have to be small compared to this numbers while the detectors inside the S-FRS and after the spectrometer could use a more massive layout. Also the expected γ -background limits the material budget of the detectors in the target area.

For the R³B project being a multi-purpose setup for very different branches of experiments the development of position sensitive time-of-flight detectors with good resolution for tracking of exotic heavy ions using minimized mass density in order to suppress parasitic reactions and multiple scattering efficiently is urgently needed. Four different types of detectors will be developed for tracking of heavy ions according to the demands of the different experiments. Diamond detectors will be used for tracking through the Super-FRS up to the R³B target. Si-strip detectors will be used for coincident detection of fragments and protons after the target as well as behind the large-acceptance magnet, where an array of Si-strip will be installed. For the second position measurement few meters behind the magnet a large-area scintillating fiber detector is foreseen. For experiments at lower energies and for lighter ions (e.g. measurements of γ, n cross sections at very low relative energy of astrophysics relevance) low-mass channel-plate detectors (with less resolution) are foreseen.

I. CVD-diamond detectors for heavy Ions

Concerning position measurements with high-intensity beams, CVD (chemical vapor deposition) diamond detectors seem the most promising development, providing also very good timing. Especially poly-crystalline material with very short signal response (1-2 ps) seems to be ideal for very high rates of heavy ions. This could comply with all tasks discussed above with one single detector type but with the risk of a very recent not fully developed technology.

Simulations

- i. Solid-state detectors have the big advantage that for vacuum applications no additional windows are necessary. Also external fields and particle properties are of minor importance for the detector performance. The diamond detectors discussed should operate in a "digital mode" without taking into account the inter-strip coupling. Thus detector simulation could be simplified to calculations of energy loss, energy straggling and angular straggling.

- ii. The expected beam properties will have a crucial influence on the design of the new detectors. Detailed MOCADI simulations will determine upper limits for the fluxes of heavy ions at the dispersive plane of S-FRS and the target area of R³B. Especially the vertical distribution will be important for the design of the mounting and readout structures of the detector. Reasonable time and position resolutions have to be verified using a full-scale tracking through the R³B setup.

Radiation hardness

The radiation hardness of CVD - diamond is the most important material property initiating the research and development of diamond detectors. For the tracking of minimum ionizing particles (mip) in the LHC experiments ATLAS and CMS [1] as well as for a variety of heavy ion applications with high luminosity beams [2] diamond detectors have been already developed. In the case of mips no increase in leakage current and unchanged collected charge is obtained for all kind of particles up to a fluence of about 10^{15} particles/cm² [1]. However, the heavy-ion dose which starts damaging CVD diamond is still unknown. A lower limit could be set by the HADES experiment using a diamond in-beam detector. Currently, about 10^{13} /cm² ¹²C ions (1-2 AGeV) have already been applied without any degradation of these detectors.

Design

The design for the in-beam diamond detectors will be very close to an ideal tracking device, providing all 4 spatial coordinates (x,y,z,t) with sufficient resolution.

Detailed studies on small samples have already been performed by the RD42 collaboration at Cern [3] for minimum ionizing particles (mips) produced at LHC.

The focus for the development of heavy ion detectors and GSI energies has to be significantly different. Due to the wide range of energy loss for heavy ions to be detected, different sets of detectors using different layers of substrate material ranging from 200 μ m for the very light carbon like species down to 20 μ m for the heaviest ones are useful.

The most critical part of the design is the size of the new detectors. For the most commonly used substrate material [1] according to CERN specification from de Beers, the maximum size available is 30×30 mm² and also the price is quite high (13 €/mm²). Other material from different suppliers has to be tested according to charge collection and signal shape. This diamond films are commonly produced for window applications and are available up to sizes of 60 mm at a more reasonable price (~2 €/mm²).

For the high momentum resolution two different segmentations in horizontal direction with a pitch of 400 μ m and 100 μ m for the larger area FRS detectors and R³B target detectors, respectively, are planned. The backsides of the detectors will have an adaptive pitch ranging between 1 mm and 5 mm each to cope with the beam profile. The final layout also depends on the individual noise dominated by the individual strip capacity. Detailed tests using the final readout electronics will be necessary.

The readout of the highly segmented front sides of the detectors will be based on the APV-25 chip developed at CERN for the CMS experiment ([APV Chip](#)). The fast shaping time of 25 ns and the included analogue daisy chains for each of the 128 channels per chip nicely fits to the planned NUSTAR readout scheme. As an important milestone the combination of ultra-fast diamond signals and frontend electronics designed for silicon readout has to be tested and signal ranges have to be adapted.

The readout of the backside strips has to provide digital y-position information as well as the time for each particle passage. A precision of $\sigma t < 40$ ps has to be achieved for mass separation around A=100 using 10 m TOF path after the large area R³B magnet. A recent development of front-end electronics (preamplifier and discriminator) for the HADES diamond detectors based on a GSI development for RPC detectors will be very similar to the R³B application.

Construction

Around the R³B target focus single detectors with a size of 50×50 mm² are sufficient to cover the beam and the reaction cone for heavy projectile fragments. For the application at the dispersive focus of the S-FRS, detectors have to consist of several segments to cover the full active area of 40×5 cm².

The detectors will be mounted on PCB boards already including the low-power frontend electronics using chip to chip bond connections. In this case only very few lines (~32 pcs.) are needed to transport

R3B

serialized hit information from the detectors to the DAQ. Different detector sets have to be mounted at parallel motor drives in the beam line vacuum for a precise online replacement.

Steps of developments and tests

The different steps of development and production are summarized in the following table.

Period	Subtask	Tests	Milestones
2005	Production of different small-size ($1 \times 1 \text{ cm}^2$) prototype detectors using different CVD - diamond substrate material, segmentation and technology. Implementation of new diamond fast timing preamplifiers. Production of $40 \times 40 \text{ mm}^2$ prototype detector	First tests of detector response, signal coupling using light-ion beams from the Munich Tandem accelerator. Preliminary tests concerning radiation hardness. Test of special efficiency using the Munich micro-beam facility.	Final selection of substrate material and production technique.
2006	Production of two full scale ($50 \times 50 \text{ mm}^2$) detectors. Adaptation of APV based readout electronics to existing GTB readout scheme.	First tests of small prototypes with low rate heavy ions from the SIS (1 AGeV). Measurement of position and time resolution.	Final design of the target detectors including specification of position and time resolution.
2007	Production of 5 full scale ($50 \times 50 \text{ mm}^2$) detectors.	Tests of first large-area detector stacks using low-rate heavy ions from the SIS (1 AGeV). Test of detectors and R ³ B readout scheme at high rates.	Proof of radiation hardness of detector and readout. Full scale prototypes ready for use.
2008	Production of 5 full scale ($50 \times 50 \text{ mm}^2$) detectors. First full scale ($400 \times 50 \text{ mm}^2$) detector array. Mechanical implementation to the beam line.	Test of full scale detectors at expected full rate using different ion species from SIS.	3 full scale R ³ B tracking stations, 1 full scale SFRS tracker.

TU München will coordinate this subtask.

Requests for test beams

Different types of parasitic beams are needed during the development phase.

Period	Beam request	Energy	Intensity	species
2006	1 week, 1/10	1 AGeV	10^5 s^{-1}	Kr like
2007	1 week, 1/10	1 AGeV	10^5 s^{-1}	Kr like
	2 days	1 AGeV	10^9 s^{-1}	Kr like
2008	2 weeks, 1/10	1 AGeV	$10^8 \text{ cm}^{-2} \text{ s}^{-1}$	C , Kr, U like

Cost and manpower estimates

The project will need continuous development of technology, setups and electronics until the end of 2007. The combination of detector production sample testing layout optimisation, readout development and mechanical construction needs a core group of at least 3 people working full time on this project.

The group will consist of 1 diploma student, 1 PhD student (already funded by FP6 EURONS Project), 50 % of a technician working for the detector production, 1 postdoc directing the group and 20% of senior scientist supervising the group for 3 years.

After successful implementation of the new tracking devices a second set of detectors with the same dimensions but different material thickness and pitch will be built for the high-resolution spectrometer (phase 2 of the project starting in 2009).

II. Silicon and scintillation detectors

As a solution B for tracking through the Super-FRS up to the R³B target, a combination of silicon micro-strip detectors for tracking and segmented scintillation detectors will be investigated in parallel. Nowadays scintillation detectors provide excellent timing information $\sigma_t = 10$ ps for heavy ions [4]. Ageing properties in very high rate heavy ion beams and the vacuum implementation of such a device that needs quite high segmentation due to a maximum flux of 10^7 s⁻¹ cm⁻² at the S-FRS dispersive focus have to be investigated.

The major drawback for such a solution is a material budget that is about ten times larger than using an optimized diamond detector setup (see section I.).

Radiation Hardness

High-resolution silicon trackers for minimum-ionizing particles are a standard component of current high-energy experiments, and radiation-hard material and electronics are available today. In reactions with relativistic heavy ions, however, non-standard problems occur that require dedicated R&D. The issues that need to be investigated are related to the large dynamic range required if protons or alphas have to be detected in coincidence with heavy-ions in the same detector. In addition, the experience on how such detectors behave in high-rate heavy-ion-beam environments is very limited.

Design

There are already existing designs and experiences of similar devices from several different experiments at the existing FRS. From the principle point of view the new design will consist of large-area (50×50 mm²) Silicon-strip detectors with a pitch also close to 100 μ m. There are different approaches for horizontally and vertically segmented scintillators which have to be tested in a high-rate environment.

For the tracking behind the target Si-strip detectors with a size of 5×5 cm² are foreseen. For some experiments, a coincident detection of protons and heavy ion in one detector is necessary. First prototype detectors and electronics based on the AMS detector design have been ordered. Integration into the R³B system and first test experiments are planned for the near future.

For position measurement directly behind the large-acceptance magnet an array of Si-strip detectors covering an area of about 30×20 cm² is foreseen. Here, a measurement of the coordinate in the dispersive plane is sufficient. The array will consist of 6 standard single-sided strip detectors with thickness of 100 μ m, a size of 10×10 cm², and a pitch of 100 μ m. The electronic readout has to be adaptable to a wide range of signal heights for detection of heavy ions with different nuclear charge.

Finally, the position in the dispersive plane is measured again a few meters behind the Si-strip array using a fibre detector (50×50 cm²) similar to the design of the presently used detectors at LAND, but with a double-layer design. The single fibres are read out by position-sensitive phototubes. This detector can be placed in air just behind the vacuum tube (with a diameter of 50 cm) very similar to the presently used setup in Cave C.

A ToF wall (50×50 cm²) will be placed directly behind the fibre detector consisting of two layers with 16 scintillator paddles each. The paddles are read out by fast phototubes. This ToF wall is already under construction and will be ready for first experiments in Cave C during 2005. A time-of-flight resolution of about 25 ps (σ) is envisaged. Within the next two years, an electronic readout scheme based on the TAQUILA digitization card with an adapted front-end module will be implemented. The intrinsic time resolution of this electronics is expected to amount to 10 ps (σ) [5].

Steps of developments and tests

Period	Subtask	Milestones
2005/2006	Purchase of Si-strip prototype detectors and electronics Adaptation of VME front-end module for connection to standard GTB bus, implementation into the R3B DAQ system. Construction and tests of ToF wall	Readout-electronics concept and first prototype for Si tracker ToF detector
2007/2008	Beam tests concerning response of tracker prototype to a) break-up of beam into p and heavy ion, b) high intensities. Implementation of TAQUILA electronic readout for ToF wall Design and purchase of Si-strip detectors Design and purchase of Scintillator fibre detector and electronics	Report with experimental results
2008	Mechanical implementation to the beam line. Test of full scale detectors at expected full rate using different ion species from SIS.	2 full scale R ³ B tracking stations, 1 full scale SFRS tracker. 1 full scale tracker behind large-acceptance magnet 1 Fibre Scintillator
2009	Implementation of detectors at Super-FRS and R ³ B experiment	

GSI will coordinate this subtask.

III. Low-mass MCP detectors:

In addition the investigation of very low-mass detectors to be placed especially close to the target focus could be an important issue. In R³B-experiments the beam detectors after the target have to be of a thickness not adding more small angle scattering (in space) than 1 mrad FWHM, resp. 0.4 mrad rms. For 400 A MeV and A/Z~2 this can be reached for thicknesses of < 10⁻³ radiation lengths; this requirement is fulfilled with Si-detectors of < 90 μm, with diamond of < 120 μm or scintillators of < 400 μm thickness. The channel plate detectors described below detect secondary electrons, produced in an Al-coated polyethylene foil which has a total thickness of 10⁻⁵ radiation lengths with small angle scattering of 0.03 mrad. The fact that the areal density of detector matter in the beam is reduced by more than an order of magnitude allows to extend a high-resolution tracking measurements to even lower energies than 400 A MeV. An additional limit on the maximum thickness of the detectors near the target comes from the requirement that the count rate produced in them is considerably lower than the one produced in the target. It is mainly this argument which makes the introduction of detectors with ~10⁻⁵ radiation length very attractive. The secondary electrons emitting foil can be made very thin fulfilling the requirement of low background generation as well as small-angle scattering. It can thus be inserted near the target and again directly before the dipole magnet. The secondary electrons are best detected in position sensitive channel plates; these require a vacuum of < 10⁻⁷ hPa, which has to be assured for at least that part of the beam line where these detectors are installed.

As will be shown below, the position resolution of such a device is limited by the spread of the emitted electron's velocity vectors to the 1 mm regime. The influence of their transverse component has been shown to be reduced by a factor of ~5 with a magnetic field of several mT causing a helical motion and resulting in a focusing of the electrons onto the detector, see [7]. Nevertheless this type of detector will

be very useful in case of experiments using light ions or low energies, where a reduced position resolution for the tracking around the target is sufficient and the material effects of the detector play an important role.

At FZR a detector setup with an electrostatic accelerator grid and electrostatic mirror has been developed, as shown in the Figure below.

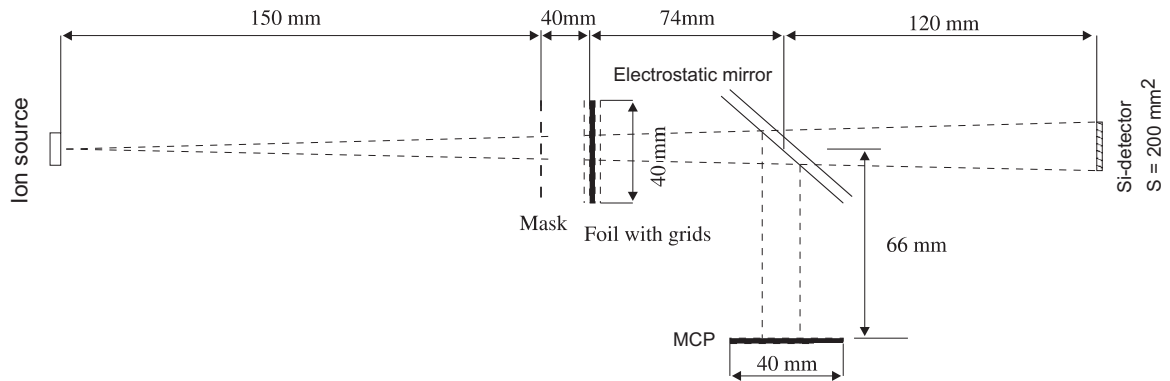


Figure 1. MCP detector set up for measuring the position resolution of a MCP stack.

Secondary electrons are emitted from a $5 \mu\text{m}$ thin, metalized polyethylene foil by a projectile passing through. They are accelerated by an electrostatic field of 10 kV/cm . The electrons are then reflected 90 degrees by an electrostatic mirror, before they hit a stack of MCPs (multi channel plates) with a position-sensitive anode. An α -source collimated by a set of circular apertures was used to test the position resolution of the setup. The α -particles were detected in a Si-detector in coincidence with signals from the MCP stack

The position resolution determined from a Gaussian fit convoluted with a box is approx. $2 \pm 0.3 \text{ mm}$ (FWHM). The position resolution is dependent on the transversal momentum spread of the secondary electrons emitted from the foil. From this resolution measurement an initial transverse momentum of approx. $1 \text{ eV}/c$ can be deduced. Channel-plate detectors have been used with a time resolution of 350 ps FWHM (corresponding to 150 ps rms) at Rossendorf. At GANIL a time resolution of 250 ps FWHM (110 ps rms) has been reached. At the radiation source ELBE with its pulses of $\sim 10 \text{ ps}$ width channel plate detectors of improved quality will be tested in the summer of 2005.

The typical design of these detectors will be very close to what is described above. So currently there is a limitation in size to several centimeters in diameter.

Radiation hardness

As only passive parts of the detector are in beam, radiation hardness should not be an issue. Nevertheless the exposure to secondaries produced close to a high intensity heavy-ion beam has to be tested.

Steps of developments and tests

Simple calculations using homogenous fields show that the system is capable to transport the secondary electrons from the foil to the MCP detector isochronously. In first order this condition can be expressed as:

$$d/(L_1+L_2) = 0.236 (\Delta V/\Delta V_f).$$

Here d is the mirror height, L_1 and L_2 are the distances between the acceleration grid and the mirror and between the mirror and the MCP (see Fig. 1). ΔV and ΔV_f are the potential differences between the foil and the acceleration grid and inside the electrostatic mirror respectively. If one fulfills this condition one could expect a significant improvement of the time resolution. Therefore, tests with an optimized geometry are planned. The setup shown in Fig. 1 will be completed with a second MCP and mirror assembly to allow simultaneous measurement of positions and time.

Additionally, a setup with secondary-electron emission from the foil in backward direction, opposite to the direction of the ion beam could also be considered.

The position resolution of the current setup seems to reach the limit given by the initial energy spread of the secondary electrons. To improve the resolution further a solenoidal magnetic field to focus the electrons on helical trajectories has to be employed. The resolution measurement so far were made with α -particles from a source, which give a lower secondary electron yield than expected from heavy ions and consequently increased fluctuations in the position resolution. At FZR we have prepared measurements with a fission-fragment source to be closer to the situation expected at a heavy ion beam. Fission fragments have typically a factor of 40 higher secondary-electron yield than α -particles, see Ref. [6].

In summary, the unique property of the MCP is the introduction of only the smallest areal density in the beam. Thus the small angle scattering in space is limited to below 1 mrad, which allows for excellent tracking capabilities. The time resolution of 550 ps (FWHM) reached so far with two MCP detectors is very promising, but still too large to separate nuclei around mass $A=100$ at 400 A MeV. The position resolution of 2 ± 0.3 mm (FWHM) is expected to be reduced to 1 mm (FWHM) by introducing a parallel magnetic field.

Technical requirements

MCP detectors require a clean UHV. The pressure should be kept in the 10^{-7} mbar range. The grids currently used for electrostatic mirrors cause an inhomogeneous areal density, which might disturb the ion optics of consecutive high-resolution spectrometer. For fast heavy-ions they can be replaced by homogeneous foils. These detectors are useful for the small-size foci around the target area. The development is being carried out by the FZ Rossendorf within the EURONS project of the 6th EU FP6 framework programme.

References

- [1] The RD42 Collaboration, Status Report 1999, CERN/LHCC 2000-011,
- [2] E. Berdermann et al., Nuclear Physics B (Proc. Suppl.) 78 (1999) 533-539
- [3] D. Meier for the RD42 Collaboration, "A CVD Diamond Beam Telescope for Charged Particle Tracking", CERN-EP-2001-089
- [4] S. Nishimura et al., NIM A 510 (2003) 377-388
- [5] K. Koch et al., *A new TAC based multi channel front-end electronics for TOF experiments with very high time resolution*, to be published.
- [6] Saro et al., NIM A 381 (1996) 520.
- [7] Odland et al., NIM A 378 (1996) 149.

B.1.4. Proton tracking

For the tracking of light charged particles, i.e. protons, behind the R³B dipole magnet two identical drift chambers (DHC) are foreseen. The chambers are designed following the concept of the SPES4- π Forward Spectrometer drift chambers [1]. The two chambers will be built during 2005 and will be operational and commissioned at GSI end of 2005, including the dedicated front-end and read-out electronics.

Design

Each DCH covers an active area of 100×80 cm², thus providing a large enough acceptance behind the magnet to detect decay protons (matched to the geometrical acceptance given by the gap of the dipole magnet of ± 80 mrad). The geometry and the operational parameters are optimized to detect minimum ionizing particles with an efficiency of larger than 95% and a spatial resolution of better than 0.2 mm (σ). The tracking through the dipole field provides a relative momentum resolution $\Delta p/p \sim 3 \times 10^{-3}$ for the protons according to Monte-Carlo simulations (including detector resolution and the straggling in the detectors at a beam energy of 500 MeV/nucleon). The hexagonal drift cells have a diameter of 16 mm. They form one plane consisting of 6 field-wire (75 μ m copper-beryllium) and 2 sense-wire (25 μ m gold-plated tungsten) layers. Each DCH comprises 2 planes (x and y) placed in one housing with in total 250 read-out channels. The chambers will be operated with the gas mixture [Ar:C₂H₆] = [50:50] at 1 atm.. In order to resolve many-particle ambiguities the two chambers will be inclined with respect to each other by ± 10 deg. relative to x, y.

Front-end electronics and read-out

Each DCH is equipped with 256 channels of dedicated front-end (FEE) and read-out electronics, based on the CROS3 read-out system being developed at PNPI [2]. The chamber –mounted FEE cards will be modified to incorporate the ASD-8 amplifier-shaper discriminator ASIC [3], with variable threshold, which is also used to read-out the HADES drift chambers at GSI [4]. Further digitization and event-building is performed according to the standards required by the GSI GTB bus interface to the SAM VME module to guarantee maximum compatibility with the R³B data acquisition and trigger system.

Time schedule

According to the Agreement on Collaboration between GSI and PNPI the chambers are expected to be at GSI beginning of 2006, after being successfully tested at PNPI. First physics experiments are planned for 2006 in Cave C. The same chambers will be used for the proton tracking at R³B behind the superconducting large-acceptance dipole magnet.

References

- [1] G.D.Alkhozov et al., Preprint PNPI EP-9-2000 #2352, Gatchina, 2000.
- [2] Internal note “CROS3 Readout System”, Electronics Department of PNPI, 2001.
- [3] F.M. Newcomer et al., IEEE Transactions on Nuclear Science, Vol. **40**, No. 4, 1993.
- [4] C. Müntz et al., Nucl. Instr. Methods A **535** (2004) 242–246.

B.1.5. Large-area ToF wall for fission and spallation measurements

Design requirements

In this section, the design and construction of a high-resolution time-of-flight (ToF) wall for charged particles and ions as a part of the R³B detection is proposed. The main requirements of such a detector are to cover the full acceptance of the charged particles and ions produced in relativistic heavy-ion collisions while providing a time-of-flight resolution such that isotopes around the mass 200 could be isotopically resolved.

Taking projectile fission at energies around 600 A MeV as the reaction mechanism covering the larger angular range, the detector should accept all particles and ions emitted within 50 mrad. Then, this detector should have an area of 1 m² at 10 m from the target and 1.5 m² at 15 m. In addition, the mass resolution we need to identify in mass all fission residues is 3×10^{-3} , then the required time resolution is $\sigma_{\text{ToF}} = 19$ ps for a flight path of 10 m and $\sigma_{\text{ToF}} = 28$ ps for 15 m flight path. Another physic cases like spallation or multi-fragmentation require the identification of heavy residues at energies around 700 A MeV. Here, the mass resolution we need is of the order of 2.5×10^{-3} and the corresponding time resolution is $\sigma_{\text{ToF}} = 9$ ps for a flight path of 10 m and $\sigma_{\text{ToF}} = 16$ ps for 15 m flight path.

Two technologies can be considered for large-area high-resolution time-of-flight detectors, organic scintillators coupled to fast photomultipliers or resistive plate chambers (RPCs). Intrinsically RPCs are much faster than plastic scintillators, however, very little is known about the response of these detectors using heavy ions. In addition, recent developments in electronics have reached a time resolution of the order or better than 30 ps (sigma). According to this, our aim is to design and build a large area ToF wall for charged particles and ions using RPCs reaching a time resolution better than 40 ps (sigma). As a fallback solution we will also consider a design based on plastic scintillators.

Design concepts

1. Resistive plate chambers

Resistive plate chambers are gas detectors based on the principle of parallel plate chambers. However, the use of rigid resistive electrodes allows to operate RPCs in avalanche mode at atmospheric pressure using very narrow gaps, of the order of few hundred μm [Par71,Cer96]. Specific gas mixtures have provided a time resolution around 30 ps (sigma) [Par71]. An alternative is a multigap RPCs working in avalanche mode with non-flammable gas mixtures [Cer96]. This solution has been used to construct large area time-of-flight detectors [Bla02] reaching a time resolution of the order of $\sigma_{\text{ToF}} < 60$ ps. Some examples are the ToF detectors for the ALICE [Aki04], STAR [Yi05] or FOPI [Sch04] experiments. However, most of the designed timing RPCs are being used with minimum ionizing particles (MIPs) and very little information is known about the response of these detectors with heavy-ions [Alv04].

Based on this principle, the design of a large area ToF-wall made of three detection planes (super-module) rotated 120° one respect to the other (Fig. 1.a) is proposed. The super-module will consist of 8 modules placed according to the geometry of Fig. 1.b. Every module will be a multi-gap resistive plate chamber with a dimension of 100x26 cm² and a segmented anode design. In principle, we are considering a stack of three glass plates, spaced one from the other with spacers of 300 μm thickness (nylon fishing line) creating two gas gaps. The outer surfaces of the two outer glass plates will be in contact with a resistive layer acting as electrodes. Then a mylar foil will isolate the system. The readout system will consist of two PCB plates surrounding the three glass plates with copper pickup strips in the inner surfaces. A cross section of this design is shown in Fig. 1.c. At the moment we are considering 10 strips (100x2.5 cm²) with 1 mm gap in between, to pickup the signals from both, the cathode and the anode (Fig. 1.d). A differential high voltage will be applied to the outer electrodes. For the readout a differential signal will be obtained from anode and cathode pickup strips. In order to reduce the number of electronic channels, the signals induced in two consecutive strips could be summed up. The two PCB plates will also constitute the main frame of the RPC module.

This design covers the required surface with 1.5 m diameter with the three RPC super-modules (Fig. 2). In addition, it will allow to reduce the time resolution achievable with a single super-module by a factor of around $\sqrt{3}$, resulting in an expected resolution is of the order of $\sigma_{\text{ToF}} = 30$ ps. This configuration also

provides individual detection cells with a surface of the order of 3 cm^2 (12 cm^2 if the signals of two consecutive strips are summed up), minimizing the multi-hit probability. The signals induced by charged particles and ions will be taken from both extremes of the RPC module. These two measurements will allow to determine the position information along the 1 m length of the RPC by the time-difference method. In addition, this position information will help to correct the time of flight improving its resolution. Using this method one expects a position resolution better than 1 cm. Since we propose to have strips along three different directions in the plane perpendicular to beam, we could determine the position in this plane with a resolution around 1 cm.

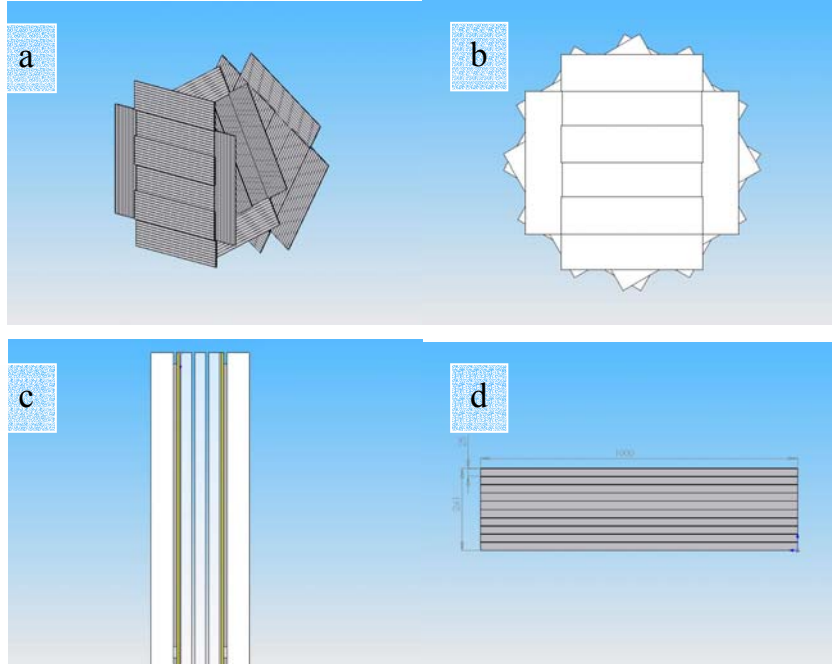


Fig. 1. Schematic representation of the design proposed for the ToF-wall detector. The upper left panel (a) shows the three super-modules configuration. The upper right panel (b) represents the proposed geometry for the eight RPC modules that constitute one super-module. In the lower left panel (c) we represent the cross section of one RPC module with the three inner glass plates surrounded by the electrodes, the mylar foils and the PCB plates with strips acting as signal pickup system and main frame of the RPC module. The lower right panel (d) shows the geometry of the pickup pads in one RPC module.

For the read-out electronics the system developed by the DVEE-department at GSI for the FOPI RPC detector is considered. This system includes a Front-End-Electronic board with preamplifier and discriminator, which is followed by a digitization card (TAQUILA) [Sch04], both housing 16 channels. However, an active impedance adapter, interfacing the RPC output with the read-out electronics would be needed. Different tests of the performances of this system have provided an intrinsic electronic resolution $\sigma_{\text{ToF}} \leq 30 \text{ ps}$. Other existing electronic designs will also be considered.

Although this is a very promising concept, specific R&D concerning the efficiency and time resolution obtained with a multi-gap timing RPC with heavy ions is planned in order to validate this proposition. In particular, questions related to the optimum gas mixture, the number of gaps or the working voltage should be answered.

II. Plastic scintillators

The second option is based in the use of standard organic scintillators coupled to fast photomultipliers. In order to achieve a time resolution below 60 ps we consider individual counters made of organic scintillator material with a dimension of $6 \times 150 \text{ cm}^2$ and a thickness of 5 mm. With this dimensions we will need 30 paddles with 1 cm overlap to cover the 1.5 m^2 total surface of the ToF wall. As in the RPC case we will have two layers of paddles being the total number of paddles 60. These scintillator paddles will be equipped with 120 light guides, photomultipliers and electronic channels.

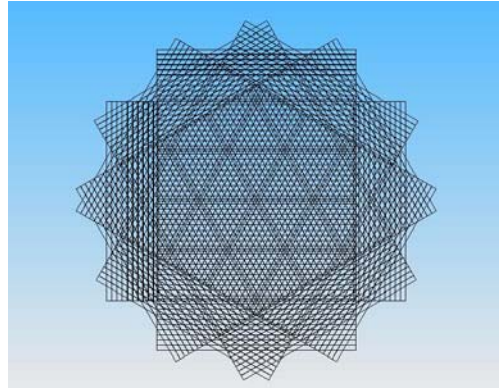


Fig. 2. Front view of the ToF wall detector with individual detection cells defined by the geometry of the pickup pads.

The use of Bicron BC420 as scintillator material coupled with light guides to Hamamatsu H2431 photomultipliers is considered. As in the RPC case, the signals will be taken from both ends of the scintillator with two photomultipliers. A similar detector with a dimension of 10x100 cm², a 5 mm thickness and equipped with Hamamatsu 2431 photomultipliers has provided a time resolution close to 75 ps (sigma) for fission fragments [Sch00]. Other detector using also BC420 as scintillator material with a dimension of 7x40 cm², a thickness of 2.2 cm and Hamamatsu R2490 photomultipliers have only reached a time resolution for MIPs of 120 ps (sigma) [Ade02].

For the readout we propose the same solution as for the RPC, although in this case, the Front-End Electronics board should be adapted to the photomultiplier output signals.

Test experiments

Different beam tests will be needed to validate the performances of the two design concepts that we propose for the charged particles ToF wall. These beam tests should be scheduled along 2005 and 2006.

Time schedule

	2005	2006	2007	2008
R&D + prototypes	xxxxxxxxxxxx	oooooooooooo	oooooooooooo	oooooooooooo
Beam test	ooooooxxxxxx	xxxxxxoooo	oooooooooooo	oooooooooooo
final design	oooooooooooo	oooooxoooo	oooooooooooo	oooooooooooo
Construction	oooooooooooo	ooooooooxxxxxx	xxxxxxoooo	oooooooooooo
Set up at FAIR	oooooooooooo	oooooooooooo	ooooooxxxxxx	oooooooooooo
Test experiments	oooooooooooo	oooooooooooo	oooooooooooo	xxxxxxoooo

Working group and personnel

The members of the working groups are given in section G of this document. This project is coordinated by Santiago de Compostela.

Additionally, a postdoc and an engineer will be needed for a period of two years

References

[Par71] V.V. Parchomchuck, Yu.N. Pestov and N.V. Petrovykh, Nucl. Instr. and Meth., 93 (1971) 269
 [Cer96] E. Cerron Zeballos et al., Nucl. Instr. and Meth., 374 (1996) 132
 [Bla02] A. Blanco et al., Nucl. Instr. and Meth. A 485 (2002) 328
 [Aki04] A.N. Akindinov et al., Nucl. Instr. and Meth. A 533 (2004) 74
 [Yi05] W. Yi et al., accepted for publication in Nucl. Instr. and Meth.
 [Alv04] H. Alvarez Pol et al., Nucl. Instr. and Meth. A 533 (2004) 79
 [Sch04] A. Schuttauf, Nucl. Instr. and Meth. A 533 (2004) 65
 [Sch00] K.-H. Schmidt et al., Nucl. Phys. A 665 (2000) 221
 [Ade02] B. Adeva et al., Nucl. Instr. and Meth. A 491 (2002) 41

B.1.6. Total γ -absorption spectrometer

Introduction

We define here the main characteristics of a 4π γ -ray calorimeter array that will surround the target of the R³B experiment. The calorimeter will be used for the study of most of the physical cases presented in the R³B Technical Proposal, though the requirements differ significantly from one experiment to the other. In some cases it is the γ -ray sum energy that is required, while in others the detector has to be able to provide γ -ray multiplicities and individual γ -ray energies for spectroscopic purposes. A key requirement of the detector is that it also has to act as the calorimeter for the target recoil detector described in B.1.7. Hence the detector has to stop and measure the total energy of high-energy light charged particles, e.g. protons up to 300 MeV, with good energy resolution.

The main properties of this device, high efficiency and good angular resolution, are imposed by the very particular kinematics of energetic γ -rays emitted by sources moving with relativistic velocities and by the typically low intensities of the secondary beams involved. A typical case to be considered is γ -rays with energies ranging from 1 MeV up to 10 MeV in the centre-of-mass (CM) reference system emitted in-flight from fragments with energies around 700 MeV/nucleon in the laboratory system, see Fig. 1. The Doppler effect introduces an angle dependent energy shift. The original CM energies are Lorentz boosted and in the laboratory system they are modified by a factor that is large for the forward angles, from 7° to 30° , see Fig. 1(a), where the maximum of the angular distribution is concentrated, see Fig. 1(b). This shift defines the final energy resolution depending on the velocity of the moving source (700 MeV/nucleon corresponds to $\beta=0.82$) and on the final angular resolution of our setup. Fig. 1(c) shows this effect for different angular resolutions.

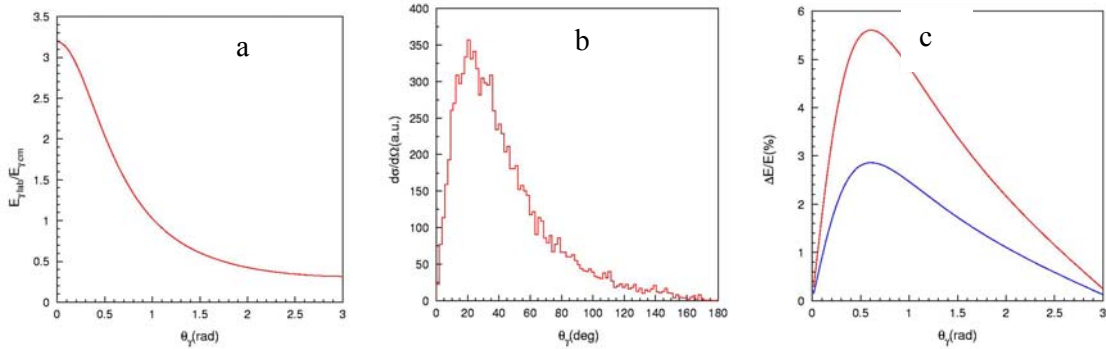


Figure 1 : Kinematical properties of γ - rays emitted by a moving source at 700 MeV/nucleon. 1(a) Doppler shift; 1(b) Angular distribution of isotropically emitted photons; 1(c) Energy resolution for $\Delta\Theta= 0.018$ rad (blue line) and $\Delta\Theta= 0.031$ rad (red line).

Design goals

The main requirements are summarised in Table 1.

Table 1: Main properties of the total absorption γ -calorimeter.

Total absorption efficiency	80 % (up to $E_\gamma=15$ MeV Lab system)
γ sum energy	$\sigma(E_{\text{sum}})/\langle E_{\text{sum}} \rangle < 10\%$
γ multiplicity	$\sigma(N_\gamma)/\langle N_\gamma \rangle < 10\%$
Good γ Energy resolution	3-5% $\Delta E/E$
Calorimeter for high energy light charged particles	Up to 300 MeV in Lab system
Good light charged particle energy resolution	$< 3\% \Delta E_p/E_p$

Geometrical considerations

High total absorption efficiency can only be reached by means of thick detectors covering a maximum of solid angle. In this sense, the use of dense crystal material would help to reduce the final volume of the calorimeter.

The length of those crystals, which will depend on the selected material, is estimated to be around 20 cm. We have chosen as a starting point a detector optimized according to the kinematical properties introduced previously. This detector is enclosing the R^3B target and will have a hole (7° aperture) for the most forward angles to ensure full fragment transmission. The inner part of the calorimeter will contain a vacuum chamber with the R^3B reaction target and the target recoil detector system as described in section **B.1.7**. The space taken by these systems determine an inner radius of 25 to 30 cm for the calorimeter. The outer radius is given by the maximum length needed to fully stop the energetic γ -rays and light charged particles up to 300 MeV. The crystal length can be reduced at backwards angles where the Doppler shift is less severe. The intensity of the γ -rays drops drastically at polar emission angles larger than 80° - 90° for the high beam energies of interest (see Fig. 1). This fact suggests that in order to reach the specification in terms of total-absorption efficiency it is not necessary to cover the full solid angle. Simulations show that by covering polar angles between 7° and 130° around 80% absorption efficiency is obtained. In order to reach the required energy resolution we have to consider the intrinsic energy resolution of the crystal material together with the energy broadening introduced by the Doppler effect. In order to minimize the angular resolution very high granularity will be needed. To keep the energy resolution $\Delta E/E$ within 3 %, crystals with an entrance area ranging from $1 \times 3 \text{ cm}^2$ for the most forward angles and $2 \times 4 \text{ cm}^2$ for the rest are considered.

Crystal Materials

The selection of the crystal material is governed by the following criteria: good intrinsic energy resolution, high probability of interaction with γ -rays and affordable cost. Different materials, $\text{LaBr}_3(\text{Ce})$, $\text{LaCl}_3(\text{Ce})$, cooled $\text{CsI}(\text{pure})$, $\text{Cs}(\text{Tl})$ and cooled $\text{NaI}(\text{pure})$, have so far been selected for study. They are inorganic crystals, are hygroscopic and are commercially available. The main advantage of $\text{LaBr}_3(\text{Ce})$ [1] is its very good energy resolution, which is of the order of 2.9 % ($\Delta E/E$) for 662 KeV γ -rays [2], and its high density (5.3 g/cm^3). However, it is a new material and it has a relatively high cost, in addition it features severe structural problems that make it difficult to grow large crystals. The intrinsic energy resolution of $\text{LaCl}_3(\text{Ce})$ [3] is still very good (3.2 % ($\Delta E/E$) for 662 KeV γ -rays [4]) but its density (3.9 g/cm^3) is lower. It seems however easier to grow long pieces and first prototypes up to 17 cm length are being produced by Saint-Gobain [5]. Recent publications have shown that cooled NaI [6] and CsI [7] could provide very good energy resolution (of the order of 4% and 4.3 % for 662 keV γ -rays and 2.5 % and 3.5 % $\Delta E/E$ for 1.3 MeV γ -rays, respectively). Such crystals are relatively cheap and can be grown to the necessary length of 20-25 cm having the disadvantage, however, that a cryostat would be needed. Last but not least we stress the interest of using standard $\text{CsI}(\text{Tl})$ scintillators coupled to optimized readout systems that would provide an intrinsic energy resolution of those devices up to $< 5 \%$ ($\Delta E/E$) for 662 KeV γ -rays [8].

Several laboratory tests are being performed within the working group to explore these different possibilities. At the same time commercial and scientific exchanges with different scintillator producers have been initiated (e.g: Saint Gobain detectors (France), Lanzhou (China) and Dubna (Russia)).

Saint-Gobain has produced 2D- NaI arrays of crystals with 1 mm^2 pixel structure and up to 15 cm length. This possibility is interesting but will need an in-depth study.

Mechanical Structure

The structure of the spectrometer should support a total crystal weight in the order of 2000 kg while keeping the volume of dead layers minimal. To reduce the interference with the measurements, the inner window of the support structure should be as thin as possible, as well as the separation between the crystals. It is planned to use epoxy-carbon fiber boxes configuring alveolar structures able to contain several crystals (up to 32 in a preliminary design). The alveolus can be made of 0.2 mm layers, having a

negligible influence on the gamma detection. Additional layers of 0.4 mm, as well as thicker support rings at different polar angles, are devised for structural purposes.

The alveolar structure allows an easier mounting as well as a natural modularization of the spectrometer, allowing a sector-like division of the full setup. Different parts of the spectrometer could be separated or accessed independently. Different sectors could be displaced for accessing to the inner detectors around the target region or for maintenance.

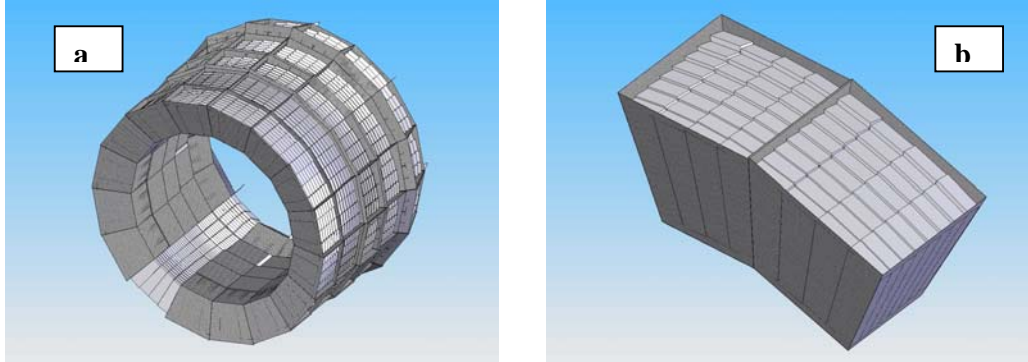


Figure 2: (a) View of the central part of the spectrometer including the epoxy-carbon fiber boxes. (b) Detailed view of two of these alveolar structures.

Simulations

The choice of the final characteristics of the total γ -absorption spectrometer for the R³B experiment depends on multiple parameters and thus it is important to carry out detailed simulations. These activities have been running during the last year using the simulation code GEANT 4 [9], developed at CERN, and will continue for the next years. We present, in the following paragraph the results extracted from the first simulations. In Fig. 3 the total-absorption probabilities simulated for very energetic γ -rays in LaBr₃, CsI and NaI crystals are shown. From the inspection of this figure we can deduce that in order to keep the nominal total absorption efficiency (80%) for 10 MeV γ -rays (Lab system) we would need crystal lengths of 16cm, 17cm, and 22 cm, respectively. If we consider 15 MeV γ -rays (Lab system), the required crystal lengths would amount to 18 cm, 21cm, and 26 cm, respectively. It is observed that even for these crystal lengths, the total γ -ray absorption efficiency drops to 60%, 55%, and 50% respectively when we consider 30 MeV γ -rays (Lab system).

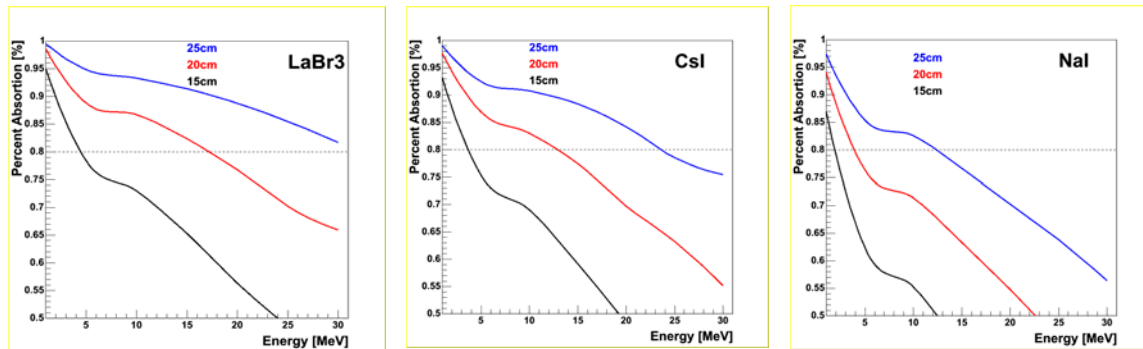


Figure 3. Total-absorption efficiency evaluated with a GEANT 4 simulation as a function of the γ -ray energy. The curve shows the results for different inorganic scintillators (LaBr₃; CsI; NaI) and different crystal lengths (black solid line corresponds to 15 cm, red to 20 cm, and blue to 25 cm).

The preliminary version of the spectrometer geometry has been simulated using GEANT4 + ROOT software, with CsI(Tl) as detection material. The full segmentation and solid-angle covering has been implemented in the simulation, including different reconstruction patterns to obtain the energy and the polar angle of the incident photon. The intrinsic resolution of the crystal has not been included in order to evaluate only the correction due to the Lorentz boost. The results show that the CM energy of the γ can be reconstructed within a 3.5 % resolution for the γ energies present in the experiment and with the proposed polar angle segmentation. A geometrical efficiency of around 80% has been observed for an isotropic γ emission by projectiles with 700 MeV/nucleon kinetic energy.

Further simulations are needed to include the support structures, the inner detectors and the beam-target interaction (large-area target).

Proposed Solution

The proposed solution consists on a detector covering a polar angle between 7-133° and divided in 5025 crystals. This detector will be subdivided in three sub-detectors: one Barrel covering the central part (1970 crystals), and two end caps: Forward (1985 crystals) and Backward (1070 crystals) End Cap (see Figure 4 and the details given in Table 2).

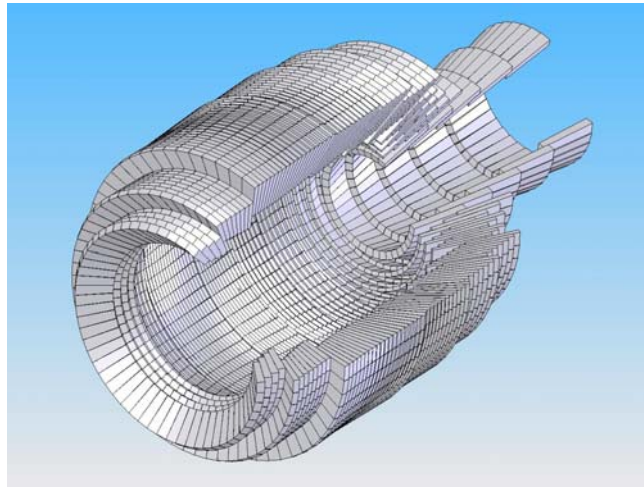


Figure 4. Proposed geometry

Table 2. Geometrical data

	Nr of Crystals	Polar-angle coverage	Crystal volume (cm ³)
Backward End Cap	1070	133° - 90°	58 443
Central Barrel	1970	90° - 50°	221 122
Forward End Cap	1985	50° - 7°	220 435
Total	5025	133° - 7°	500 000

The crystal segmentation yields an energy resolution (due to the polar-angle segmentation) in the order of 3.5 % and a total-absorption efficiency in the order of 80% is achieved with a typical crystal length of 20 cm.

The intense R&D activity in new scintillator material going on worldwide will open new and very interesting possibilities that we do not want to discard. The fast evolution of this field will finally determine the final decision on the “optimum” scintillation material. The proposal presented above based on CsI as scintillator material is what we think the most plausible option at the moment. In this case the total detection volume would amount to 500 dm³ with a weight of 2000 kg. The intrinsic energy resolution of the system is around 5% (for 662 keV γ and readout with Large Area APDs) if we consider

the option CsI(Tl). This value could be improved if one uses pure CsI at cryogenic temperatures. This last option would need of a different readout system (namely Photo Multiplier tubes that better fit the spectral response of the crystal). This solution would allow keeping the final resolution within the limit imposed by the polar-angle segmentation.

Readout and electronics

The readout will depend upon the choice of crystal material and on the sizes of individual crystals. PIN-diodes, APDs or LAAPDs as well as PMs are considered. To make the right choice, tests have to be performed using the different crystal materials in combination with the different readout concepts. Concerning the readout electronics one can make use of solutions developed for other detectors. A possible solution could be based on the ASIC card MATE developed at CEA Saclay for the MUST2 detector. It is important to note that the detection of both γ -rays and light charged particles with energies up to 300 MeV in the same crystal implies a very large dynamic range in the charge collection. The readout device and the whole electronics chain has to be optimized for this function. Clearly an already existing, commercially available, design might not be available, in which case the development of a new design for the readout electronics will be necessary.

Test Experiments

The following test experiments are foreseen during the ongoing R&D phase:

- bench test of crystal performances: each module (ensemble of different crystals and readout in a common aluminium housing) has to be tested on an optical bench at the collaborating institutions
- beam test: to be performed under realistic conditions with γ -rays emitted by relativistic secondary beams at the actual GSI facilities and with proton beams at GSI or at other institutions.

Time Schedule

	2005	2006	2007	2008	2009
Simulations	xxxxxx	xxxxx-	-----	-----	-----
R&D prototypes	--xxxx	xxxxx-	-----	-----	-----
Final design	-----	-----X	-----	-----	-----
Crystal tests	-----	-----	----XX	xxxxxxx	-----
Construction	-----	-----	xxxxxxx	xxxxxxx	-----
Beam tests	-----	-----	--XX--	--XX--	--XX--
Implementation	-----	-----	-----	-----	xxxxxxx

Working group

The members of the working group are given section G of this document. This project will be coordinated by Santiago de Compostela.

References

- [1] Brilliance 380. Thecnical Data sheet. Saint-Gobain detectors. <http://www.detectors.saint-gobain.com>
- [2] E.V.D. Van Loef et al., Applied Physics Letters 79 (2001) 1573
- [3] Brilliance 350. Thecnical Data sheet. Saint-Gobain detectors. <http://www.detectors.saint-gobain.com>
- [4]] E.V.D. Van Loef et al., Applied Physics Letters 77 (2000) 1467
- [5] Saint-Gobain detectors. <http://www.detectors.saint-gobain.com> (private comunication)
- [6] M. Moszynsky et al., NIM A505 (2003) 63
- [7] M. Moszynsky et al., NIM A537 (2005) 357
- [8] T. Ikagawa et al., NIM A538(2005) 640
- [9] GEANT 4 code. S. Agostinelli et al., Nucl. Instr. and Meth., A506 (2003)250.
<http://wwwasd.web.cern.ch/wwwasd/geant4/geant4.html>

B.1.7. Target recoil detector

Overall design

The detector for light (target-like) particles is a substantial part of the R³B setup. It allows registration of recoils in coincidence with the heavy fragments, neutrons and the γ -rays. This set-up gives thus a unique possibility to study elastic, inelastic and quasi-free scattering, knockout and breakup reactions. The recoil particle detector provides precise tracking, vertex determination as well as energy and multiplicity measurement with high efficiency and acceptance. The latter two parameters are very important when dealing with radioactive beams. A general overview of the light-ion detector has been described in the R³B LoI [1].

A thick liquid-hydrogen target ($100 - 250 \text{ mg/cm}^2$) will be used to reach the required luminosity for the radioactive beams. It allows for almost background-free data taking. The use of an extended ($3 - 4 \text{ m}$ long) target requires a detector set-up with the possibility to determine the interaction vertex with the precision of $1-2 \text{ mm}$. This precision corresponds to an effective target thickness below 20 mg/cm^2 , and allows the energy loss of the recoils in the target to be corrected for.

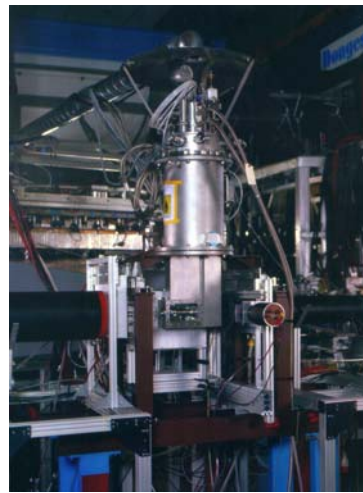


Figure 1. Photographs of the existing liquid hydrogen target.

We will employ a modified version of the liquid-hydrogen target that was used for the elastic and quasi-free scattering experiments at GSI [2] (see fig. 1). A new vacuum chamber will be designed which will be placed in the γ -ray calorimeter described in section B.1.6. The calorimeter will cover approximately 75% of the total solid angle with an opening in the backward hemisphere. This space, free of detectors, will be used for the infrastructure of the liquid hydrogen target (tubes, etc.) and the readout electronics of the tracker detectors.

Study of knockout reactions and quasi-free scattering in inverse kinematics requires detection of recoils in an energy-range of $50 - 300 \text{ MeV}$. The typical angular range which has to be covered is 20° to 70° for an incident projectile energy of 700 MeV/u . The tracking system consists of two layers of position-sensitive detectors. The general scheme of the recoil-detector system is shown in Fig. 2.

Detection of the Recoils

The main requirements are high resolution for momentum and energy of the recoiling target-like nuclei. According to previous experience, for the case of (in)elastic scattering, the angular resolution (in centre-of-mass and laboratory system) should be around a few mrad and the resolution in excitation energy, E^* , better than 1 MeV .

Some initial simulations have already been carried out that show the feasibility of the system. Extended simulation studies of the performance of the suggested detector scheme should be performed taking into account the size of each individual sensor and the mechanical structure. The simulation package is based on the general purpose transport tool Geant4 [3].



Figure 2. General scheme of the recoil detector. The red cylinder represents the first layer and the green cylinder the second layer of the tracker. The calorimeter is indicated in blue.

Geant4 is used to trace particles through the various materials, generate other particles according to the interaction cross sections and decay probabilities, as well as to calculate their energy loss and time-of-flight. The analysis of the simulated events is done using the histogramming tool ROOT [4]. The recoil particles are generated using external event generators. The main results of the simulations carried out so far have been obtained for one of the most demanding types of reaction – inelastic scattering.

The aim of the simulation is to optimize the detection system in terms of its tracking capability and detection with good energy resolution and particle identification. In particular the focus is on the following points:

- Geometrical configuration of the two tracking layers, their thicknesses and strip pitch
- Thickness, material and configuration of the vacuum chamber wall
- Thickness and material of the calorimeter
- Energy resolution of all detectors

The key parameters of the detector system are the resolutions in excitation energy and centre-of-mass scattering angle. These values are calculated for a ‘standard’ detector geometry that has been used as a starting point:

- first layer of Si detectors – 2.5 cm distance to the target, 100 μm thickness, 100 μm pitch size, 50 keV (FWHM) energy resolution;
- second layer – 10 cm distance to the target, thickness is 300 μm , pitch size is 100 μm , energy resolution is 50 keV (FWHM);
- calorimeter – CsI crystals with 20 cm thickness and 1% energy resolution;
- the wall of the vacuum chamber is 50 μm of stainless steel.

All coordinates and energy losses are folded with the resolutions. The coordinate determination is based on the strip size as in real micro-strip detectors. The energy resolutions are based on known test results. The resolution in excitation energy ΔE^* (σ) versus proton recoil energy E_p for the case of inelastic scattering of $^{12}\text{C}(p,p')$ with $E = 400$ MeV/u is shown on the right panel of Fig. 4. The resolution in the centre-of-mass angle $\Delta\theta$ (σ) versus E_p for the same reaction is shown in the left panel of Fig. 4. The resolution on the angle in laboratory system $\Delta\theta$ (σ) versus E_p for the same reaction is displayed in Fig. 5 (left frame).

The results of the simulations for higher energies (700 – 1000 MeV/u) and heavier ions show a similar performance. In case of (in)elastic scattering, the required resolution would be $\Delta\theta \leq 3$ mrad for the CM angle and $\Delta E^* \leq 1$ MeV for the excitation energy.

First simulations for quasi-free scattering have been performed using an external event generator and the same configuration of the detector as for the inelastic scattering. The reaction chosen is $^{12}\text{C}(p, 2p)$ at a beam energy of 700 MeV/u. The aim of the simulation was to estimate the accuracy of the separation energy E_{sep} measurement for the given energy resolution of the calorimeter and the given pitch-size of the tracker. An example of the ΔE_{sep} calculation for $E_{\text{sep}} = -15.8$ MeV is shown in Fig. 5 (right panel).

Some results for ΔE_{sep} are presented in a Table 1. One can see that with the designed energy and position resolution the accuracy of the order of $\Delta E_{\text{sep}} = 2\text{-}3$ MeV is reachable and it will be enough for most of the quasi-free scattering experiments. The precision of the transverse momentum distribution of the cluster

p_x is an important observable to show the performance of the system. We can reach $\Delta p_x = 3-4$ MeV/c and relative momentum resolution $\sim 3-4 \cdot 10^{-4}$ for the present geometry that is compatible with the performance of the high resolution spectrometer. At the present stage, the simulations of the observables for the quasi-free scattering have been made without Geant4 using separate programs. Multiple scattering was not taken into account but the estimations show it will increase the values of ΔE_{sep} and Δp_x by 30-40%.

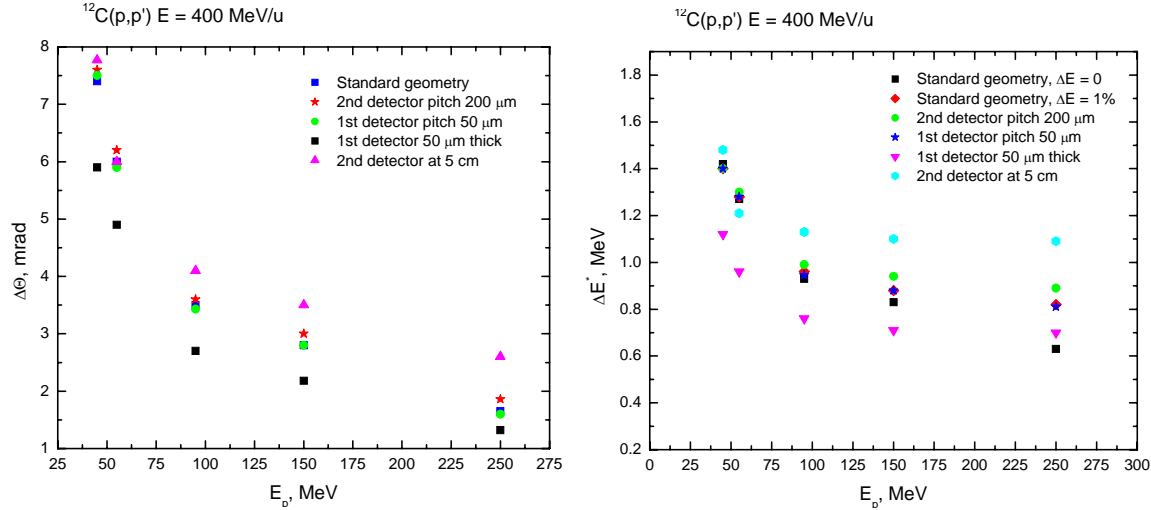


Figure 4. Right panel: excitation energy resolution versus the proton recoil energy E_p for the case of inelastic scattering of $^{12}\text{C}(p,p')$ with $E = 400$ MeV/nucleon. Left panel: resolution on the centre-of-mass angle $\Delta\theta$ (σ) versus E_p for the same reaction.

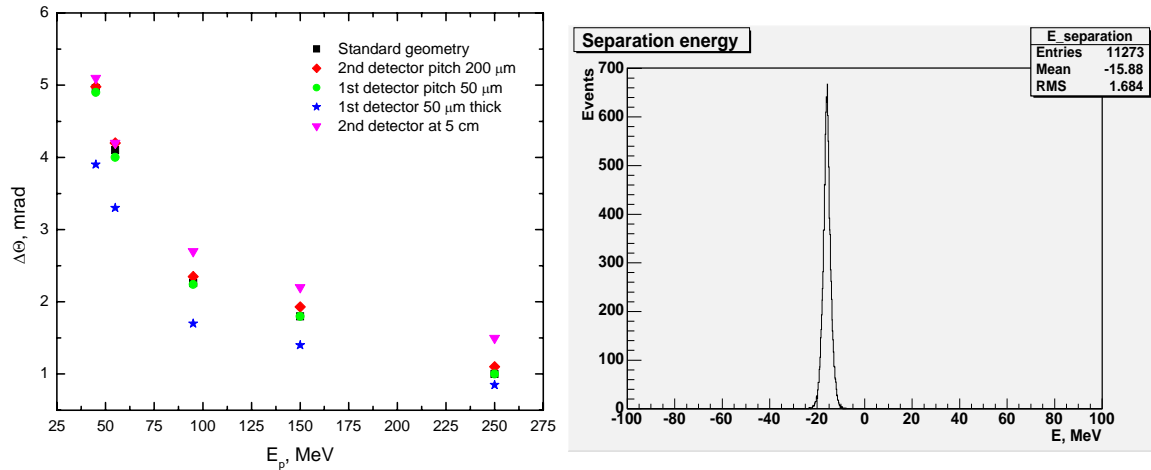


Figure 5. Left: Resolution on the angle $\Delta\theta$ (σ) in laboratory system versus E_p for the case of inelastic scattering of $^{12}\text{C}(p,p')$ with $E = 400$ MeV/nucleon. Right: Separation-energy resolution for the QFS reaction $^{12}\text{C}(p,p')$ with $E = 700$ MeV/nucleon.

Table 1.

Strip size, mm	Energy resolution, %	ΔE_{sep} , MeV	Δp_x , MeV/c
0.01	0.5	0.5	0.5
0.05	0.5	2.1	2.1
0.05	1.0	2.2	2.2
0.1	1.0	4.0	3.5
0.1	3.0	4.1	3.7

The first conclusions are the following:

- ✓ The first layer should be placed close to the target. It improves the precision of the vertex determination and reduces the size and cost of the system. For the time being we consider the first layer composed of 50 μm thick detectors at 2.5 cm distance from the centre of the target. 100 μm thick detectors would introduce larger multiple scattering, but could be used if the lowest energy of the recoiling protons is about 100 MeV. The individual detectors are arranged to form a barrel with a length of 13 cm, surrounding the target.
- ✓ The second layer, made from 300 μm thick sensors, can be positioned at a distance of 5 cm from the centre of the target. The detectors will be fixed on 17 cm long ladders with the electronics on one side to reduce the dead zones.
- ✓ The energy resolution of the calorimeter for detection of the proton's detection can be 3% (FWHM) without large influence on the overall performance.

An example of such a ladder is shown in Fig. 7. The maximum active area of the first layer is about 200 cm^2 and of the second one about 500 cm^2 . In the real situation it will be smaller due to the infrastructure of the target and a mechanical arrangement of the individual sensors. The exact geometry of the calorimeter (which is simultaneously used as the γ -ray detector, see section **B 1.5**) and the crystal type – CsI, NaI or $\text{LaBr}_3(\text{Ce})$, will depend on the results of detailed simulations (including segmentation of the calorimeter, dead zones etc.) and the tests of prototypes. In general, the scheme described above should fulfill the requirements.

A possible solution for the first layer of the tracker is double-sided Si detectors (DSSDs) but such detectors are normally thicker – 200 μm or more. Thinner sensors (30 – 100 μm) with a reasonable size of 20 – 25 cm^2 are commercially available (Micron Semiconductor). This solution requires some R&D and prototyping to prove the performance of such thin detectors. The advantage of this solution is the moderate number of readout channels (40k or less) and the experience gained by several high-energy experiments [5, 6, 7]. In any case, additional simulations should be made including realistic rates of all reactions. If the probability of getting two hits in the same strip within the integration time of the front-end chip is large, we need to reduce the strip length or even use pixels.



Figure 6. Left: Example of the arrangement of the double-sided Si detectors on a ladder (a part of the tracker system of the AMS experiment). Right: Prototypes of the MAPS detectors on 6" Si wafer.

Another prominent solution is based on Monolithic Active Pixel Sensor (MAPS) technology [8]. These devices have projected thicknesses down to 30 - 50 μm , single-point resolution of 5 μm and an efficiency of 99%. The maximum active size is at the moment $\sim 3 \text{ cm}^2$. R&D in high-energy physics is going towards larger area detectors. Two members of the collaboration, namely CEA Saclay and the consortium of UK universities, participate in this R&D. An example of the detectors made on a 6" wafer is shown in Fig. 6 (right picture).

An attractive feature of MAPS is that they allow a System-on-a-Chip by integrating signal processing micro-circuits (amplification, pedestal subtraction, digitization, and discrimination) on the detector substrate. The resulting chip may be thinned down to a few tens of microns. There is extensive R&D

going on with the aim to use MAPS as the vertex detector in the CBM experiment [9] and in other future experiments in nuclear and high-energy physics.

Another solution for the first layer is the Image Sensor with In-situ Storage (ISIS) pixel detector that is being developed for the future linear collider [10]. It is based on CCD technology and the existing prototypes already have a size of 10 cm^2 (Fig. 7). The arrangement of sensors mounted on a ladder also fits the geometry of the first layer. The position resolution of ISIS can be of the same order as MAPS ($\sim 5 \mu\text{m}$) and there is no problem to make larger pixel sizes. This detector can also be made $30 \mu\text{m}$ thick [10]. The drawback of the MAPS or ISIS detectors is, of course, the large number of pixels ($\sim 2 \times 10^6$) that requires a special readout scheme. The energy-loss measurement might be difficult using such thin sensors. In this case the total energy will be measured by the second layer of the tracker and the calorimeter and corrected for the missing energy in the first layer. Simulations show that the error, introduced because of this is very small.

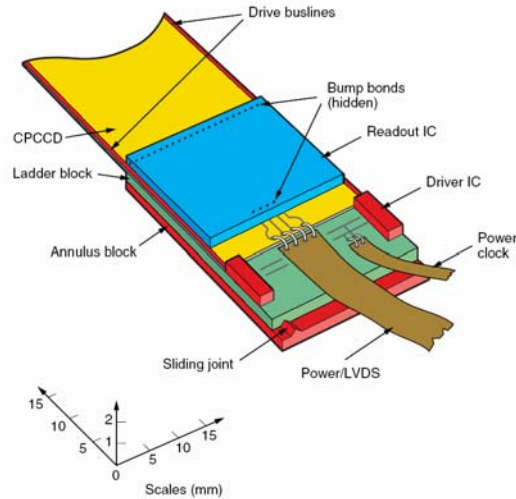


Figure 7. Prototype of the ISIS detector on the ladder.

The second layer of the tracker can be made from double-sided Si detectors with a standard thickness of $300 \mu\text{m}$. The number of readout channels for this layer is estimated to be 50k.

There are some considerations about the readout electronics and especially about the front-end chips. On the one hand, a smaller thickness (l) introduces less multiple scattering ($\sim \sqrt{l}$), less leakage current ($\sim l$) and smaller full depletion voltage ($\sim l^2$). On the other hand, the reduction of the detector thickness implies a reduction of the signal-to-noise ratio S/N that depends on the relative contributions from the series (ENC_s) and parallel (ENC_p) noise:

$$S/N = \frac{r_L \cdot S_{300} \cdot (l/300 \mu\text{m})}{\sqrt{ENC_s^2 + ENC_{p300}^2 \cdot (l/300 \mu\text{m})}}$$

where S_{300} is the most probable charge deposition (for the given energy of the protons) in a $300 \mu\text{m}$ thick detector and r_L accounts for Landau fluctuations and charge collection deficits. Energy losses in the Si detectors will be between 5 MeV and 150 keV. This implies a moderate dynamic range of 1:30 which can be handled by many commercially available readout chips. The situation will be more difficult with the first layer of the tracker since thin detectors ($50 - 100 \mu\text{m}$) are mechanically less stable and the S/N ratio is smaller, especially for fast protons. Taking into account realistic values for ENC_s and ENC_p of about $700 e^-$, we expect $S/N \geq 10$ that should be sufficient for tracking. One should mention that there will be an extensive R&D on Si detectors and their readout electronics within the EXL project. Their requirements are in general higher, in particular the detectors and the front-end electronics are required to work in UHV conditions. In addition, a precise time measurement is foreseen and the dynamic range of the signals is higher. Nevertheless, if the performance of the detectors and the electronics as developed for EXL fulfills the requirements of the R³B tracking detector we consider using the same solutions for R³B. There will be a permanent exchange of information and ideas between the collaborations.

The readout of analog information from the strips is based on the multiplexers and the serial line for the data transmission. The custom receiver modules are digitizing the amplitudes; the service module SAM providing a fast DSP makes the pedestal suppression and data processing in real time.

Both layers of the tracker will operate inside a vacuum chamber with a radius of about 25 cm. The support structure for the detectors and the readout electronics will be made from carbon fiber. The material is strong enough and has low density minimizing the scattering of the particles in the support structure.

The Si sensors will be optically aligned and the alignment will be verified using cosmic rays (high energy muons) giving the relative position of each sensor with respect to the others. The final alignment of the total system will be made after mounting it into the experimental setup with the laser metrology system.

The power dissipation of the detectors and the corresponding front-end electronics should be kept as small as possible due to the vacuum conditions. In any case, it will be less than 300 W for the whole tracker system. This will require cooling, but without any cooling media like water or other liquid. The typical consumption of one ADC VME module is on the order of 30 W so the consumption of the VME part, including 5-6 VME crates, can be of the order of 5-6 kW.

Radiation hardness

The recoil detector will be used for detecting the secondary particles from nuclear reactions in the target. Taking into account a maximum rate of $10^8 - 10^9$ radioactive ions/s and a 1% interaction probability, we estimate a maximum flux for the recoils of $10^6 - 10^7$ particles/s for the whole detector system or $10^4 - 10^5$ particles/s per cm^2 . Assuming typical beam time of 2 months per year, the detector must stand a total dose of up to $5 \cdot 10^{10}$ particles per cm^2 per year. This dose is much smaller than the estimated doses for the Si detectors in vertex systems of the LHC experiments, which are typically $10^{14} - 10^{15}$ charged particles per year [5, 6, 7].

Space requirements

The system will be very compact and fit into the inner part of the γ -ray detector, which is a sphere with an inner diameter of 50 cm and an outer diameter of 100 cm. The support structures will be designed to accommodate either liquid (hydrogen, deuterium, helium, etc.) or solid targets. Additional space of the order of $6-8 \text{ m}^2$ is required for the electronic racks.

Test experiments

The collaboration has already purchased several Si microstrip detectors equipped with their readout and these will act as the first prototypes of the second layer of detectors. Each detector has a size of 30 cm^2 and a readout pitch of $100 \mu\text{m}$ on both sides of the sensors. Test experiments using proton and light ion beams are inevitably required in order to prove the simulations and make a decision on the best suitable detector technology. A first test experiment using ^{12}C at 250 MeV/u and lighter nuclei from the fragmentation of ^{12}C has been made in November 2005. The detectors show very good performance in terms of signal-to-noise ratio, energy and position resolution. These prototypes will be implemented in the existing LAND setup in Cave C at GSI and will allow valuable experience to be gained. Further tests will be necessary as the new prototypes are developed. The energy of the protons and some light ions should be in the range of 50 - 500 MeV/u. Test experiments using high rate accelerator facilities are foreseen to check the radiation hardness of each prototype.

R3B

Milestones

2005 – 2006	Simulations and optimization of the geometry, tests of prototypes
End of 2006	Decision on the detector concept, Technical Design Report
2007	Preproduction of prototypes, concept of installation and alignment
2008 – 2009	Production of the detectors and electronics, installation

Working group and personnel

The members of this working group are given in section G of this document. This project is coordinated by University Mainz.

Our working group includes people from the Universities of Mainz, Darmstadt, Chalmers and GSI who have experience in tracking detector design and simulations. They will be involved in optimization of the calorimeter surrounding the tracker and the tests of the prototypes. The participants from CEA-Saclay have built several detector systems for nuclear physics (MUST, MUST2) and developed front-end ASICs and corresponding electronics. Several UK universities and laboratories participate in the R³B and EXL projects and have been involved in many experiments in nuclear and high-energy physics. Their MAPS development program is world-leading and they are heavily involved in designing ASICs for both the ATLAS and CMS experiments for the LHC at CERN. They also have expertise in hybrid pixel detectors (sensor bonded directly to ASIC) and in general building blocks such as low noise preamps, shaping amplifiers, multiplexers, ADCs, analogue pipelines (to increase the apparent ADC sampling rate) and detector readout. The R³B recoil detector is, in many aspects, similar to the one that will be built for the EXL project. Therefore we can profit from the partial overlap of R&D with EXL.

References

1. R³B LoI, GSI, 2004.
2. F. Aksouh, PhD Thesis, Université de Paris XI, Orsay, France, 2002.
3. S. Agostinelli et al., Nucl. Instr. and Meth., A506 (2003) 250.
4. R. Brun and F. Rademakers, Nucl. Instr. and Meth., A389 (1997) 81.
5. CMS The tracker project, Technical Design Report, CERN/LHCC 98-6, TDR 5, 1998.
6. ATLAS Inner detector, Technical Design Report, TDR 5, 1997.
7. ALICE Technical Design Report of the Inner Tracking System (ITS), CERN/LHCC/99-12, ALICE TDR4, 1999.
8. M. Deveaux et al., Nucl. Instr. and Meth., A512 (2003) 71.
9. CBM LoI, GSI, 2004.
10. T. Goji Etoh et al., IEEE Trans ED (2003) 144.

B.1.8. Active target

Physics case

The study of the structure of exotic nuclei poses unique experimental challenges, raised both by the constraints arising from the production of such nuclei and also by the experimental tools necessary to explore their properties. A general constraint is that such nuclei are typically produced with low intensities, which need a detection system with very high efficiency. Furthermore, the information on the structure of exotic nuclei is most readily extracted using reactions in which one of the participants has a relatively simple structure, e.g. ^1H or ^4He . In this instance the use of radioactive beams necessitates the use of ^1H or ^4He targets and inverse kinematics. For some of the reactions to be studied the most interesting information is concentrated in the region of very low momentum transfer, and therefore demands for high resolution detection of very slow target-like recoil particles.

A very promising solution to such experimental challenges is the use of an active target detector, where the gas constitutes both the target and the detection medium. Such a detector may have a very high efficiency, very low particle detection thresholds, and may use different gases, which can therefore be chosen to best suit the experiment purpose.

The physics case addressed within R³B with the active target concept is quite similar to that of the EXL project, but the two different projects are well complementary. The EXL project will allow to reach high luminosities for all cases where the nuclear lifetime of the exotic beam particles is sufficiently long (> 500 ms) to allow for beam preparation in the CR/NESR rings and for continuous accumulation and staging. Keeping in mind that the rate capability of the active target technique will be limited, especially for very heavy projectiles, to about 10^5 s^{-1} or less, luminosities of the order of $10^{28} \text{ cm}^{-2} \text{ sec}^{-1}$, as expected for EXL, will not be reachable with external active targets. On the other hand there exist many cases of exotic beams of high interest for nuclear structure and nuclear astrophysics, which are located far outside the valley of stability, and consequently have half-lives much shorter than 1 s, and relatively low production rates considerably below 10^5 s^{-1} (see figure 1). For such cases the technique of active targets is presently considered as the only way to perform high resolution experiments at low momentum transfer with sufficient luminosities to extract the cross sections of interest.

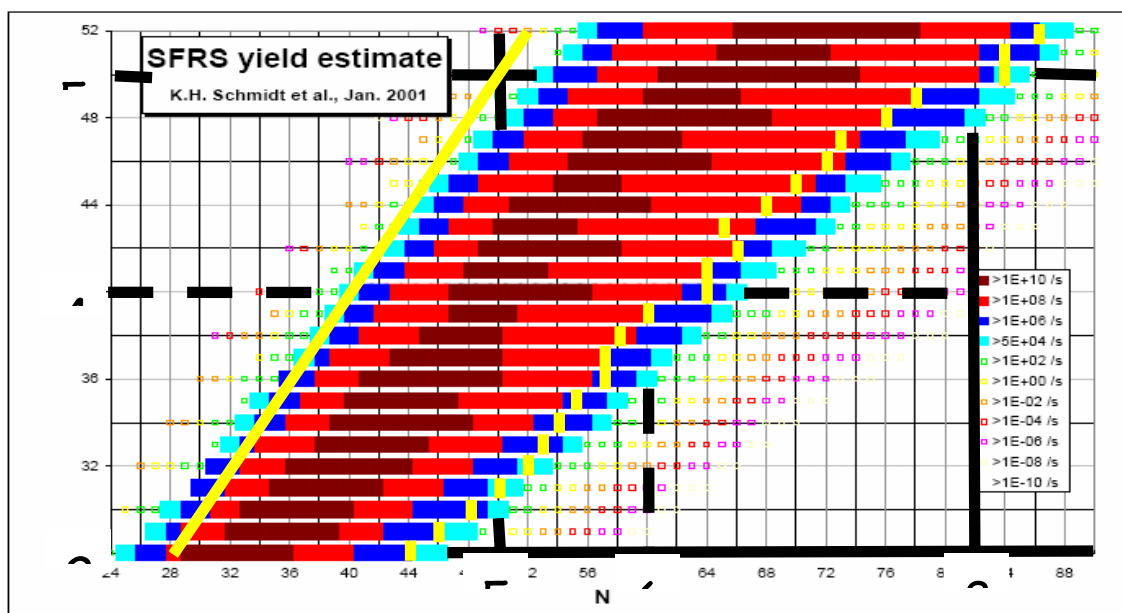


Fig.1: Estimation of production rates with the Super-FRS (without transmission losses) for nuclides with $28 < Z < 52$. The yellow lines mark the regions on the neutron- and proton rich side where nuclear lifetime becomes smaller 1 sec.

To illustrate the experiments that can be performed with the active target, we consider here 2 examples:

- i) elastic scattering of very exotic species ($T_{1/2} < 1s$) on a light target. Such investigations, as for example elastic proton scattering at intermediate energies allow to accurately determine the nuclear matter radii, and the radial shape of the nuclear matter distributions of these nuclei. The active target will be used to measure the kinematical characteristics of the light recoil, and the high energy ejectile will be detected through the large acceptance dipole.
- ii) (${}^3\text{He}, t$) charge exchange reactions. At energies of about 50-70 GeV/nucleon, mainly the Isobaric Analogue Resonance State (IAS) and at somewhat higher energy (100MeV/n), mainly the Gamow-Teller (GT) resonance are populated. The GT resonance strength can be compared to large-scale shell model calculations that should become possible for nuclei of mass up to 100 in the near future. The GT-strength is also of astrophysical interest. The IAS is a powerful spectroscopic tool to study single particle properties of neutron rich nuclei. Consider as an example the reaction ${}^{133}\text{Sn}({}^3\text{He}, {}^3\text{H}){}^{133}\text{In}(\text{IAS})$. The IAS is the analogue of ${}^{133}\text{Sn}$. The Coulomb displacement energy, determined by the Q-value of the reaction, is directly related to the radius. The IAS will decay by a strong branch via proton emission to ${}^{132}\text{Sn}$. The recoil energy of the triton is very low, in the 1 MeV region. The active target is ideally suited to detect both this very low energy recoil particle, together with the decay proton in the R³B device, in order to sign the reaction.

Detector concept

The active target detector is a relatively novel gas detector concept where the gas constitutes both the target and the detection medium. Mostly, inverse reactions will be used where the target gas is p, d, ${}^3\text{He}$ or ${}^4\text{He}$, either pure or mixed with standard detection gases such as isobutane C_4H_{10} . The recoil particles have mostly very low energy for the most important center of mass angles near zero degree in quasielastic reactions (see figure 2).

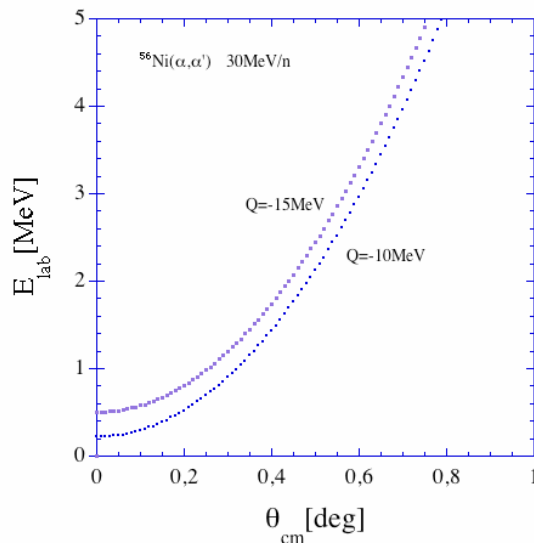


Fig. 2. Kinematics curves for inelastic scattering to giant monopole resonances.

The identification and good resolution of such low energy particles together with high efficiency is most uniquely realized in a gas detector. The working principle of such detectors as the one used at GSI, IKAR [1], and the one tested and used at Ganil, Maya [2], can be characterized as Charge Projection Chamber by analogy with the Time Projection Chambers (TPC) used in Particle Physics. Primary electrons produced by charged particles passing through the gas drift under the influence of an electric field to the readout plane of the chamber where they produce avalanches on anode wires. The induced charge from the avalanches is detected on a cathode plane that has been divided into pads. Typically the induced charge from one avalanche will spread over several pads and the resultant distributions can be used to obtain the localization of the hit in two dimensions. The signal on each of the pads is also sampled in time and from these samples the arrival time of the pulse can be determined, providing a

measurement of the height of the track above the given pad. In this way three dimensional track reconstruction can be achieved.

Such a detector needs a very good position resolution in three dimensions for track reconstruction, and a large dynamic range. This may necessitate the incorporation of magnetic fields in the detector design. It also leads to a very large number of readout channels implying the development of high-density electronics using ASIC technology.

Fig. 3 and 4 show schematic drawings of IKAR and MAYA. IKAR was built several years ago and used to measure the elastic scattering at high energies (1 GeV/nucleon) of light exotic nuclei at PNPI, CERN and GSI [3]. The detector IKAR consists of six in-line axial ionization chambers and has a 2π acceptance in azimuthal angle for the recoil registration. Each anode in IKAR is subdivided into an inner part, permitting the registration of signals from adjacent cells separately, and an outer part, which registers signals from neighboring cells simultaneously. Low-noise current-sensitive preamplifiers coupled to flash-ADCs were used for recording the signals induced by the drifting electrons on the anodes A and B, and the cathodes. This technique permits to deduce not only the energy of the recoils in each one of the six active volumes of IKAR but also the respective recoil angles and the Z-coordinate of the vertices along the chamber axis.

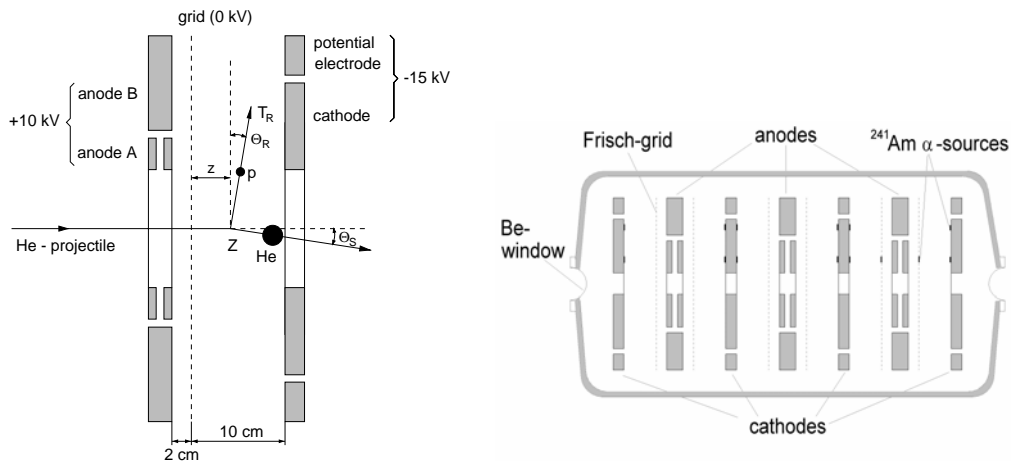


Fig 3: Typical scattering event in IKAR detector and the arrangement of the electrodes inside the chamber

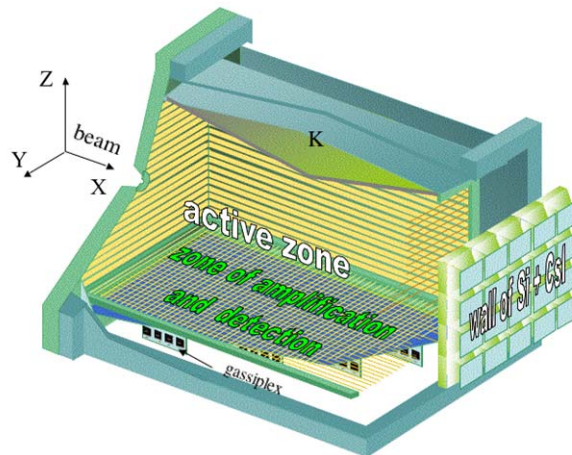


Fig 4: The MAYA detector

The MAYA detector was built more recently at GANIL, where it has been used to measure several types of direct reactions at lower energies (< 50 MeV/nucleon). While these prototype detectors have proven the usefulness of the principle of the active target concept, they have limited dynamic range, position and multi-track resolution. The readout electronics used in MAYA, has not allowed individual pad waveform sampling to be implemented. Both devices are not able to work in the magnetic field, restricting the dynamic range of the devices.

Required R&D

The research and development on the active target concept will be carried out within the ACTAR project of I3NS. There is a large overlap between the groups involved in this JRP and the R³B collaboration. The R&D of ACTAR includes:

- Physics simulations in order to establish the resolutions needed in position, energy, charge and mass, the required dynamic range in energy and charge, and the requirements related to ancillary detector coupling.
- Technical simulations to optimize the geometrical, electrical and magnetic field configurations of the detector.
- Construction of test modules. Several elements of the active target will require dedicated test modules in order to decouple the different problems: investigation of different solutions for read-out chambers (multiwire proportional chambers, micropattern gas detectors), study of properties of gas mixtures, at normal temperature and at low temperature, investigation of gas recycling, search for an optimized geometry of an eventual magnetic field.

The Electronics and data acquisition, and in particular the conception of a dedicated ASIC chip was included in the first draft of the ACTAR collaboration. However, due to the budget reduction applied in the final approval of the I3NS JRP, this part of the R&D had to be abandoned. Therefore it will have to be taken in charge by the participating laboratories outside ACTAR.

As already mentioned, the active target will be used with ancillary detectors in order to cover the complete dynamic range of the outgoing particles. It will be necessary to study whether the other detection systems of the R³B project, in particular the proton and heavy fragment detectors are suitable or if additional ancillary detectors have to be provided.

Test experiments

When the test modules have been designed and constructed, together with their electronics and data acquisition, they will be tested in-beam at several laboratories. These will be GANIL (low-intermediate energy range), GSI (medium-high energy) and JINR Dubna (intermediate energy). This will allow detailed evaluations to be made of the various concepts in a real experimental situation. It will also allow optimization of the particle tracking algorithms to be made.

Manpower

During the three years of the ACTAR project (2005-2007), the estimated manpower is around 200 man-months, 138 man-months for the physicists/engineers from the different institutions involved, and 65 for post-docs financed by EU.

The development of a new ASIC for the digitalization of the signals would require 100 man-months. This development should be made in collaboration with other sub-groups.

Schedule

2005	2006	2007	2008	2009
Design simulations Detailed design study	Construction of test modules	Construction of test modules	In beam tests at GANIL/GSI/Dubna Design of new ASIC	In beam tests at GANIL/GSI/Dubna Design of new ASIC

The members of this working group are given in section G. This project will be coordinated by GANIL.

References

- [1] A.A. Vorobyov *et al.*, NIM in Physics Research 119 (1974) 509.
- [2] MAYA, GANIL Internal Report 27.2002.
- [3] S. Neumaier *et al.*, Nucl. Phys. A712 (2002) 247.

B1.9. Low-energy neutron detector

Design goals

Spin-isospin giant resonances can be strongly excited in (p,n) reaction using inverse kinematics. One can use at the same time thick targets, without disturbing the energy spectrum of the recoiled neutrons, which has an importance in experiments with rare isotope beams.

As a typical example, we assume radioactive beam of ^{132}Sn with an energy of 400 AMeV. The angular dependence of the energy of the recoiled neutrons is shown in the Figure below. We want to measure the differential cross section for the 1-5° C.M. angular range in order to resolve the states populated with $L=0,1$ and 2 angular momentum transfer. The excitation-energy range of 10 MeV to 50 MeV would contain most of the strength of the relevant giant resonances. We are aiming at an energy resolution of 1 MeV in excitation energy.

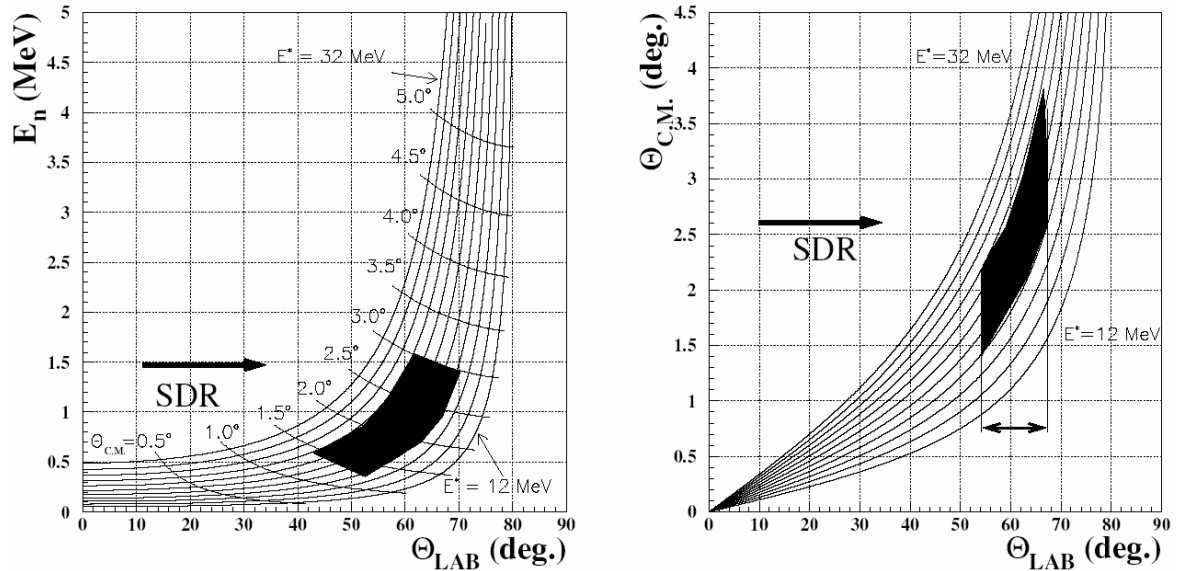


Figure 1. Energy (a) and CM-angle (b) of the recoiling neutrons in the $^1\text{H}(^{132}\text{Sn}, ^{132}\text{Sb})n$ reaction at 400 AMeV bombarding energy. The best regions for investigating the Spin Dipole Resonance (SDR) are indicated in the figure.

To achieve this goal we should measure the energy of the neutrons with better than 10 % resolution and the scattering angle in laboratory frame with better than 1° angular resolution. We require also high efficiency for the spectrometer. The best candidate for such a setup is a time-of-flight (TOF) ball consisting of plastic scintillators.

Realization of a TOF ball

The relative energy resolution of the TOF method is given by:

$$\frac{\delta E}{E} = 2 * \sqrt{\left(\frac{\delta d}{d}\right)^2 + \left(\frac{\delta T}{T}\right)^2},$$

where d is the flight path, T is the flight time, and δd , δT are the respective resolutions (FWHM). For infinitely good time resolution ($\delta T = 0$), the energy resolution is limited by the finite detector thickness δd , since the interaction can occur anywhere within the detector.

The efficiency requirement of at least 30% constrains the thickness of the scintillator to be more than 4 cm. If we combine this with the necessary energy resolution of 10%, then the necessary flight path should be 1 m. The flight time of a 5 MeV neutron in this spectrometer would be 33 ns so if we can

R3B

measure the time of flight with a resolution of 1 ns then the error coming from the TOF measurement would be less than 6%.

The main problem of such a TOF detector is detecting the low-energy neutrons. Using plastic scintillators the lowest energy threshold is typically about 50 keV electron equivalent, which causes a considerable efficiency loss already at a neutron energy of 1 MeV. However, a recent R/D using a conventional plastic scintillator wrapped in a special plastic foil (VM2000 developed by 3M) resulted in much better results. With this special wrapping one could go down to 5 keV and still could produce a clean trigger. Assuming a threshold of 5 keV in the neutron detector we can safely go below 0.5 MeV neutron energy without losing too much efficiency.

Simulations in Debrecen

The exact geometry of the setup is under discussion. It depends on multiple parameters and we need a reliable simulation of the setup. We have started Monte Carlo simulations with the code GEANT 4 to define the optimum geometry.

Test experiments in Debrecen

We have built already one detector unit with a 100x45x10 mm fast plastic scintillator and tested its efficiency as a function of the neutron energy using a ^{252}Cf source. Standard NIM and VME electronic modules were used for processing and digitizing the signals. We are planning to do this kind of tests also with mono-energetic neutrons produced by our 20 MeV cyclotron.

Time schedule

	2005	2006	2007	2008
Simulations	xxx			
Final design	xxx			
Construction		xxx		
Beam tests			xxx	
Implementation				xxx

This subproject is coordinated by Debrecen.

B.1.10. High resolution neutron time-of-flight spectrometer

a) Design goals

A high-resolution neutron time-of-flight spectrometer is required to determine the momenta of high-energetic neutrons resulting from the decay of the projectile [LoI-04]. A momentum resolution of $\Delta p/p$ of 10^{-3} similar to that for the charged particles is desired, resulting in resolution requirements for the time of flight of $\sigma t < 100$ ps and a position resolution of $\sigma_{x,y,z} \approx 1$ cm for given flight paths in the range from 10 to 35 m. For an experiment on a medium mass nucleus at about 500 MeV/nucleon, invariant-mass resolutions of about $\Delta E = 10$ keV at 200 keV above the neutron threshold ($\Delta E = 30$ keV at 1 MeV respectively) will be reached using the maximum flight path.

With the existing neutron detector LAND (Large Area Neutron Detector) [Bla-92] invariant-mass resolutions of the order of 200 keV at 1 MeV above the neutron threshold are obtained. This detector is built in a modular sandwich structure using iron converter and organic scintillator providing a time resolution of $\sigma t = 250$ ps and a position resolution of 10 cm. The detection efficiency for neutrons with energies above 400 MeV is larger than 90% [Bor-03].

For the new detector, a similar or even improved neutron detection efficiency is demanded together with a high multi-hit capability for up to 5 neutrons.

An active area of 2×2 m² of the neutron detector at a distance of 12.5 m to the target will match the angular acceptance of ± 80 mrad for the neutrons defined by the gap of the superconducting dipole magnet.

b) Neutron detection – hadronic shower properties

High-energetic neutrons are detected via their hadronic interactions leading to the emission of charged particles and gamma rays. Detailed knowledge about the properties of the neutron induced hadronic showers is indispensable for the design studies of a neutron detector. Therefore recently, simulation studies were started [Rad-04] investigating neutron interactions on iron using the Monte-Carlo simulation code FLUKA [FLUKA], resulting in double-differential yields for protons, pions, and gammas as produced by neutrons with energies of 200, 500 and 1000 MeV hitting an iron plate with a thickness of 5 mm.

Figure 1 shows the absolute proton yield calculated for 500 MeV neutrons. The solid line connecting the dots represents the yield integrated over the whole angular range, underlying are curves for $\theta = 0-5^\circ$ (solid), $5-20^\circ$ (dashed), $20-80^\circ$ (dashed-dotted), $80-120^\circ$ (dotted) and $120-180^\circ$ (densely dotted). It turns out, that to about 50%, the energy of the proton is larger than 110 MeV, to about 75%, E_p is larger than 60 MeV.

The contributions from charged pions are found to be one to two orders of magnitude suppressed compared to protons for 500 MeV neutrons. There is a substantial amount of γ -emission found with γ -energies up to 10 MeV, the distribution is dominated by transitions from the first and second excited state in ⁵⁶Fe.

Figure 2 shows the integrated proton yield per incident neutron as a function of the neutron energy.

As a next step, more detailed simulation studies will be carried out, allowing also for correlations between different particles originating from one neutron interaction and for a propagation of the particles through realistic detector geometries and materials.

c) Design concepts

Detection based on resistive plate chambers

General design considerations

Resistive Plate Chambers (RPC) are detectors for ionizing particles and presently, these types of detectors are used in many different experiments involving cosmic rays and accelerators such as STAR, RICK, CMS and ATLAS at LHC, CERN, AGRO etc. [RPC-0 4]. Excellent time resolutions down to

$\sigma t < 50$ ps [Fon-00] were achieved for minimum ionizing particles using multi-gap resistive plate chambers (MRPC), introduced by [Cer-96]. Building of large detector arrays with high granularity is feasible, thus RPC detector systems partly take over the classical application of scintillators for ToF-arrays. A. Blanco et al. [Bla-02] showed that a large area MRPC (160 cm \times 10 cm, 2 strip readout) can provide good time resolutions of $\sigma t \sim 50$ -70 ps and a position resolution of 1.2 cm along the strips using time the difference method. In addition, an efficiency for minimum ionizing particles of more than 95% was reached.

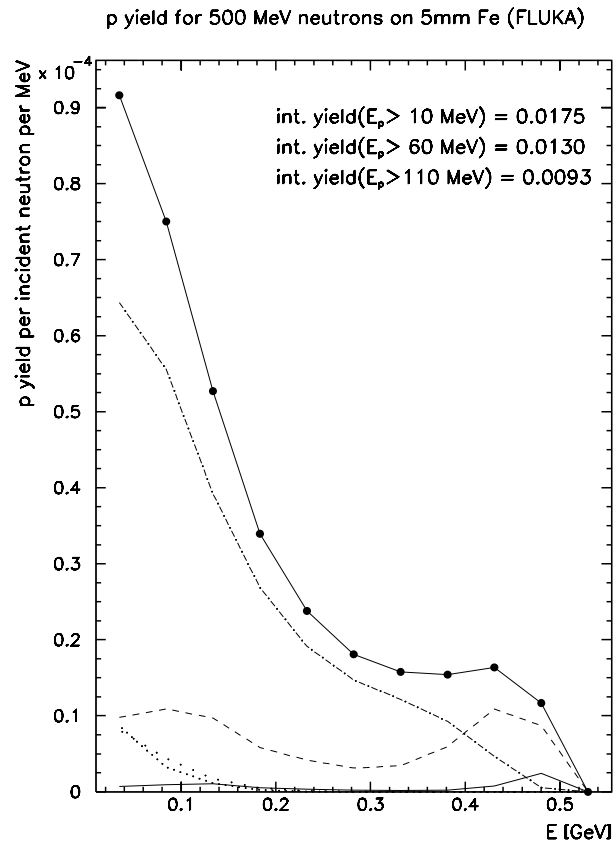


Figure 1. Absolute proton yield calculated for 500 MeV neutrons. The solid line connecting the dots represents the yield integrated over the whole angular range. The other curves show the yield for angular ranges of 0-5° (solid), 5-20° (dashed), 20-80° (dashed-dotted), 80-120° (dotted) and 120-180° (densely dotted).

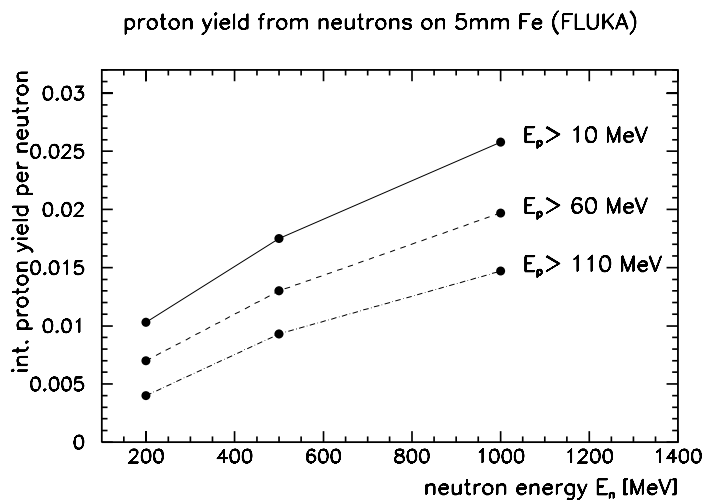


Figure 2. Integrated proton yield per incident neutron as a function of the neutron energy.

With the impressive time resolutions accompanied by good positional resolutions using either a strip readout, pad readout, or using the granularity of the system, MRPCs appear to be ideally suited for the detection of the charged part of the hadronic shower induced by neutrons. Improved resolution should also allow for a much improved tracking of the induced hadronic shower and thus for a more efficient multi-hit resolving power.

A neutron detector concept based upon RPCs is investigated in the following. A sandwich structure of converter material (iron, tungsten) and RPC arrays is foreseen.

Exemplarily, a detector is visualized with $2 \times 2 \text{ m}^2$ active area and about 0.8 m depth formed from alternating layers of iron converter of 1 cm thickness followed by arrays of RPCs built up from modules of $100 \times 3 \text{ cm}^2$ with a depth of $\sim 1.1 \text{ cm}$, arranging 2×67 modules to cover the active area. With stacking of 35 of these combined converter/RPC structures, the depth of the detector material corresponds to more than 3 interaction lengths ($\lambda_1 \approx 17.8$ (33) cm for Fe (RPC materials)) in order to provide a detection efficiency for fast neutrons of more than 90%.

The time signals induced by a hadronic shower particle are taken from the anode for both far sides of the RPC chambers, thus allowing for mean timing information and for position information within the length of the chamber via the time-difference method.

The position of the hit in the two additional dimensions is obtained from the granularity of the detector system, i.e., by the width of the RPC chambers (3 cm) and the depth of the converter/RPC structures (2-3 cm), respectively, leading to resolutions of $\sigma_{y,z} \approx 1 \text{ cm}$.

This example amounts to a total number of 4690 RPC chambers (35 planes, 2×67 RPC's per plane) and a number of 9380 signals to be read out. The active area covered by RPC's sums up to 140 m^2 . Alternatively a width of the RPC chambers of about 10 cm is considered, using multi-strip anodes to obtain the position resolution, leading to about 1600 RPC chambers needed for the neutron detector.

Enlarging the size of the RPC modules from 1 m to 2 m length would reduce the number of channels by a factor of two, reducing the price for the electronics by a factor of two. The technical feasibility for these long chambers will be proven.

Simulation studies and prototype tests

According to our knowledge, no explicit experimental studies exist up to now for the response of RPC detectors to high energy neutrons (50-1000 MeV) and the charged particles produced from the neutron induced reactions (see section on hadronic shower). For the neutron sensitivity of a double-gap RPC, simulations were performed over a wide neutron energy range [Alt-01]. Experimental data on neutron sensitivity exist only for neutrons with 2 and 20 MeV being in agreement with the simulation [Abb-03].

Therefore, extensive studies comprising test experiments using RPC prototypes and detailed simulations of the RPC performance for neutrons, respectively protons, with energies from 50-1000 MeV will be carried out within the next two years.

The simulations will comprise i) studies of the neutron induced shower production allowing for optimizations on the geometrical design and ii) studies of the intrinsic time response for MRPCs, allowing for optimizations of dimensions and type of resistive plates, number of gaps, gas mixtures etc. Monte-Carlo model calculations exist for the avalanche development considering space charge effects [Fon-0b], [Rie-03], also analytical calculations exist [Man-04].

For the geometrical design of the RPCs we have to take into account mechanical stability, different readout schemes, multi-hit capabilities, chamber size versus number of readout channels etc..

Additionally, the possibilities of using the RPC structure as a supplementary neutron converter have to be investigated, i.e., a double-stack multi-gap RPC with an increased thickness of the anode is conceivable, using this anode as an additional converter material.

Alternative: detection based on scintillator

General design considerations

In parallel to the investigations on the above discussed RPC neutron detector concept, we prepare another detector solution based on the technique used for LAND using alternating iron converter and organic scintillator layers arranged in a paddle structure and readout from both sides via photomultipliers. In order to reach the design goal for the spatial resolution of 3 cm, the size of the paddles has to be decreased to 2m×3cm×3cm (now 2m×10cm×10cm). Simultaneously, an improved time resolution is expected from the decreasing paddle depth, additional optimizations of light guides, scintillator, and photomultipliers will be investigated.

A detector built similar to LAND using 2 m long and 3 cm high paddles comprising 1.5 cm iron and 1.5 cm scintillator each needs 67 paddles per plane ($2 \times 2 \text{ m}^2$) and 34 planes to fulfill the efficiency goals, thus leading to more than 4500 photomultiplier signals.

Since the costs of the scintillator-based concept are dominated by the amount of photomultipliers, methods of reducing the number of photomultipliers without losing resolution are under discussion, i.e. replacing the one-dimensional paddle structure with 3 cm width by a crossed scintillator structure with 10 cm width using the time-difference method for the position determination in two dimensions. Using this geometry could save up to 30% for the photomultipliers and its power supplies. The mechanic efforts, however, would be much increased.

As a matter of fact, the neutron efficiency, the neutron time and positional resolutions, and the multi-neutron recognition, would gain from abandoning the sandwich structure with converting the neutron in a passive volume. Inorganic scintillators with high densities would allow for such a detector concept, i.e., BaF_2 or PbWO_4 are possible candidates. Especially PbWO_4 has an impressive high density of 8.3 g/cm^3 and an interaction length of $\lambda_I=18 \text{ cm}$, thus reducing the detector depth to about 60 cm. Unfortunately, the costs for inorganic scintillators (BaF_2 , PbWO_4) are in the order of some US\$/ cm^3 and the needed quantity is about 2 m^3 thus making such a concept unaffordable.

d) Radiation hardness

The detector will be used for experiments with radioactive beams with maximum production rates of 10^8 to 10^9 particles/s. Assuming a target thickness corresponding to 1% interaction probability, maximum neutron fluxes of 10^6 to $10^7/\text{s}$ are expected, distributed over the 4 m^3 volume of the detector. Most of the experiments will deal with very rare ions (down to 100/s), therefore for the estimation of the overall dose on the neutron detector, a mean value of 10^6 ions/s and equivalent 10^4 neutrons/s are taken into account.

With a running time of 2 months per year, 5×10^{10} neutrons/year will be deposited in the detector volume, neglecting duty cycle.

RPCs are widely used in high energy physics, where rates/ cm^2 are usually up to 5 orders of magnitude larger than in our experiments (typically 0.02 Hz/cm^2). Therefore, radiation hardness of the RPC neutron detector is uncritical, nevertheless, in the following, we give an evaluation of the effect of the dose on the neutron detector. The 5×10^{10} neutrons/year hitting the detector translates into 10^6 counts/ cm^2/year assuming 3 RPC counts per neutron hit. Aging effects for RPC's are evaluated by the total charge flow across the detector during its lifetime, assuming an average avalanche charge of 10 pC, the total charge integrated over a period of 10 years amounts to about 0.1 mC.

Recent studies for MRPCs operated in the avalanche mode showed no aging effects up to 10 mC/cm^2 [Aki-04] and even for 800 mC/cm^2 [Lop-04].

Also for the scintillator concept, aging effects due to deposited energy seem to play a minor role. The accumulated dose due to the 5×10^{10} neutrons/year is estimated to be of the order of 1 mGy. [Abr-98] performed detailed studies on radiation hardness of detectors built from organic scintillator combined with WLS bars, and it was shown, that a neutron dose of nearly 500 Gy leads to decrease of the light output of the order of 10%.

The active size of the detector will cover, similarly to the existing LAND, $2 \times 2 \text{ m}^2$ area, while the active depth depending on the detailed structure of the detector will not exhaust 2 m (1m actually foreseen). Including the support structures, the outer dimensions should not exceed $4 \times 3 \text{ m}^2$ on the floor with a height of 4m. Additional space is needed for electronic racks, power supply, cooling and possibly gas supply, amounting to 30 m^2 . The detector is designed to be moveable from a position of about 10 m from the target to a maximum distance from the target of 35 m.

f) Test experiments

During the next two years, test experiments are indispensable, in order to investigate the response to fast neutrons (respectively to their products) for both RPC detectors and for scintillator concepts also. The maximum achievable time resolution has to be determined, depending on detector size and geometry. Therefore, proton beams with energies of 50-1000 MeV are necessary, as turned out in the simulations, and for the prototype tests, neutron beams of 200-1000 MeV, produced from deuteron and triton break up.

g) Calibration

After having set up the neutron detector, one calibration run is needed using tagged neutrons from the deuteron (and triton) breakup varying the beam energy in the range of 200 to 1000 MeV to investigate in detail the neutron efficiency and the neutron response behaviour for one- and multi-neutron hits. The time adjustment of the modular detector system can, as it is done for LAND, be performed by tracking cosmic rays passing the detector volume.

h) Milestones

2005-2006	Simulation and detector tests (RPC and scintillator), prototyping
End 2006	Final decision on detector concept
2007	Production and test of "Module 1", investigations on serial production
2008-2010	Construction, installation, tests, commissioning

i) Personnel estimates and responsibilities

In addition to the persons actually involved in the neutron detector working group (see section G), we need for the R&D and test phase (2005-2007) at least 4 people to work full time on the project for 3 years, e.g., 3 post-docs and 1 engineer, for the construction phase at least 1 engineer working full time on the project for 3 years is needed. Additionally 1 post-doc for about 3 years is needed for the development of slow control and software for the operation of the neutron detector.

Within our working group, people from universities of Cracow, Frankfurt and Mainz and GSI are involved, who were involved in the development of the existing neutron detector LAND.

One part of our working group from SINP, Kolkata, India has some expertise in the development of RPCs for the iron calorimeter type detector system for the India based Neutrino Observatory. They are interested to take the responsibilities of developing the prototype RPC detectors for the neutron detector. Additionally, at GSI, we can profit from in-house knowledge, since the FOPI RPC detectors were developed here and parts of the HADES RPC concept also. Within the R³B working group, RPC chambers are also developed for heavy ions by the Santiago de Compostela group, and we can profit from the partial overlap of investigations.

This project is coordinated by GSI.

References

- [Abb-03] M. Abbrescia et al., NIM **A508** (2003) 79-82
- [Abr-98] V. Abromov et al., NIM **A419** (1998) 660-666
- [Aki-04] A.V. Akindinov et al., NIM **A533** (2004) 93-97
- [Alt-01] S. Altieri et al., NIM **A461** (2001) 57-59
- [Alv-04] H. Alvarez-Pol et al., NIM **A535** 277-282
- [Biz-03] A. Bizetti et al., NIM **A515** (2003) 348-353

R3B

- [Bla-92] Th. Blaich et al., NIM **A314** (1992) 136
- [Bla-02] A. Blanco et al., NIM **A485** (2002) 328-342
- [Bor-03] K. Boretzky et al., PRC **68** (2003) 024317
- [Cer-96] E. Cerron Zeballos et al., NIM **A374** (1996) 132-135
- [FLUKA] <http://www.fluka.org> and reference therein
- [Fon-00] P. Fonte et al., NIM **A449** (2000) 295-301
- [Fon-00b] P. Fonte et al., NIM **A456** (2000) 6-10
- [LoI-04] NUSTAR Letters of Intend, April 2004, p95 ff.,
<http://www-w2k.gsi.de/superfrs/documents/nustar/LoI/NUSTAR-LoI.pdf>
- [Lop-04] L. Lopes et al., NIM **A533** (2004) 121-125
- [Man-04] A. Mangiarotti et al., NIM **A533** (2004) 16-21
- [Rad-04] T. Radon, private communication
- [Rie-03] W. Riegler et al., NIM **A500** (2003) 144-162
- [RPC-04] Proceedings of the seventh international workshop on resistive plate chambers and related detectors, Clermont-Ferrand, France, 20-22.Oct 2003, NIM **A533** (2004) 1-238
- [Sch-04] A. Schuettauf, NIM **A533** (2004) 56

B.1.11. Multi-track ion detector for spallation and fission measurements

This subsection describes the principles of a multi-track detector to be installed downstream of the R³B magnet in order to detect and reconstruct multi-particle final states of nuclear reactions such as spallation or fission reactions. In order to be fully efficient, such a detector has to be combined with three other devices: A multi-hit position detector in-between the target and the magnet entrance, a high-resolution time-of-flight counter and a thin hydrogen target. The new type of hydrogen target is described below while the position and the time-of-flight counters are only briefly mentioned since they are described in other sections of the present proposal.

The most demanding requirements for his detection setup come from the experiment aiming at a kinematical complete measurement of spallation reactions of heavy nuclei, which is discussed in more detail in the following.

Final states of spallation reactions $A+p$ with $A \sim 200$ at energies around 1 $A.GeV$ have the following features:

- 1 or 2 heavy fragments, depending on the de-excitation channel (evaporation of the projectile or fission)
- Average neutron multiplicity: 15 - 20
- Maximal neutron multiplicity: 35-40
- Average multiplicity of light-charged spallation fragments: 3 or 4 with a kinetic energy in the center of mass frame below 30 MeV
- Maximal multiplicity of light-charged fragments (including protons): 12
- Roughly 2/3 of the particles with a center of mass kinetic energy below 20 MeV , an estimate which depends only lightly on the theoretical models.

The neutrons will be detected with the neutron time-of-flight spectrometer described in section B.1.10 similar as in the SPALADIN experiment performed at the present facility using the ALADIN LAND setup, see Figure 1. An event by event determination of their multiplicity will be performed.

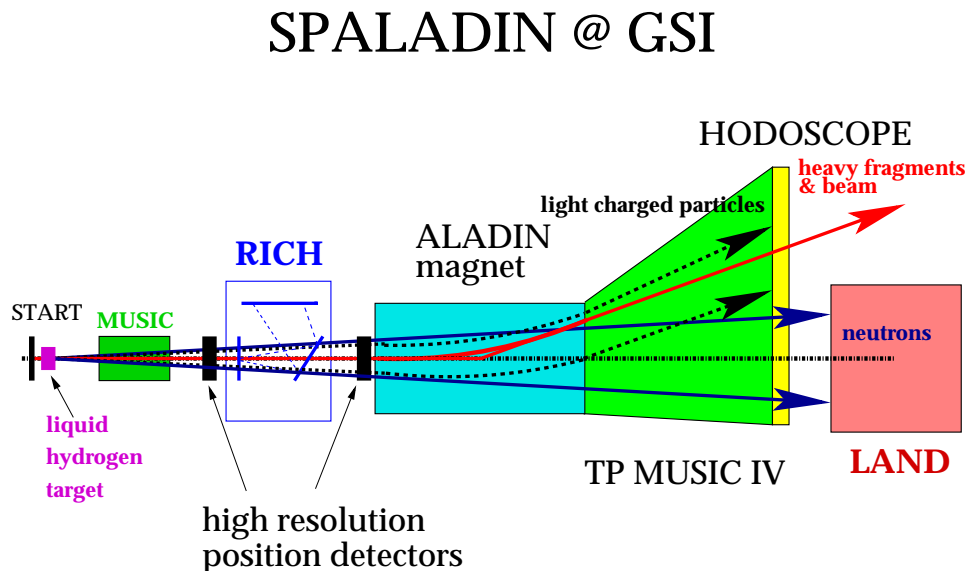


Figure 1. Schematic view of the SPALADIN set-up in Cave B of GSI.

Contrary to the present SPALADIN set-up, given in Fig. 1, it is mandatory for the spallation studies of heavy fragments to have as much as possible vacuum on the paths of the produced fragments, from the reaction vertex to the detectors downstream of the magnet. For heavy projectiles, the major experimental constraints in spectrometry and mass identification are multi-scattering and secondary reactions. Multiple scattering destroys the angular and position information of the ions. Secondary reactions, whose

probability is greater for heavy ions, perturb the correlation between the projectile residue and the other fragments emitted in the reaction of the compound nucleus mass, charge and energy balance of the events. Both constraints are related to the presence of matter on the flight path of the ions. This implies that the target detectors for position and velocity determination should represent very thin layers of material. In such a scheme, a RICH (ring imaging Cerenkov) with a thick radiator cannot be used, as in SPALADIN, and high resolution ToF measurements techniques combined with accurate flight path length determination from the magnetic analysis are necessary.

As it is the case in the present ALADIN / LAND / MUSIC IV set-up, a multi-track charged- particle detector has to be studied, designed and built to cover the exit aperture of the large-acceptance R³B dipole magnet (GLAD). This will be the subject of the first sub-project of the next section. Furthermore, to ensure a good reconstruction of the heavy fragments magnetic rigidity, it is necessary to measure the position at the entrance of the R³B-GLAD magnet. In order to cope with fission decays and IMF production channels, these position detectors have to be equipped with multi-hit readout capability. Such detectors will be described in the second sub-section. Mass determination needs a precise measurement of the time of flight (ToF) of the heavy ions as will be briefly discussed in the third sub-section. Finally, a fourth sub-section will describe the design of a new type of hydrogen target. There are two possibilities for this target: The first is the use of a solid hydrogen target with which we can get rid of the cell walls; the second one is to use a low pressure target to reduce drastically the thickness of the target cell walls. With such a new type of target, the contribution of empty target events will be very small relatively to $A+p$ events or will be even zero without target cell walls.

Multi-track detector

Two main goals have to be reached with the multi-track detector:

- The spectrometry of reaction fragments at the 10^{-3} level in momentum resolution in the laboratory frame,
- The charge identification of these fragments from $Z = 1$ to $Z = 92$.

Furthermore it has to be added that, since we intend to measure absolute cross-sections for the different final states of spallation reactions, this detector has to provide a detection efficiency very close to 100 % even for light fragments ($Z = 1$ or 2).

For light reaction products, such a detector will allow for the reconstruction of the kinematics at the reaction point in angle and momentum and thus for the kinematical reconstruction of the variables in the center of mass frame. For heavy fragments, fission products or projectile evaporation residues, this detector, whose information will be combined with that of the position detectors upstream of the magnet, will provide the magnetic rigidity of the fragments with a resolution in mass of $A/\Delta A \sim 300$ (FWHM) in conjunction with high-resolution ToF measurements, necessary for a clean identification of the isotopes in the final states. Combined with the analyzing power of the magnet, this means that a spatial resolution of roughly $100 \mu m$ (FWHM) has to be aimed at in the detector design.

This detector will have to assure a multiple sampling measurement of trajectories. There are three reasons for this:

- To perform Z identification with ΔE measurements for charges from 1 to 92, the sampling of the primary energy loss signal has to be large enough (to be specified quantitatively, depending on the detector and its active material)
- Distinguishing efficiently the tracks for relatively high-multiplicity events (as expected for spallation of heavy nuclei) with points taken on different planes (as with MWPCs for example) implies working on a huge combinatory of points which can only be avoided if continuous measurements of tracks are performed
- This is all the more difficult as the magnetic optics constraints given by the transport in GLAD are small because of its large acceptance so that many different types of trajectories (position and angle combinations in both the dispersive and the non-dispersive plane) have to be taken into account. In practice, in such a set-up, events with multiplicities larger than 4 cannot be efficiently reconstructed with MWPC's, as was shown by simulations [14].

To do this, a gaseous detector such as a time projection chamber (TPC) is required. For such a detector, we will need to have:

- Vertical drift lines for the primary signals in order to assure the highest position resolution in the horizontal plane (the magnet dispersive plane) by charge division using collecting pads,
- Multi-hit readout with flash-ADCs in order to distinguish two trajectories on the top of each other in the detector.

The density of trajectories in this detector will be quite reasonable once the distribution of δ -rays around the beam and the heavy fragments will have been considered. The light-fragment multiplicity of about 4 (and up to 12 in very excited systems) as given above, will have to be detected in a surface orthogonal to the main component of the momentum (the direction of the beam at the exit of the magnet) of around $50 \times 50 \text{ cm}^2$ for the major part of it (corresponding to an acceptance in kinetic energy of 40 MeV in the center of mass frame). This means in particular that the probability that two fragments trajectories are parallel and closer than 5 mm is very small. This implies that the spatial transverse extension of the primary signal before amplification can be of the order of $3\text{-}5 \text{ mm}$ (FWHM) with a very small probability that two primary signals overlap. Thus if pads are used to collect primary drifting charges in such a detector, their size can be of the order of $0.5 - 1 \text{ cm}$. Of course, all these quantities will have to be estimated precisely with proper tests and detector simulations. A compromise between the number of channels (price) and the granularity of the detector (performance) will have to be found.

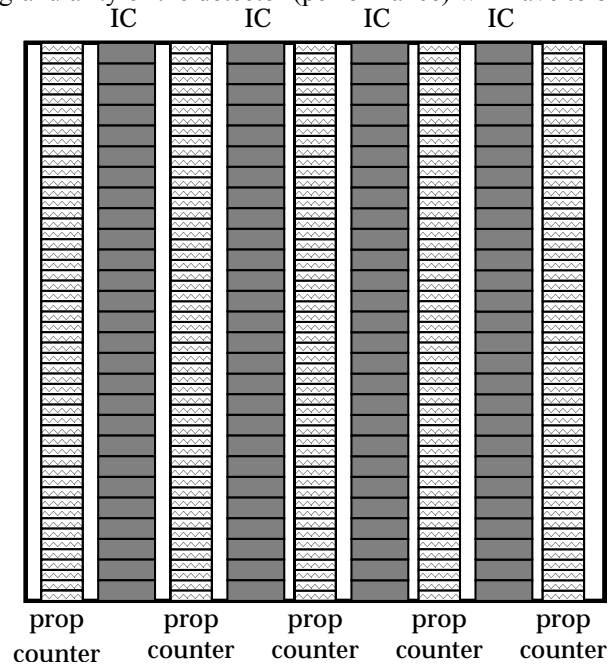


Figure 2: Detection scheme (top view) for the TPC. **IC**: Ionisation chambers (counters **without** primary signal amplification for the heavy residues); **Prop counter**: Proportional counters (counters **with** linear anode wire amplification for light fragments). The beam comes from the left. Typical dimensions for the TPC are 1 meter in the beam direction and 2 meters in the orthogonal direction (dispersive plane).

One of the major concerns for such a detector is the fringe field of the large acceptance GLAD magnet. In fact, for a good collection of primary signals after the drift along a few 10 cm lines, the active area of the detector has to be shielded against the magnet fringe field. As far as the latest designs of the magnet are concerned, this fringe field may be large at the exit so that we will have to install our multi-track detector further downstream and/or protect it against magnetic field with iron, which means then that it will have to be larger and thus more expensive. A good magnetic shielding scheme has first to be found in order to make this detector performing, not too large and, thus, not too expensive. A first “guess” for the distance between the exit plane of GLAD and the active volume of the TPC is 200 mm , value based on the existing TOSCA maps of the conceptual design.

Other issues have been already identified and are being worked-out:

- Is there a need to protect the active volume from the beam passing through and generating δ -rays in the gas of the detector?
- How can δ -rays be handled in the detection as well as in the subsequent data analysis?
- Performances of the detection and readout system with a dynamical range from 1 to 10000 with 1 bit resolution (for Z identification through ΔE measurement and digitization on 14 bits if a unique readout is used)
- High efficiency in both the detection and the track reconstruction of light-charged fragments.

This detector design will begin by studying the possibilities offered by the already existing MUSIC IV, recently upgraded by the ALADIN group of GSI [spall15] and used in the SPALADIN experiment. With respect to the new R³B GLAD magnet, concerns come mainly from the dimensions of this detector compared to the physical aperture of the magnet and the fringe field of this magnet. With respect to SPALADIN experiments, three issues have to be solved:

- The higher multiplicities of tracks from charged fragments to be efficiently reconstructed,
- The efficiency of the proportional counters of this detector which needs to be large even for $Z = 1$ particles (mainly protons and deuterons in spallation reactions),
- The need for a measurement in the same counters and ADC's of fragments of charge going from $Z = 1$ to $Z = 92$.

A proper consideration of these problems leads to the definition of the detection scheme of Fig. 2.

Table 1. Tracking efficiencies (P_{TRACK}) for a given single-proportional-counter detection efficiency (P) in two geometries (4 & 5 planes) according to the different conditions demanded to the tracks of an event (X/Y : X planes with a hit out of Y planes).

4 planes	4 / 4	3 / 4	2 / 4	
$P = 0.8$	$P_{\text{TRACK}} = 41 \%$	$P_{\text{TRACK}} = 82 \%$	$P_{\text{TRACK}} = 97 \%$	
$P = 0.9$	$P_{\text{TRACK}} = 66 \%$	$P_{\text{TRACK}} = 95 \%$	$P_{\text{TRACK}} = 100 \%$	
$P = 0.95$	$P_{\text{TRACK}} = 82 \%$	$P_{\text{TRACK}} = 99 \%$	$P_{\text{TRACK}} \sim 100 \%$	

5 planes	5 / 5	4 / 5	3 / 5	2 / 5
$P = 0.8$	$P_{\text{TRACK}} = 33 \%$	$P_{\text{TRACK}} = 74 \%$	$P_{\text{TRACK}} = 99 \%$	$P_{\text{TRACK}} \sim 100 \%$
$P = 0.9$	$P_{\text{TRACK}} = 59 \%$	$P_{\text{TRACK}} = 92 \%$	$P_{\text{TRACK}} = 99 \%$	$P_{\text{TRACK}} \sim 100 \%$
$P = 0.95$	$P_{\text{TRACK}} = 77 \%$	$P_{\text{TRACK}} = 98 \%$	$P_{\text{TRACK}} \sim 100 \%$	$P_{\text{TRACK}} \sim 100 \%$

The optimal gas for the detection in this TPC has not been so far the subject of investigation. However, as in the TP-MUSIC IV, P10 gas seems to be a good candidate in order to have a good drift velocity at a reasonable E/P ratio: $5.5 \text{ cm}/\mu\text{s}$ at $E/P \sim 150\text{-}160 \text{ V}/\text{cm}/\text{bar}$ which gives 8000 V of electrostatic voltage for a drift dimension of 50 cm which remains in quite conventional standards for commercial DC power supplies. In the following, we will take P10 at atmospheric pressure for the detection gas in the TPC.

According to the necessary resolution for the energy loss of the fragments in order to be able to discriminate between their different charges, a sampling of 100 cm of P10 at atmospheric pressure is needed. This parameter is fixed by considering the Landau distribution of energy losses of fragments inside the gas: The distribution width has to be smaller than the distance between the two most probable energy losses of fragments of charge Z & $Z+1$, taking into account the work of G.D. Badwahr [spall16].

As can be seen on Fig 2., the TPC will consist of a series of five proportional counters (“prop counters” on Fig. 2), i.e. with amplification of the primary signals on an anode wire, “dedicated” to the detection of light-charged fragments and four ionization chambers (IC on Fig. 2, without amplification of the primary signals) which will be dedicated to the proper identification of heavier fragments. This distinction allows for a reduction of the dynamics needed for the readout electronics if we allow for a certain saturation of the ADC signals of the proportional counters. In such a case, we have to make sure that this saturation

does not create too large a distortion of the time-sampling readout, preventing thus a complete detection of the tracks close to the passage of the heavy fragments. In such a detection scheme, different pad widths can be used since the multiplicity of heavy fragments will be small in spallation events (“heavy” means here $Z > 6$) which permits to reduce the numbers of pads (and thus of readout channels in the detection).

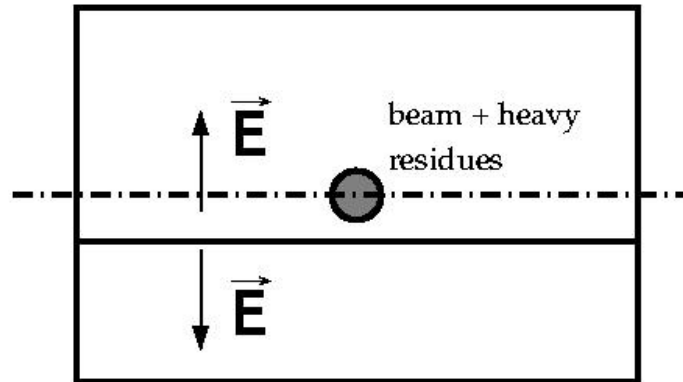


Figure 3. Schematic view of the TPC from the beam direction downstream (front view). The beam and the heavy-residue envelope are drawn in grey. The cathode dividing the electrostatic volume into two parts is shown below the beam and heavy-residue envelope.

The number of detection planes is not fixed yet. The first choice of five planes for the proportional counters is based on the calculations presented in Tab. 1 and on our present experience of the TP-MUSIC IV as we could use it during the SPALADIN & S254 runs. We can see in Tab. 1 that (i.e. with a hit on 3 different planes, the tracking efficiency inside a 5 planes TPC is almost 100 % even with a single plane efficiency of only 80 %). Since 80 % is so far the value of the detection efficiency we have in the proportional counters of the TP-MUSIC IV for $Z = 1$ charge particles, with an upper limit which will be hard to pull above 90 % for reasons not yet understood (but the data analysis is still going on), we have to take into account such a possibility for this multi-track detector for spallation experiments with GLAD. Let us mention anyhow that the single-plane detection efficiency for fragments of charge $Z = 2$ or 3 is much higher and of no concern in the SPALADIN data. This should be the same for the TPC for GLAD. Furthermore, since we want to measure cross-sections and compare, for given compound nuclei, branching ratios of different de-excitation channels with thus different fragment species and different detection efficiencies on the single-plane-proportional-counter level, we have to have tracking efficiencies very close to 100 % for an accurate experiment. Moreover, but this will be an outcome of, the requirement to have 2 hits in two planes may not be constraining enough on the proportional-counter hit patterns in order to distinguish between real tracks, δ -rays and accidentals. This will be studied in details in the present data analysis of the S254 and SPALADIN experiments. This issue is all the more important as the geometry of the tracks at the exit of GLAD will be wide and will not allow for very narrow cuts, generating this way small optical constraints on these tracks. Demanding for three aligned hits will help a lot in the data analysis and will also provide in-line control of the detector resolution as well as of the single-plane efficiencies according to each particle type.

The optimization of the detection scheme (pad width, minimal requirements for track identification in terms of number of planes and of neighbor pads in a plane to define a hit and the geometry) is the subject of a dedicated numerical simulation including geometry considerations, simulation of the drift of the primary signals and the generation of δ -rays on the way of the heavy fragments.

In Fig. 2 (top view), it is shown that the primary signals will be collected on pads. These pads will be read-out individually. In such a scheme, the charge division technique for coordinate reconstruction (center of gravity and other methods) will be used for the horizontal plane coordinate (dispersive plane of GLAD). Indeed, this coordinate requires the best achievable resolution in order to get the best spectrometry. With charge division, a resolution of $100 \mu\text{m}$ (FWHM) can be reached without any unconventional requirements on the noise level in the readout electronics or on the geometry of the pads. Furthermore, such a choice will avoid the need for a very accurate drift velocity calibration to determine

the dispersive coordinate of the fragments at the exit of GLAD, the drift velocity being a potential source for systematic errors at the $100\ \mu\text{m}$ level.

The detection volume will be divided into two halves as it is the case in the TP-MUSIC IV. The division will be horizontal, not vertical like in MUSIC IV. The cathode plane providing the electrostatic volume division will be placed below the beam position in order to prevent the beam to go through it as shown on Fig. 3. This division allows for:

- A limitation of the drift length of the primary signals with thus a reduction of the dead-time of the detector and of the transverse size of the primary signals,
- a reasonable high voltage between cathode and anode in order to define the correct value of the electrostatic field which governs the drift velocity of the signals
- a check, in the data analysis, of the measurement and identification of the fragments, with one half which will detect heavy residues, the beam, half of the fission fragments and light-charged particles and the other through which only the second half of the fission fragments and the light-charged particles will go.

Fig. 4, based on geometrical considerations, gives an idea of the necessary active volume of a TPC at the exit of GLAD. The active volume of the TPC is placed $200\ \text{mm}$ downstream of the exit plane of GLAD in order to limit the influence of the fringe field (inhomogeneous both in modulus and orientation) on the drift lines of the signals. In the detection geometry proposed on Fig. 2, using $5\ \text{mm}$ pads for the proportional counters (lighter fragments) and $20\ \text{mm}$ pads for the ionization chambers (heavier fragments) we obtain 4 k channels for the TPC.

The readout of these channels will be performed by flash-ADCs. A sampling rate for these ADCs of $40\ \text{MHz}$, as used in the TP-MUSIC IV should be considered since the primary signal space dimensions and rates will be comparable with those of the TP-MUSIC IV.

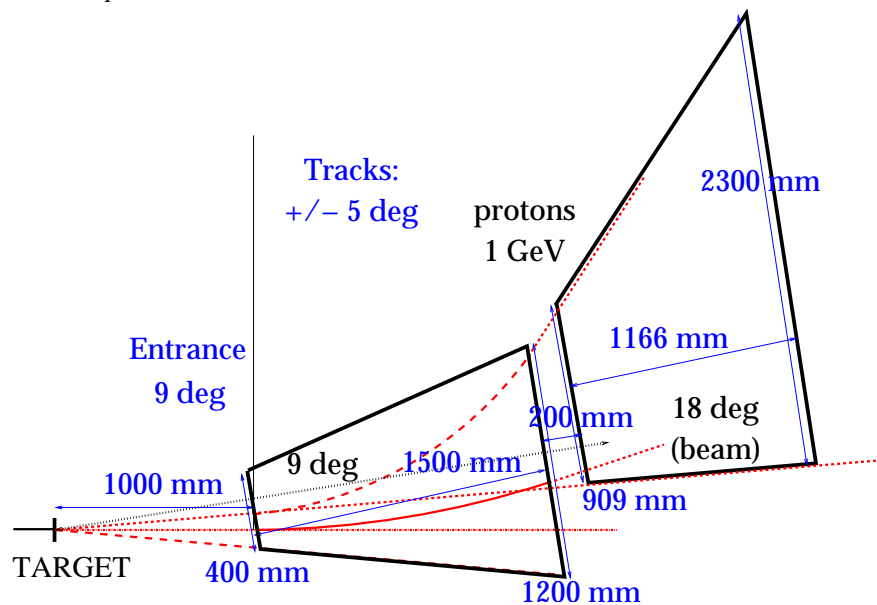


Figure 4. Geometrical scheme of the installation, target + GLAD's active volume + the multi-track detector at the exit of GLAD with different trajectories on which the GLAD's design is based.

Heavy-fragments multi-hit position detectors up-stream the dipole

The multi-hit high resolution position detectors to be used in spallation measurements with R^3B and placed upstream of the GLAD magnet will allow for a reconstruction of the magnetic rigidity of the heavy fragments (fission products and evaporation residues) in combination with the multi-track detector and the ToF measurement downstream of the magnet. Their performances have to be compatible with those in this last detector: $100\ \mu\text{m}$ of spatial resolution, around $1\ \text{mr}$ of angular resolution (combination of two position detectors). These counters will be designed to detect primarily heavy fragments ($Z \geq 10$)

as it is the case in the SPALADIN experiment. This threshold in sensitivity will provide them with a protection against the high-background environment where they will be placed: δ -rays from the beam and heavy fragments going through the target, light spallation fragments produced in coincidence with the projectile residues we want to detect etc...

Contrary to the detectors standing upstream of the magnet that are being used in the SPALADIN experiment in cave B, these detectors upstream of R³B-GLAD will have to be placed in vacuum, in order to reduce multiple scattering of the fragments. There are two possibilities with this constraint: Either solid material detectors such as silicon strips detectors or low pressure gas detectors.

Silicon strip detectors are being studied and will be used in the R³B collaboration. Such detectors will be developed for angle measurements at the target for quasi-elastic scattering in reverse kinematics. The constraints for them are quite similar in terms of resolution and granularity to what we need here. Their size (around $5 \times 5 \text{ cm}^2$) is roughly what we would need for the spallation experiments, their thickness is around $300 \mu\text{m}$, which creates little multiple scattering for heavy ions at 1 A.GeV . For such detectors, it would be anyway of great interest to have larger areas ($10 \times 10 \text{ cm}^2$) in order to place them closer to the magnet entrance and, with the kinematical reconstruction provided by the magnetic analysis, discriminate between events from the target and reactions occurring in this detector.

Gaseous detectors, if chosen for such position detectors will thus have to be low pressure (around a few 10 mbar) to avoid thick interfaces with the vacuum. This is favorable to avoid detection of very light fragments but will necessitate amplification higher than what is being used so far in the SPALADIN experiment.

As for the multi-track detector downstream of GLAD, these gaseous position detectors will have to have vertical drift lines in order to assure the highest resolution in the dispersive plane of the magnet by center of gravity coordinate determination and will have to be equipped with multi-hit readout. It has to be investigated whether a higher sampling rate has to be used for this readout with respect to that of the multi-track detector since the trajectories of the fragments are closer in these detectors than downstream of GLAD because these detectors are much closer to the target and are placed before the magnetic analysis which in average pull apart the different fragments (of different magnetic rigidities and of different kinematics). Furthermore, these detectors will not be able to work at the magnet entrance where the magnetic field is already large, contrary to the silicon strip ones.

Time of flight (ToF) detector

Since the set-up for spallation measurements will be designed to have as little as possible material on the way of the reaction products, the velocity of the heavy fragments whose determination is necessary for their proper isotopic identification, will be provided by time of flight (ToF) measurements. In order to get a clear isotopic identification, such a detector will have to have a resolution of at least 100 ps (FWHM) which seems to be within reach in the near future. This will be ensured not only by the properties of the detectors itself but also by the very small amount of matter along their trajectories through the experimental set-up, which will allow for a narrow energy loss straggling of the fragments. The surface of such time-of-flight detectors should be of the order of $50 \times 50 \text{ cm}^2$. According to Fig. 4, the ToF detector will be placed at least 3.5 m downstream of the target, i.e. behind the multi-track detector.

In section B.1.5 a large-area ToF wall based on resistive plate chambers (RPC) is described, which is designed to provide the required time resolution. The area will be large enough for a full-acceptance measurement of spallation and fission reactions.

Thin hydrogen target

The measurement of spallation reactions in reverse kinematics, i.e. using the heavy ion as the projectile impinging on a proton target, has to face a problem not easily solvable. This problem is twofold:

- Double scattering of the ions *inside the liquid hydrogen* of the target itself
- Ion reactions on the target walls (empty target contribution).

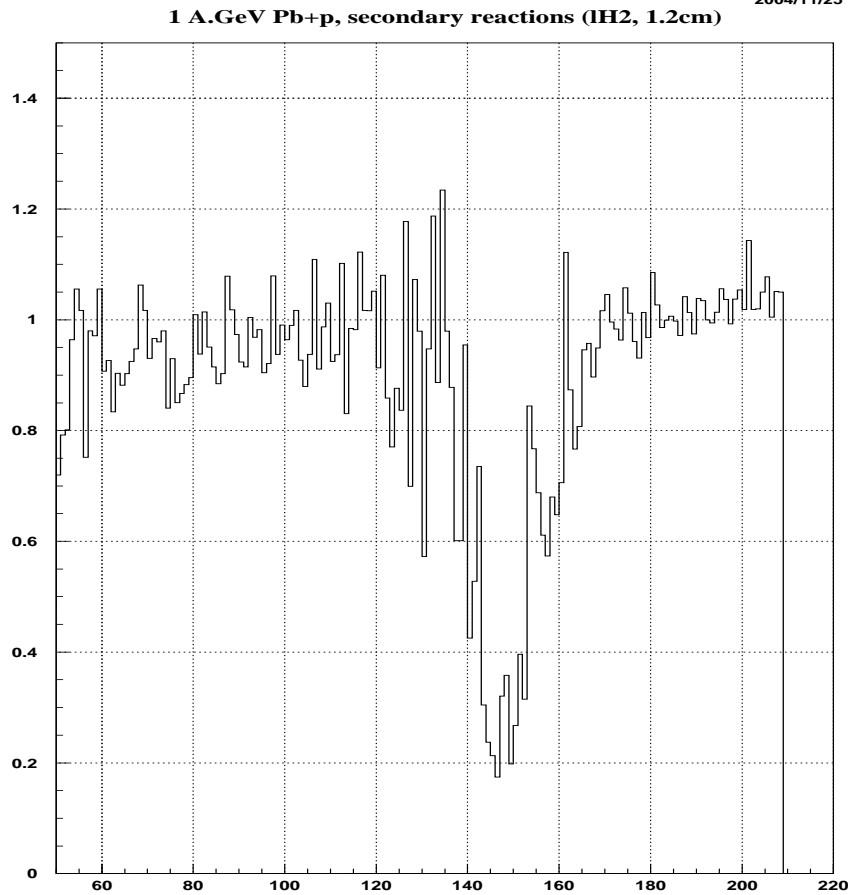


Figure 4. Correction factor used for projectile residue cross-section measurement at the FRS as a function of the mass of the detected fragment. Here, the beam is ^{208}Pb impinging on a 1.2 cm IH_2 target. The measured cross-sections are divided by this correction factors to obtain data without any contribution from secondary reactions in the IH_2 .

The contribution from secondary reaction inside the liquid hydrogen in the target cell is shown on Fig. 4. On this figure, the correction factor to be applied to the data is given, for the measurement $^{208}\text{Pb} + \text{p}$ at 1 A.GeV beam energy, as a function of the mass of the detected fragments. The data are corrected by multiplying the measured cross-sections with this factor. It can be seen on Fig. 4 that although in most cases the correction is of the order of 10 %, it can be as large as a factor 2 to 5 for some isotopes. The larger corrections are explained by the fact that the most probable double scattering is the combination of the production of a heavy residue (the largest cross-sections) which subsequently undergoes another fragmentation. This mechanism populates lighter-mass production for which the spallation cross-section is small. Thus, the relative contribution of double scattering with respect to the basic cross-section becomes large.

The empty target contribution is illustrated on Fig. 5 where the isotopic distributions of the counting rates of the reactions $^{208}\text{Pb} + \text{p} \rightarrow \text{Re}$ (target) and $^{208}\text{Pb} + \text{Ti} \rightarrow \text{Re}$ (cell walls) are given for a kinetic energy of the projectile of 1 A.GeV. The contribution of the reactions on the Ti windows is, isotope by isotope, between a few and up to 10 %.

The problem of double scattering and empty target contribution prevents the experiments from getting pure $A + \text{p}$ events. In inclusive experiment, this can be handled. The empty target contribution can be subtracted from the total contribution on a spectrum basis. The double scattering contribution can be computed accurately using *ad-hoc* models providing correction factors as on Fig. 4, as performed in the FRS experiments [spall1-spall12].

Making exclusive measurements of spallation reactions, whose final states can be complicated because of the presence of many fragments, requires these contributions to be negligible. In fact, these contributions correspond to a loss of information on an event by event basis which cannot be corrected for on such a basis

To that end, it is necessary to reduce both the IH_2 and the target cell walls thicknesses. For that, there are two possibilities: either low pressure liquid hydrogen (IH_2) or solid hydrogen targets (ice, sH_2). In the two cases the number of atoms per cm^2 is of the same order, the hydrogen ice being of roughly the same density as liquid hydrogen. In both cases, both thicknesses can be reduced.

The advantage of using ice targets is threefold:

- Once the ice has been formed, the windows can in principle be removed, the target being then of pure ice.
- Using solid targets allows for the use of thin targets which is of importance for spallation studies on heavy fragments for which multiple scattering of the fragments within the hydrogen itself increases with respect to lighter projectiles.
- Moreover, solid hydrogen targets have a constant thickness across the beam emittance whereas liquid ones have a profile which increases by as much as 10 % with respect to its value on the border of the cell, making the determination of cross-sections from counting rates very sensitive to the beam quality.

The drawback of solid hydrogen targets is essentially the non-uniformity of their thickness, depending on the system used to cool the hydrogen, with the possible presence of bubbles and physical thickness non-uniformity.

Thin solid hydrogen targets are also needed for other experiments foreseen in the R^3B collaboration, for example the measurement of elastic and inelastic scattering of exotic nuclei with the coincidence measurement in the final state of the recoiling proton of low momentum and of the projectile fragment.

The use of liquid hydrogen targets implies the necessity to change the concept on which the target is regulated and change from temperature regulated targets, as it is the case in the SPALADIN experiment, to pressure regulated ones. For such pressure regulated targets, working pressure of 100 *mbar* can be achieved, which allows for the use of a wall thickness 10 times smaller than what is presently done. Working at such a low pressure requires that hydrogen is under-cooled to be in a liquid phase with a density of 0.07 g/cm^3 , its value at atmospheric pressure.

The concept for such a target is completely different from what is presently working for example in GSI-Cave B / SPALADIN:

- The hydrogen pressure is regulated with a piston which controls an expansion volume directly connected to the primary circuit (a kind of vacuum storage tank)
- The control system is of course totally different from the existing one since the probes are different (more pressure sensitive probes have to be used) and the problem handling procedures are also different. The control system has thus to be re-designed completely.

To be fully efficient, such a reduction of the target cell wall thickness has to be combined with the use of fast closing valves (a few ms closing time) on the beam line in order to avoid windows in between the different vacuums (beam line vacuum, scattering chamber vacuum and magnet vacuum).

In such a scheme, by using for example a 10 mm diameter target cell, the amount of Titanium needed could be reduced from $4 \times 15 \mu\text{m}$ to $2 \times 1 \mu\text{m}$, which means a *factor 10 reduction*. This would reduce the cell wall contribution to negligible levels with respect to the hydrogen contribution to the counting rate.

One advantage of such a type of liquid hydrogen target is that it uses only a reduced amount of hydrogen (8 liters of gaseous hydrogen at STP) in a *closed system* which, conceptually, cannot let in more hydrogen in case of leakage.

The choice between solid or liquid hydrogen targets have to be made carefully and all the parameters, among which the cost of this equipment, have to be taken into account. The use of this new target with small window protection to contain the hydrogen in case of a failure in the cooling system or of a blow-up of a vacuum window on the beam line will necessitate a careful study of safety issues and protection to be used on the beam line upstream and on the set-up downstream.

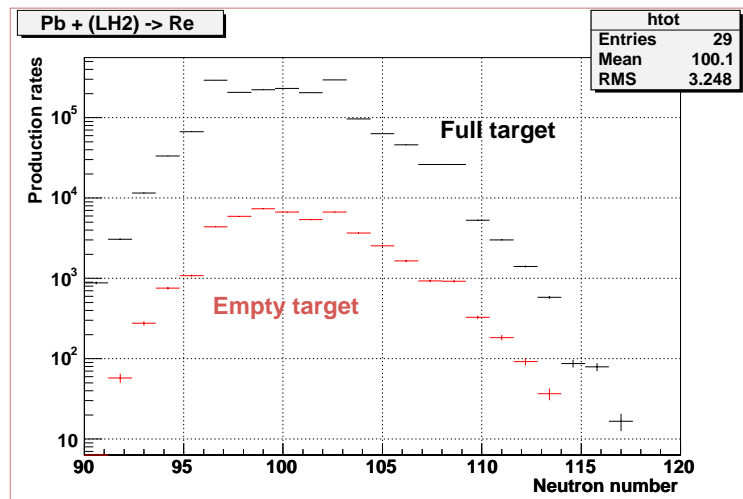


Figure 5. typical isotopic distributions for $^{208}\text{Pb}+p \rightarrow \text{Re}$ (spallation) and $^{208}\text{Pb}+\text{Ti} \rightarrow \text{Re}$ reactions [14]. The spallation reaction occurs in the hydrogen itself whereas the second reaction occurs in the target cell wall. The difference of production rate takes into account the difference in the number of atoms per cm^2 between the hydrogen and the cell walls.

Physics Performance

The physics performances of this detection system for spallation studies have to be done with an accurate simulation which will be started once a geometry for the magnet and for the TPC will be fixed. However, the goal of the present set-up is to provide as complete as possible the reconstruction of the spallation events through the mass and charge identification of heavy residues as well as lighter fragments and cover the largest acceptance available with the future magnet. We will then have a complete set of data on spallation of heavy projectiles.

Implementation and Installation

There will be two special requirements for the spallation set-up:

- The use of a hydrogen with thin walls for the cell (or even without walls), which will necessitate the installation of fast valves on the beam pipe (10-20 *m* upstream). Hydrogen will be present anyway in very small amounts (a few liters at STP), as explained above.
- The use of a large volume of P10 gas (the TP-MUSIC IV contains roughly 1 m^3 of P10) but in a *closed loop* with a purification system, as it is actually the case for MUSIC IV.

References and Acknowledgements

- [spall1] W. Wlazlo *et al.*, Phys. Rev. Lett. **84**, 5736 (2000)
- [spall2] J. Benlliure *et al.*, Nucl. Phys. A **683**, 513 (2001)
- [spall3] F. Rejmund *et al.*, Nucl. Phys. A **683**, 540 (2001)
- [spall4] T. Enqvist *et al.*, Nucl. Phys. A **686**, 481 (2001)
- [spall5] J. Benlliure *et al.*, Nucl. Phys. A **700**, 469 (2002)
- [spall6] T. Enqvist *et al.*, Nucl. Phys. A **703**, 435 (2002)
- [spall7] J. Taieb *et al.*, Nucl. Phys. A **724**, 413 (2003)
- [spall8] M. Bernas *et al.*, Nucl. Phys. A **725**, 435 (2003)
- [spall9] M.V. Ricciardi *et al.*, Nucl. Phys. A **733**, 299 (2004)
- [spall10] P. Napolitani *et al.*, Phys. Rev. C **70**, 054607 (2004)
- [spall11] P. Armbruster *et al.*, Phys. Rev. Lett. **93**, 212701 (2004)
- [spall12] B. Fernandez-Dominguez *et al.*, Nucl. Phys. A **747**, 227 (2005)
- [spall13] A. Boudard *et al.*, Proposal S248 to the GSI-EA, Dec. 2000
- [spall14] J.E. Ducret, private communication, 2002
- [spall15] C. Sfienti *et al.*, GSI Scientific Report 2002, p. 220 & contributed paper to the 18th Nuclear Physics Division Conference, Prague, Czech Republic, 23-29 Aug. 2004
- [spall16] G.D. Badhwar, NIM **109**, 119 (1973)

B.2. Data acquisition system

NUSTAR DAQ

The NUSTAR data acquisition (DAQ) concept tries to incorporate and deal with the changes that are related to the discontinuation of production and support of all CAMAC and FASTBUS modules, together with the much increasing number of channels in the different experiments. Dedicated front-end electronics boards are foreseen in most experiments for NUSTAR. The other main issue is to provide a maximum interoperability of the different setups of the NUSTAR facility as many parts of particular setups, detectors systems and their associated DAQ systems. As an example may serve the in-ring instrumentation of the NESR that will be used in parallel by the EXL and ELISE collaborations. The same holds for the combination Super-FRS instrumentation – R³B setup, or gamma spectroscopy arrays in conjunction with reaction setups. As the communities overlap to a large extent it is favourable to come up with a combined DAQ framework that allows sharing expertise, thus saving manpower and running cost. The GSI MBS [1] system is an example for such a flexible DAQ scheme, that provides a generalized multi-processor environment, suitable for the readout, control and data storage of heterogeneous setups. The necessary extensions of the scheme have to be evaluated and integrated into the developing system by the NUSTAR DAQ group. A major part of this will be the integration of ‘foreign’ stand-alone DAQ systems or similarly the control and operation of various front-end electronics. System integration should be possible at different stages of the DAQ system.

- (a) **“NUSTAR” DAQ systems:** It should be possible to couple different standalone “NUSTAR” DAQ systems, together in a simple way. Typically the individual DAQ systems are used to setup and debug detector groups or experiments. By foreseeing the necessary interconnects for triggers and control signals and by keeping the modularity of the system in mind while building local triggers and event buffer capabilities, such a scheme can be realized. The R³B/CaveC setup together with the current FRS is an example where the necessary prerequisites are currently specified. Note, that different schemes of coupling might be used here: (i) the systems are synchronized with one common trigger (ii) the DAQ systems run standalone and are synchronized via timestamps (see section Time and trigger distribution systems).
- (b) **Front-end electronics (FEE):** For the common NUSTAR DAQ system, specific front-end electronics together with its digitization part is seen as part of the detector. This has the advantage that all analogue signal processing is done by the working groups with the most experience on the particular detector system. Only the control, trigger and data flow will be specified as interface description by the common NUSTAR DAQ system. This includes the necessary trigger types to be implemented, like data, calibration and synchronization triggers together with a prescription how to lock the FEE to realize a clearly defined dead time of the total system. The timestamp-data interface has to be specified and slow control issues like version numbering, firmware revisions, software up/download from e.g. databases to particular FEE boards require R&D work. A first implementation for the digital interface that allows slow control and experiment data transfer from and to FEE boards already exists and is in use; the GTB-BUS a GSI development.
- (c) **Inhomogeneous DAQ systems:** From our operating experience we know, that especially the large gamma arrays come with their own customized DAQ systems. As has been seen e.g. for the RISING2 experiments at the FRS, a certain flexibility of the host (here the NUSTAR) DAQ system is mandatory to couple these systems together. The development and implementation of the TITRIS timestamp module together with the time-ordered writing to mass storage within the MBS framework is an example for such integration efforts.

Implementation: As a first step we want to implement within the years a standardized front-end electronics (e.g. for the R³B/CAVEC) for fast signals. It will consist of a taquila [3] front-end board that has been developed for the upgrade of the FOPI experiment at GSI. These boards can be used to record 16 channels of time-signals, amplitude- or charge-signals at a moderate channel cost of about 50-60€. As interface to the detector additional FEE (e.g. [4]) boards are used, that are used to amplify, shape and split the signals prior to their input the digitizer board. Such a system can be thought of being already a replacement for a full e.g. NIM based pre-amplifier, discriminator and CAMAC/FASTBUS based digitizer chain. The taquila boards provide also a simple time stamp mechanism. We will study the

behaviour of such a system within the next two years at the R³B/CAVEC setup using the LAND neutron-detector readout as reference implementation. Further R&D steps will be accomplished to come to a fully operable FEE environment. The FEE is digitally attached via the GTB bus to a VME based processor board [5] that can be used to control the FEE readout process and to perform online data reduction (see Figure 1).

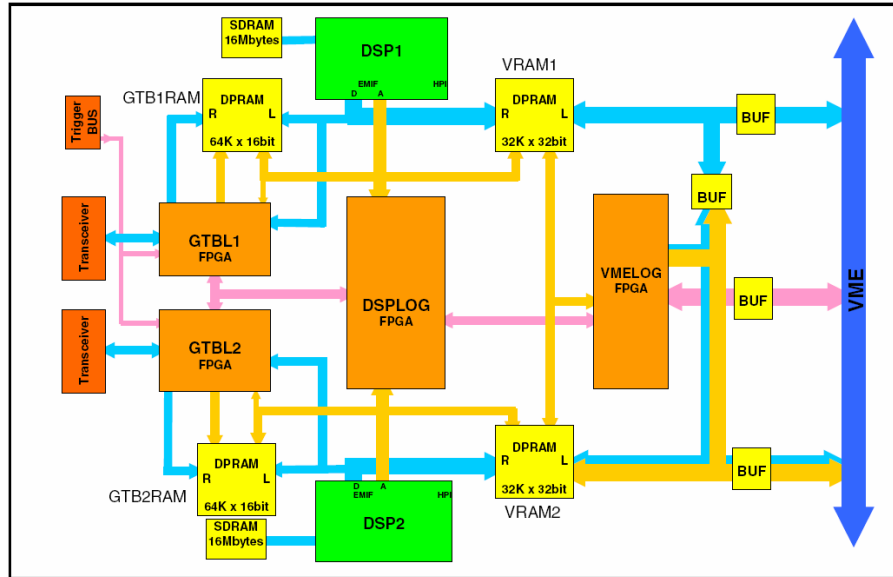


Figure 1.

Block diagram of the VME based SAM3 processor board. Two TMS320C6711 digital signal processors running at 100 MHz are used. It is foreseen to provide this module's functionality within the framework of the NUSTAR DAQ system.

Known requests: Apart from the R³B/FAIR experiment that will be the continuation of the R³B/CAVEC experiment the EXL community has already come up with detailed requests to the NUSTAR DAQ group. The EXL front-end electronics which includes the ADC will have its own Time stamp & slow control facilities. The slow control facilities will allow a level of hard and software debugging. The slow control will allow the modification of e.g. the sub-trigger, choice of pre-amplifiers and amplifiers, the shaping, the gain, discriminators, sampling, ADC functions, calibration and test sequences, cable redundancy, high voltage, and bias settings. The structure required to manage the above should, is requested from the NUSTAR DAQ system. Apart from the control aspects, also the data collection chain from the digitized data has to be implemented, where the expected data rates for both experiments are approaching the 100 MBytes/sec limit.

Controls: We foresee two kinds of data from the experiments: event-wise data that is taken with the physics and control triggers and what we call slow control data, like scaler readouts, beam profiles and so on. These data are of interest for the distributed slow control system throughout the NUSTAR facility and the accelerator. For this example, profile data may be taken to generate a feedback loop in order to perform automatic beam steering, whereas scaler data can provide information on the sanity of the particular setups.

Time and trigger distribution systems

As can be seen from the above discussion one of the main infrastructures delivered by the NUSTAR DAQ framework will be a hierarchical time distribution system. Existing architectures for large scale time and trigger distribution systems are given e.g. by the TTC for LHC experiments [6], or the TCS [7,8] build for the COMPASS experiment, both at CERN. The Accelerator Division is currently working on the technical concept of the next generation timing system [9]. This activity was originally prompted by the requirement of the PHELIX experiment to synchronize a laser shot with the arriving pulse to a precision of 100 ps, thus the internal name "BuTiS" for 'Bunchphase Timing System'. This scope has of course widened, the objective is now to provide the timing reference for all FAIR accelerator components, and if there is interest, also the experiments. The current specifications call for a long term stability of 100 ps across the whole GSI site, and a timing jitter of well below 100 ps. The system will

provide a campus reference for standard frequencies (current plan is 200 MHz and 10 MHz) and standard time (UTC) which will be derived from a GPS based reference. In addition, auxiliary information channels are foreseen which will provide for example triggers for specific accelerator events. Getting this performance over distances of up to 1 km has a price, the technologies and components used in BuTiS seem to be too expensive to be used in a local time distribution system of an experiment, where several end nodes have to be served over quite short distances. However, it seems prudent to use BuTiS as master clock/time reference for the local time distribution systems of experiments. This would also allow a more modular approach, using a local time distribution system per detector sub-system. This is of particular interest for experiments where parts of the setup are in different locations, like in many Super-FRS experiments.

Local time-stamps: A campus wide synchronisation method allows for common timestamps between different experiments. The common clock is not enough on its own for full synchronisation - one needs to be able to correlate particular clock edges with particular values of the timestamp counters in order to start from the same timestamp value everywhere. Existing local time distribution systems like e.g. the GSI TITRIS [10] modular, which is similar to the CENTRUM built by GANIL [11] and also the proposed AGATA GTS [12], have to be adapted to allow for the synchronization to the BUTiS clock with a defined phase. Different types of FEE will also provide their local clocks. One may consider the following scenarios:

- a) Self-made timestamps, where a specification of the latency of the front-end trigger with respect to the timestamps is needed in order to be able to synchronize the particular data to the overall system. The latency can be automatically determined e.g. by using generated synchronization events from the host DAQ system to the particular timestamp generating system. Another question is how to couple local systems to BuTiS. One BuTiS receiver per local timestamping system might be too expensive it is a subject to further R&D whether an additional (experiment-wide) time distribution layer is desirable.
- b) For the standardized NUSTAR DAQ one should consider to build a novel “Titris II” module in different form factors, to be used in VME crates or attached to the FEE, which can be coupled to the BuTiS system.

We can base our studies e.g. on the already existing use the techniques of time-stamping followed by software filters and triggers which were developed for GREAT. Within GREAT these items are handled by the Metronome and its interface to the ADC cards. Within the next years we need to specify latencies for trigger decisions depending on the physics of the trigger, taking into account the limited pre-processing buffer depths, and their associated acceptance window. Here dedicated input from the different experiments is needed to come up with a generalized and flexible scheme.

Data collection and storage

Data collection and mass storage is another issue. If one deal with 10-100 Mbytes/sec data form the experiments at maximum as estimated for the EXL and R³B setups, the total data produced per day is in the order of 1-10 TBytes. This means, for the NUSTAR experiments we expect not more than 500TB/year data. The requested band-width for data transfer is in accordance with the expected rates that can be transferred using standard network components.

The demand to run independent NUSTAR DAQ modules that can be combined in a flexible manner poses certain requirements to the transport layer in between the experiments and to the mass storage.

1. Standardized sub-event format; this is favourable in order to facilitate to event building from different data sources.
2. Flexible event builder combinations; one may consider to use different parts of the data stream at different locations to perform different tasks: mass storage; online analysis; slow control feedback.
3. Standardized event format; to be used to use a common unpacking scheme for data analysis.

The NUSTAR DAQ system will provide the necessary data collection procedures for standard electronics module (e.g. VME) and collection form FE-boards that follow the conventions for the

standardized digital interfaces (e.g. GTB). The necessary R&D work will be done in parallel to the various electronic developments in the NUSTAR community in close collaboration with the respective groups, co-ordinated by the DAQ responsible for the particular experiments.

Slow control and monitoring

The slow control requests for the NUSTAR DAQ system go two ways. First the sub-systems should provide certain information in order to be in the monitoring process of the total experiment specific combination of different DAQ systems at different locations. This functionality exceeds the implemented acquisition controls: a command dispatcher and log message facility the sense, that also e.g. different online scalers providing dead-time and rates should be available. This implies also that there should be an extended way to be able to probe the actual configuration of the setup (this means an extended object with distances between the different parts of several 100 meters) including software revisions on the FE-boards and other related information. Probing means in this context, that the individual sub-systems provide information about the parameters and interlock conditions to be monitored. One may also think of status requests that return FPGA codes, hard- and software-revisions and related information.

The other way is the information that will be provided by the experiments DAQ and analysis stage to:

1. the accelerator; to allow e.g. automatic beam steering [13] like it is done at CERN PSB to continuously adjust experiments settings without manual interference.
2. the general slow controls of the experiment or setup, allowing to define interlock and warning conditions.
3. any other item not mentioned here that requires information of the experiments status extracted from the online data.

The advantage of such a scheme is that controls get their information from the different local systems so that the expertise is kept locally also.

The implementation of the above scheme will be an adaptive process, where tests of the method are and can be already done at existing setups, which will lead to a final design, also with the input of the locally existing controls group. The final specification will be provided in the Technical Design report.

References

-
- 1 The New data Acquisition System at GSI, H.G. Essel, J. Hoffmann, N. Kurz, R.S. Mayer, W. Ott, D. Schall, IEEE Trans. Nucl. Sci. **43** (1996), 132; The General Purpose Data Acquisition System MBS, H.G. Essel, N.Kurz, IEEE Trans. Nucl. Sci. **47** (2000), 337
 - 2 J. Hoffmann and N. Kurz, RISING Data Acquisition with MBS:Event Synchronization with Time Stamp Modules, GSI Scientific Report, p. 224.,2002
 - 3 A New TAC Based Multi Channel Front-End Electronics for TOF Experiments with Very High Time Resolution, K.Koch, H.Hardel, R.Schulze, E.Badura, J.Hoffmann (GSI), IEEE Conf Proc. Nucl. Sci. Symp., Med. Im. Conf., Symp. Nucl. Power Sys. and 14th Int. Workshop on Room Temp. Semic. X- and Gamma- Ray Det., Oct. 16-22, 2004, Rome, Italy, to be published
 - 4 FOPI-Collaboration, "Upgrading the FOPI detector system", GSI Scientific Report, p. 177, 1998; A.Schüttauf et. al., "Timing Resistive Plate Counters (RPC) in FOPI", GSI Scientific Report, p. 231, 2003
 - 5 Development of New Readout Processor SAM3, J.Hoffmann, W.Ott, GSI Scientific Report, p. 193, 2002
 - 6 <http://ttc.web.cern.ch/TTC/intro.html>
 - 7 I. Konorov at al., The trigger control system for the COMPASS Experiment. IEEE Nuclear Science Symposium Conference Record (2002)
 - 8 L. Schmitt et al., The DAQ of the COMPASS Experiment. IEEE Trans. Nucl. Sci. (2004)
 - 9 P.Moritz (P.Moritz@gsi.de), private Communication.
 - 10 http://www-linux.gsi.de/~mbs/v43/manual/gm_r.pdf

-
- 11 <http://nnsa.dl.ac.uk/documents/edoc421/edoc421.pdf>
 - 12 <http://agata.pd.infn.it/documents/week9152003/MarcoBellato.pdf>
 - 13 'INTELLIGENT' AUTOMATIC BEAM STEERING AND SHAPING, A. Jansson and M. Lindroos, CERN, Geneva, Switzerland, Proceedings of EPAC 2000 conference.

B.3. Beam/target requirements

The experiment requires CW or CW-like beams. In most cases, secondary beams will be used, which will be produced and separated with the Super-FRS. Many experiments will ask for the maximum reachable intensity at the Super-FRS target with energies up to 1500 MeV/nucleon. This means that SIS100 as well as SIS300 (as stretcher ring) will be needed. Typical secondary beam intensities will be in the range of one to 10^6 ions/s. The use of the Super-FRS implies that no other experiments with radioactive beams, e.g., low-energy branch or ring branch, can be operated in parallel. Parallel operation with other programmes is possible to some extent, which will, however, reduce the duty cycle implying longer runs in consequence. The experiment will accept beams from Super-FRS making use of the full acceptance, i.e. with an emittance of 200π mm mrad and a momentum spread of $\pm 2.5\%$. A beam spot size of 3×3 cm² is considered.

Typical experiments to be performed at R³B need two to three weeks of beam time. A total requirement of 3 months/year beam on target is estimated. The different experiments to be performed at R³B make partially use of different setup configurations. In such cases breaks of several weeks in between the experiments are needed for setting up the experiment. The experimental area has to be accessible in no-beam time periods, e.g., also while the Super-FRS is in operation delivering beam to other branches.

B.4. Physics performance

Tracking through the large-acceptance dipole magnet (Identification of reaction products)

The basic information needed for reaction studies with radioactive beams is the identification of incoming ions and reaction products. The incoming beam is identified by standard techniques making use of ToF and ΔE measurements. Since the acceptance of the separator is larger than the difference in $B\rho$ of neighbouring nuclei, the rigidity has to be measured in addition, which can be accomplished by a position measurement at the dispersive mid focus of the separator. A moderate position resolution of about 5 mm is sufficient to obtain a $B\rho$ resolution of about 10^{-3} . For high resolution measurements, better position resolution plus angle measurement are necessary. The identification of reaction products is more demanding for heavy beams since the large-acceptance dipole provides only moderate dispersion. In the following we describe the scheme in more detail and simulation results are presented.

The superconducting large-acceptance dipole provides a field integral of 5 Tm which is sufficient to bend a 15 Tm beam, e.g., 1 GeV/nucleon ¹³²Sn by 18°. The magnetic rigidity $B\rho$ can be measured by tracking the ions through the magnetic field. In principle, three position measurements are sufficient to uniquely

determine the trajectories if the magnetic field is of dipolar character. In R³B, the position will be measured twice before and two times after the dipole. The rigidity can thus be calculated either by using two position measurements before and one after the magnet (method 1) or by using the position measurement just before the magnet and two after the dipole (method 2). The optimum location of the detectors for the position measurements is different for method 1 and method 2, e.g., for method 1 the detector behind the magnetic field should be as close to the magnet as possible while for method 2 a large distance will yield a better resolution.

The required resolution is defined by the necessity that fragments emerging from the target have to be uniquely identified for heavy ions up to mass $A=200$. A separation by $2\times\text{FWHM}$ corresponds to a relative $B\rho$ resolution of about 10^{-3} . For reactions with longitudinal momentum transfer of significant more than 10^{-3} times the total beam momentum an additional measurement of the velocity is required to be able to determine the mass from the $B\rho$ measurement. In this case, a similar relative resolution of the measurement of $\beta\gamma$ by time-of-flight (ToF) has to be reached, corresponding to a ToF resolution of about 25 psec (σ) at 700 GeV/nucleon, which can be reached with organic scintillator and fast phototubes.

The four position measurements used are:

- 1) Target position as determined from two position measurements in front of the target;
- 2) Position measurement 1 m behind the target, directly in front of the dipole;
- 3) Measurement directly after the dipole;
- 4) Position 10 m after the dipole.

The influence of the detector resolution and the straggling in the detector on the rigidity measurement is simulated using a Monte-Carlo procedure. The magnetic field of the dipole is modelled by transport matrices, two matrices describing the fringe fields at the entrance and the exit, and one matrix for the dipole field. Those matrices are calculated to describe the properties of the large-acceptance dipole as close as possible. The transport of particles through the magnetic field is calculated up to third order using the Monte Carlo code MOCADI. The effects due to passage of material, e.g., angular straggling in the detectors is taken into account in the MOCADI calculation based on the ATIMA code. Fragments are generated randomly according to initial angular, position and momentum distributions with realistic parameters. The generated data are stored in PAW ntuples including the information of the position, magnetic rigidity and angle at the locations of the trajectories corresponding to the detector positions. These data are analyzed in a second step in order to reconstruct the momentum from the position measurements similar as in the experiment. Here, the detector resolutions are taken into account. As an example, a beam of 1 GeV/nucleon ¹³²Sn was considered.

The procedure of reconstructing the rigidity from the position measurements is performed by using a first order matrix formalism. Although only a small fraction of the total acceptance of the magnet is used by the heavy fragments, higher order effects are clearly visible and have to be corrected. Without this correction, the resolution is limited to about 1.7×10^{-3} even without effects due to straggling and detector resolution. A correction depending linearly on the entrance angle in the dispersive plane is sufficient to reach a precision in the reconstruction of $B\rho$ of about 1.5×10^{-4} , much better than the resolution finally obtained. The left part of Figure 1 shows the reconstructed value versus the true rigidity. Such a correction can easily be done in an experiment using the non-reacting beam with known momentum. Now the detector resolution and the angular scattering in the detectors are introduced. The individual contributions to the final resolution in momentum are summarized in Table 1. A position resolution of 50 μm σ (corresponding to a pitch size of about 200 μm) was assumed. It can be seen that the obtainable resolution is finally limited by the angular straggling in the detectors. A thickness of 0.2 mm silicon was assumed for the detectors at position 2 and 3. The last detector can be thick and does not need very good position resolution since it can be placed at a distance of a few meters.

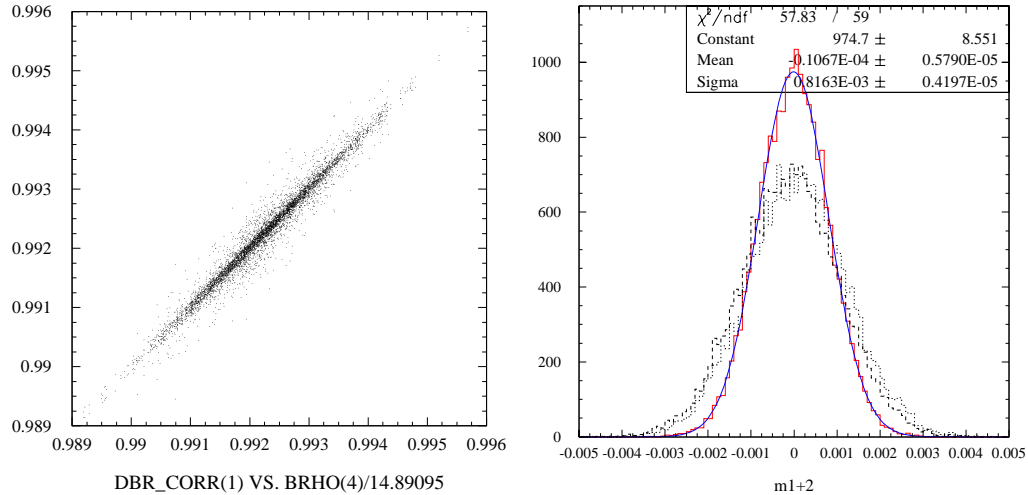


Figure 1. Left panel: Reconstructed versus true magnetic rigidity (relative to the reference of $B\rho=14.89\text{ Tm}$). The rigidity is reconstructed in first order and empirically corrected for higher-order effects resulting in a precision of the reconstruction of about 1.5×10^{-4} (without detector effects). Right: Difference of measured and true relative rigidities using method 1 (dotted) and method 2 (dashed) taking into account detector resolution and straggling. The solid curve shows the difference for an averaged value using both methods resulting in a relative $B\rho$ resolution of 0.82×10^{-3} . Detector thicknesses and resolutions are given in Table 1.

Table 1. Individual contributions to the relative $B\rho$ resolution due to the position resolutions Δx at locations 1 to 4 as defined above, and due to the angular straggling.

Position	Δx (sigma) (μm)	thickness (mm)	Contributions to the $B\rho$ resolution (sigma $\times 10^3$)			
			Method 1		Method 2	
			Δx	$\Delta\theta$	Δx	$\Delta\theta$
1 (target)	50		0.35	0	0	0
2	50	0.2	0.44	1.0	0.18	0
3	50	0.2	0.17	0	0.42	1.0
4	300	1.0	0	0	0.34	0
total			0.55	1.0	0.53	1.0
			1.1		1.1	
average			0.82			

The results are similar (slightly better) for diamond with the same thickness of $200\ \mu\text{m}$, which is nowadays technically easily reached for detector sizes of about $5\times 5\ \text{cm}^2$. The most difficult part is the detector 3 if method 2 is used. In that case a comparable thickness has to be reached, but for a larger detector size of about $20\times 10\ \text{cm}^2$. It should be noted, that a resolution of 1 mm pitch for detector 3 is sufficient if only method 1 would be used, as provided, e.g., by fibre detectors. An array of diamond or silicon detectors at position 3 consisting of several small detectors with 0.2 mm maximum thickness is considered making a redundant measurement of the momentum by the two methods possible. This results in a well balanced system concerning the individual contributions to the momentum resolution as can be seen from Table 1. The values obtained from the two methods can be averaged resulting in a final relative resolution (sigma) of $\Delta B\rho/B\rho=0.82\times 10^{-3}$, see right panel of Figure 1. The system thus provides mass resolution which is sufficient for unique identification even for heavy systems with mass $A=200$ and with beam energies around 1 GeV/nucleon.

If the detector thicknesses can be further reduced, a better resolution can be obtained. Using silicon detectors with $50\ \mu\text{m}$ thickness and corresponding better spatial resolution ($15\ \mu\text{m}$ sigma corresponding to a pitch size of $50\ \mu\text{m}$) a relative momentum resolution of 0.55×10^{-3} is reached by both methods and 0.4×10^{-3} if the average of both values is used.

C. Implementation and installation

1. Cave and Annex Facilities

The R³B experiment will be located at the focal plane of the high-energy branch of the Super-FRS. An experimental hall of about 50 to 60 m length and 20 m wide is required (depending on the final design of the magnetic spectrometer) with standard technical infrastructure including crane (8 t) and air condition. The length of the hall of at least 50 m is also required for the high-resolution measurements of neutrons, and time-of-flight measurements.

The configuration of the experimental setup is different for individual experiments. The area not occupied by the actual setup will be used to store big detector components and for mounting and setting up the individual experiments. The size of the hall as given above provides sufficient storage area, e.g., for the liquid hydrogen target systems (used for particular experiments), the active target (few meters length, used for (in)-elastic scattering), the multi-track ion detector and large-area ToF wall (used for spallation and fission experiments), or the old LAND detector (to be used for quasi-free scattered neutrons under 45 degree) (or for the respective detection systems replaced by those detectors). Such big devices have to be handled by crane and/or will be moved by air pads, e.g., the heaviest systems like the neutron detector (~20 t). The floor of the hall has to be foreseen for that.

A cooling system for the super-conducting magnets (large-acceptance dipole and high-resolution spectrometer), gas supply system for detectors, as well as safety installations for the use of liquid and gaseous H targets are required. Liquid hydrogen targets with thin cell walls will be used. The experimental vacuum has to be decoupled from the ultra-high vacuum of the separator. In addition, fast valves have to be installed.

Access has to be provided to bring in large and heavy equipment. Partly, large equipment will be installed later, after the first period of commissioning and first physics experiments. The magnets for the high-resolution spectrometer, for instance, will be installed in the experimental hall in 2012, two years after start of phase 1.

The R³B experimental area has to be accessible independent of operation of other Super-FRS beam lines, e.g., the ring branch and the low-energy branch.

The height of the beam line should be at least 2.0 meter. Typical beam intensities used for R³B experiments will range between few ions/s up to 10⁷ ions/s. All beams up to uranium have to be considered.

In addition to the experimental hall, counting rooms, rooms for on-line data analysis, and an area for mounting and storage of smaller detector components (e.g. tracking detectors) should be foreseen close to the experimental hall with a size of about 40 m².

2. Detector-machine interface

The experimental vacuum has to be decoupled from the ultra-high vacuum of the separator. In addition, fast valves have to be installed. The setup contains vacuum chambers with big volumes (several m³, behind the large-acceptance magnet) and large exit windows (with about 1 m diameter).

Machine and in particular separator parameters have to be provided for the data-event stream (see DAQ section). Timing interface to the accelerator cycles is required in case of pulsed beams.

Radiation shielding is discussed in section F.

3. Assembly and installation

The space provided by the experimental hall plus the external 40 m² area mentioned above should be sufficient for mounting and installation of the various sub-systems, as well as for later re-arrangements as discussed above.

D. Commissioning

Several detector components will be tested already in Cave C. These are the tracking detectors, the low-energy neutron detector, and the proton tracking system. They will be fully operational before installation in the new experimental area. Therefore, test beams at the existing facility, Cave C, are required, as well as for testing of prototypes.

The large-acceptance dipole will be installed in the experimental area in 2009. The magnet will be commissioned and a field map will be measured during this year. In parallel, the components of e.g. the neutron detector will be assembled in the cave including the electronics. This detector system will go into operation already in 2009 and will be commissioned and calibrated using cosmic rays. The gamma calorimeter will be assembled and tested with sources elsewhere.

The complete setup will be ready for commissioning with beam in 2010.

The installation of the high-resolution spectrometer is foreseen in 2012 subsequently to the installation and commissioning of the other Super-FRS stages and beam-lines.

E. Operation

The experiment will be operational beginning of 2010.

F. Safety

The main safety aspects which have to be dealt with are the radiation shielding, the installations for the hydrogen targets, and the vacuum system including large-area vacuum windows.

Expected radiation doses in the high energy experimental area

The shielding of the high energy experimental area should limit the radiation exposure to the working staff and to people in general. The intention is to assure a dose rate of less than 1mSv per 2000 working hours in areas which are not kept under radiation surveillance. This leads to the limit of the average dose rate of 0.5 μ Sv/h. Inside the experimental halls certain areas with higher radiation levels may have to be accessed. When the yearly dose in an area may exceed 6mSv a so-called radiation controlled area has to be installed. Thus, if the access to the area shall be free of a control system the average dose rate has to be smaller than 3 μ Sv/h.

In the high energy experimental area heavy ions up to uranium with kinetic energy of up to several GeV/amu are made available for nuclear physics research. The interaction of the primary beam with a target will lead to the production of secondary radiation. From the radiation protection point of view the neutrons consider the most important radiation component as they are able to penetrate thick shielding layers. The production of neutrons was measured in a dedicated beam time in November 2001 with a neutron telescope detector and the Large Area Neutron Detector (LAND) in Cave B. The measured double differential neutron spectra were put into a Monte-Carlo simulation of a model of the planned high energy hall. The radiation transport code Fluka [fluka1+2] was used with the defaults set to "SHIELDING". The attenuation of the dose rate through the solid concrete walls is shown in figure 1 for a beam of 1E8 uranium ions per second of kinetic energy 1GeV/amu.

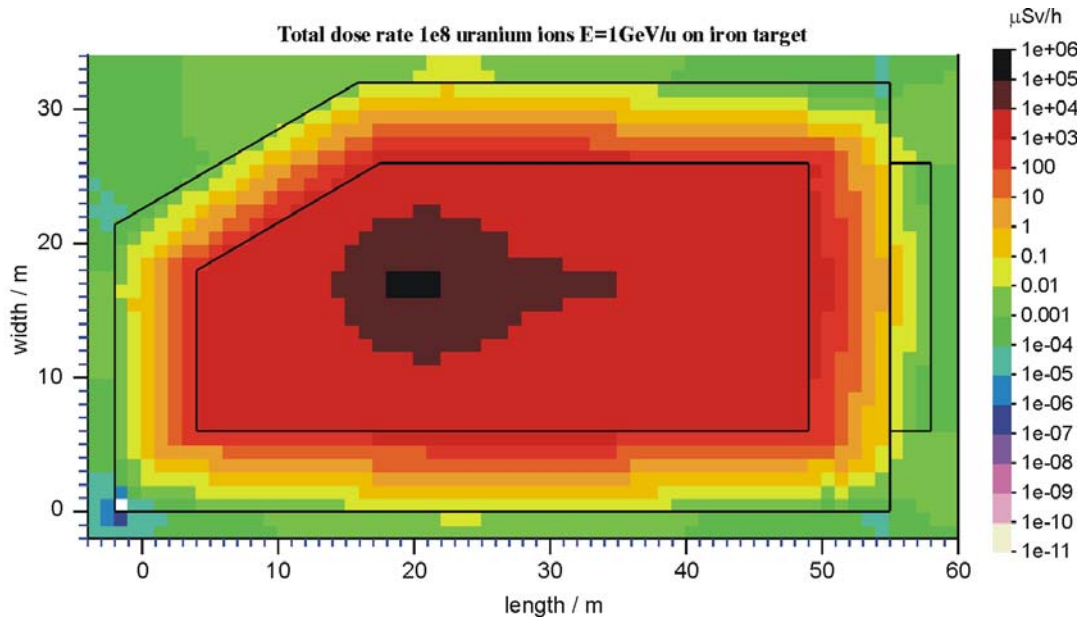


Figure 1: Dose rate at the high energy experimental area for radioactive ion beams. The transport of the radiation was simulated with the Monte-Carlo code Fluka [fluka1+2]. A beam of $1E8$ uranium ions per second with kinetic energy of 1 GeV was assumed to be fully stopped in the target.

In the model of the high energy hall the concrete walls are made 5m thick in the lateral and upstream direction and 8m thick in the downstream direction. For the uranium beam with kinetic energy 1GeV/amu and intensity of $1E8$ ions per second the dose rate outside the building is smaller than $0.1\mu\text{Sv/h}$ mostly smaller than $0.01\mu\text{Sv/h}$. The situation can be different for other beam intensities and energies and if the target position changes. Figure 1 demonstrates that the dose rate outside the shielding can be kept under $0.5\mu\text{Sv/h}$. The concrete shielding employed is 5m in the lateral and 8m in the downstream direction to the beam. For higher beam intensities and energies and for target positions closer to the walls the shielding might have to be adjusted: One meter of ordinary concrete shield will reduce the dose rate approximately by one order of magnitude. Nevertheless the simulation of the radiation transport can be repeated with a more refined geometry and a more realistic modelling of the primary beam losses before the civil construction of the building will start.

References

- [fluka1] A. Fassò, A. Ferrari and P. R. Sala: Electron-photon transport in FLUKA: status, Proceedings of the MonteCarlo 2000 Conference, Lisbon, October 23-26 2000, A.Kling, F.Barao, M.Nakagawa, L.Tavora, P.Vaz - eds., Springer-Verlag Berlin, 2001, pp 159-164
- [fluka2] A. Fassò, A. Ferrari, J. Ranft and P. R. Sala FLUKA: Status and Prospective for Hadronic Applications, Proceedings of the MonteCarlo 2000 Conference, Lisbon, October 23--26 2000, A.Kling, F.Barao, M.Nakagawa, L.Tavora, P.Vaz - eds., Springer-Verlag Berlin, 2001, pp 955-960

G. Organization and responsibilities, planning

1. R³B collaboration and project structure

The R³B collaboration has a steering committee or collaboration board. The members of this board are the signatories of the R³B Memorandum of Understanding (MoU). In this MoU, the signatories document their intention to take responsibility for design and construction of subsystems of the R³B experimental setup and express their intention to seek to raise the necessary resources needed with individual emphasis as indicated in Table 1. The present members of the collaboration board are given in Table 2. This process is not finalized yet, though. The management board consists of the spokesperson, the co-spokesperson the chair person of the technical board, his deputy, and a GSI contact person. The present constellation is given in Table 3. The management board is responsible for the coordination of the project. The R³B project consists of several sub-projects as described in this document. The project leaders of the individual sub-tasks form the technical board (Table 4). The technical board will meet regularly together with the management board to monitor the progress and to ensure coherence of the developments. Table 5 gives an overview on the working-groups responsible for the different projects.

Table 1. Involvement of the participating institutes

Systems:

- | | |
|----------------------------------|-----------------------------------|
| (1) Large-acceptance dipole | (7) Target recoil detector |
| (2) High-resolution spectrometer | (8) Active target |
| (3) Tracking detectors | (9) Low-energy neutron detector |
| (4) Proton tracking | (10) Neutron ToF spectrometer |
| (5) Large-area ToF wall | (11) Multi-track detector |
| (6) Gamma spectrometer | (12) DAQ and slow control |
| | (13) Simulation, Analysis, Theory |

Institute	System												
	1	2	3	4	5	6	7	8	9	10	11	12	13
Chalmers		x					x					x	x
UK		x				x	x	x				x	x
CSIC Madrid		x				x						x	x
Universidad Madrid						x							
Santiago		x			x	x		x					x
Krakow										x		x	
GSI	x	x	x	x		x	x	x		x		x	x
Univ. Mainz							x			x			
TU München		x	x									x	
Univ. Frankfurt				x						x			x
TU Darmstadt		x	x				x						x
FZ Rossendorf										x			
Univ. Köln						x							
CEA-Saclay	x						x				x		
GANIL								x					
IPN Orsay						x							
ISS Bucharest										x			
SINP Kolkata										x			
Tata Mumbai						x							
Bergen													x
Moscow													x
Debrecen									x				
PNPI			x										

Table 2. Collaboration Board / Steering Committee

T. Aumann	GSI, Germany
B. Jonson	Chalmers, Sweden
J.V. Kratz	University of Mainz, Germany
M.J.G. Borge	CSIC Madrid, Spain
R. Palit	Tata Mumbai, India
U. Datta Pramanik	SINP, Kolkata, India
M. Freer	University of Birmingham, UK
J. Benlliure	Santiago de Compostela, Spain
R. Krücken	TU München, Germany
R. Lemmon	Daresbury, UK
M. Chartier	Liverpool, UK
W. Catford	Surrey, UK
A. Botvina	Moscow, Russia
J. Vaagen	Bergen, Norway
J.-E. Ducret	CEA Saclay, France
A. Krasznahorkay	Debrecen, Hungary
L.M. Fraile	Universidad Complutense, Madrid, Spain
J. Stroth	University of Frankfurt, Germany
A. Zilges	TU Darmstadt, Germany
P. Roussel-Chomaz	GANIL, France
A. Heinz	Yale University, USA
A. Khanzadeev	PNPI, Russia
R. Kulesa	Jagellonski University, Krakow, Poland
D. Hasegan	Institute of Space Sciences Bucharest, Romania
E. Grosse	TU Dresden and FZ Rossendorf
P. Reiter	Uni Köln

Table 3. Management Board

Spokesperson	T. Aumann (GSI)
Co-spokesperson	B. Jonson (Chalmers)
Project Manager	T. Aumann (GSI)
Chair person of Technical Board (TB)	R. Lemmon (Daresbury)
Deputy chair person of Technical Board	O. Tengblad (CSIC Madrid)
GSI contact	unneeded in present constellation

Table 4. Technical Board

	member	Affiliation	deputy	Aff.
Chair	R. Lemmon	Daresbury	O. Tengblad	Madrid
Dipole magnet	B. Gastineau	CEA	J.E. Ducret	CEA
Spectrometer	R. Lemmon	Daresbury	H. Geissel	GSI
Tracking detectors	H. Simon	GSI	R. Gernhäuser	TUM
Proton detectors	J. Stroth	Frankfurt	A. Khanzadeev	PNPI
ToF	J. Benlliure	Santiago	K. Sümmerer	GSI
Gamma spectrometer	D. Cortina-Gil	Santiago	J. Gerl	GSI
Target recoil detector	O. Kisselev	Mainz	T. Nilsson	TUDa
Active target	P. Roussel-Chomaz	GANIL	P. Egelhof	GSI
Low-energy n	A. Krasznahorkay	Debrecen	H. Emling	GSI
Neutron ToF spectr.	K. Boretzky	GSI	U. D. Pramanik	SINP
Multi-track detector	J.-E. Ducret	CEA		
DAQ / slow control	H. Simon	GSI		
Simulations/Analysis	H. Alvarez-Pol	Santiago	M. Labiche	Paisley
EXL representative	M. Chartier	Liverpool	P. Egelhof	GSI

Table 5. R³B working groups and responsibilities
(Coordinators, deputies, participants)

Project	Members
Large-acceptance dipole	CEA Saclay (B. Gastineau , <i>J.-E. Ducret</i>) GSI (T. Aumann)
High-resolution spectrometer	UK (R. Lemmon) GSI (T. Aumann, <i>H. Geissel</i> , M. Winkler) MSU (B. Sherrill) Argonne (J. Nolen)
Tracking detectors (R ³ B group of common NUSTAR group)	TUM (M. Böhmer, <i>R. Gernhäuser</i> , R. Krücken) GSI (H. Simon , T. Aumann, A. Kelic, K. Sümmerer) FZ Rossendorf (<i>A. Junghans</i> , A. Wagner)
Proton detection	Frankfurt (J. Stroth , C. Müntz) PNPI (<i>A. Khanzadeev</i>) GSI (T. Aumann, H. Simon, K. Sümmerer) Mainz (O. Kiselev)
Large-area ToF	Santiago (J. Benlliure , E. Casarejos, I Duran) GSI (<i>K. Sümmerer</i>) SINP (U Datta Pramanik) TUM (<i>R. Gernhäuser</i> , M. Böhmer, R. Krücken)
Gamma spectrometer	Santiago (D. Cortina-Gil , H. Alvarez-Pol, J. Benlliure, E. Casarejos, I. Duran,) CSIC Madrid (<i>Olof Tengblad</i> , M.J.G. Borge, M. Turrion, D. Obradors) Universidad Madrid (L.M. Fraile, J.M. Udias) Valencia (B. Rubio) Barcelona (F. Calvino) IPN Orsay (F. Azaiez, D. Beaumel, Y. Blumenfeld, B. Genolini, E. Khan, J. Peyré, J. Pouthas, J.A. Scarpaci, F. Skaza, T. Zerguerras) GSI (J. Gerl, T. Aumann) Köln (P. Reiter) IFJ Krakow (A. Maj, M. Kmiecik, M. Zieblinski) MPI Heidelberg (H. Scheit) UK (K. Spohr, D. Cullen, S. Freeman, M. Labiche, P. Nolan) Lanzhou (Y. Zhang) Tata Mumbai (R. Palit)
Proton-recoil detector	Mainz (O. Kiselev , J.V. Kratz) TU Darmstadt (<i>T. Nilsson</i> , G. Schrieder) CEA (E. Pollacco) Chalmers (G. Nyman) UK (R. Lemmon, M. Chartier, W. Catford, M. Freer, M. Labiche) GSI (T. Aumann, P. Egelhof, H. Emling, H. Simon) Mumbai (A. Shrivastava)
Active target	GANIL (P. Roussel-Chomaz , W. Mittag) GSI (<i>P. Egelhof</i>) UK (M. Chartier, Ch.-E. Demonchy, R. Lemmon, B. Fernandez-Dominguez) Santiago (D. Cortina-Gil, H. Alvarez-Pol)
Low-energy neutrons (common with EXL)	Debrecen (A. Krasznahorkay) GSI (<i>H. Emling</i>)
Neutron ToF spectrometer	GSI (K. Boretzky , T. Aumann, H. Emling, Y. Leifels) SINP Kolkata (<i>U Datta Pramanik</i> , S. Bhattacharya) ISS Bucharest (M. Haiduc, A. Sevcenco, C. Mitu, M.Potlog) Krakow (R. Kulesa) Mainz (J.V. Kratz) Frankfurt (J. Stroth) FZ Rossendorf (E. Grosse, A. Junghans, A. Wagner) TU Darmstadt (J. Enders, A. Zilges) Santiago (J. Benlliure) Tokyo (T. Nakamura)
Multi-track detector	CEA Saclay (J.-E. Ducret , A. Boudard, E. Le Gentil, S. Leray, S. Pietri, C. Volant) GANIL (F. Rejmund)
DAQ and slow control (R ³ B group of common NUSTAR group)	GSI (H. Simon , N. Kurz, J. Hofmann) Krakow (R. Kulesa) UK (Ian Lazarus, V. Pucknell, S. Letts) GANIL (NN) Chalmers (B. Jonson) CSIC Madrid (O. Tengblad) Chalmers (T. Nilsson) TUM (M. Böhmer)
Simulation and analysis (R ³ B group of common NUSTAR group) and Reaction Theory	Aarhus (H.O.U. Fynbo, K. Riisager) Mainz (O. Kisselev) Kurchatov (L. Chulkov) Santiago (H. Alvarez-Pol, D. Cortina-Gil) Chalmers (B. Jonson) CSIC Madrid (M.J.G. Borge, E. Garrido) Valencia (J.L. Tain) UK (M. Labiche, M. Chartier, B. Fernandez Dominguez, R. Lemmon, K. Spohr, S. Paschalis) INR-Moscow (A. Botvina) Arizona (C.A. Bertulani) UK (J. Al-Khalili , R. Johnson, M. Oi, P. Stevenson, I. Thompson, J. Tostevin)

2. Schedule and milestones

In the following table, the most important steps in the design and construction are summarized. More details are given in the respective subsections.

Year	Project	Tasks / milestones
2005	1. dipole 2. spectrometer 3. tracking 4. proton tracking 5. large ToF wall 6. γ -calorimeter 7 target recoil det. 8. active target 9. low-nergy n 10. neutron ToF	Decision on budget and start of the project (Q4) Ion-optical calculations and simulations Test of prototypes for diamond detectors and Si-tracker, decision on substrate material Construction, delivery of detectors in Q4 Prototype tests of RPC based ToF-wall modules Simulations, prototype tests Simulations, tests of prototypes Design studies Simulations and final design of the low-energy neutron detector Simulations and detector tests (RPC and scintillator)
2006	1. dipole 2. spectrometer 3. tracking 4. proton tracking 5. large ToF wall 6. γ -calorimeter 7 target recoil det. 8. active target 9. low-nergy n 10. neutron ToF	Order of superconductor and start fabrication (Q2) Ion-optical calculations and simulations, decision on the design (Q4) Final design, production of first full-scale diamond detector Commissioning and first experiment Beam tests, final design, start of construction (Q3) Simulations, prototype tests, final design, Technical Design Report (Q4) Simulations, tests of prototypes, final design, Technical Design Report (Q4) Construction of test modules Construction of low-energy neutron detector Final design, Technical Design Report (Q4)
2007	1. dipole 2. spectrometer 3. tracking 5. large ToF wall 6. γ -calorimeter 7 target recoil det. 8. active target 9. low-nergy n 10. neutron ToF	Superconducting cable delivery (Q4) Technical Design Report for the spectrometer Production of large-area diamond, beam tests, design of Si-strip array and fibre detector Construction, setting up in Cave C (Q3-Q4) Start construction, crystal tests, beam tests Preproduction Construction of test modules Beam tests Start production and performance tests of first modules
2008	1. dipole 3. tracking 5. large ToF wall 6. γ -calorimeter 7 target recoil det. 8. active target 9. low-nergy n 10. neutron ToF	End of winding (Q2), integration in cryostat (Q4) Production and test of large-area diamond, Si-strip, and fibre detectors Commissioning and first experiment in Cave C Construction, crystal tests, beam tests Production In-beam tests, design of new ASIC Implementation and first experiment Construction
2009	1. dipole 3. tracking 6. γ -calorimeter 7 target recoil det. 8. active target 10. neutron ToF	Tests at Saclay (Q1), installation at R ³ B/FAIR (Q2), commissioning and field map (Q3) Implementation of tracking detectors at Super-FRS and R ³ B experiment Tests, implementation of calorimeter in R ³ B setup Installation of recoil tracker in R ³ B experiment In-beam tests, design of new ASIC Construction, installation of neutron detector in R ³ B hall, commissioning
2010	Phase 1 2. spectrometer 8. active target	Commissioning of full setup (excluding spectrometer and active target) Physics experiments (Phase 1) Production of spectrometer magnets Final design of active target, Technical Design Report, start of construction
2011	Phase 1 2. spectrometer 8. active target	Physics experiments (Phase 1) Delivery of spectrometer magnets Construction of active target
2012	2,8	Installation of spectrometer and active target, commissioning (Q4)
2013	Phase 2	Physics experiments (Phase 2)

H. Relation to other projects

Several detector developments and in particular the readout-electronic systems are to a large extent similar to those discussed, e.g., for the experiments using internal targets in the storage ring (see the technical proposal of the EXL collaboration). Although the geometries of the EXL detectors are rather different compared to those of R³B, many developments can be performed commonly. This is in particular planned for the target recoil detector (Si tracker), the gamma calorimeter, and the neutron detector. A common development is already evident from the fact that the members of the respective working groups in the EXL and R³B collaborations are partially identical. In addition, the spokesperson of the EXL collaboration is a member of the R³B Technical Board to ensure that all possible synergies are exploited, and to guarantee information exchange. Similarly, the chair person of the R³B Technical Board is a member of the EXL board.

Wherever possible, common developments are planned for the whole NUSTAR project. Here, in particular, the Data-Acquisition-System is planned to be identical as far as possible. Common NUSTAR working groups have been established for DAQ systems, tracking detectors, as well as for the development of common software tools for simulation and data analysis.